UNIVERSITÀ DEGLI STUDI DI CASSINO E
DEL LAZIO MERIDIONALE

Ph.D. course in
Imprese, Istituzioni e Comportamenti

Curriculum: Imprese e Ambiente

XXXVI cycle

Multidisciplinary approach on environmental contaminants in wastewater

SSD: ICAR/03

Course Coordinator
Prof. Rosella Tomassoni

Ph.D. Student
Gelsomino Monteverde

Supervisors
Prof. Patrizia Papetti
Prof. Marco Race

ACKNOWLEDGEMENTS

The authors would like to thank the “Istituto Nazionale di Previdenza Sociale” (INPS) for funding the doctoral scholarship of Gelsomino Monteverde.

ABSTRACT

This doctoral thesis explores various strategies for environmental remediation and management, encompassing the use of biodegradable extracting agents for soil washing techniques to avoid the accidental release of persistent pollutants into the environment, the employment of affordable adsorbents to mitigate the spread of micropollutants (i.e., microplastics), and the mitigation of emerging contaminants such as methylisothiazolinone (MIT) through a biological process.

Different aspects related to the soil washing techniques, in both ex-situ and in-situ configurations are here discussed, particularly focusing on the application and effectiveness of the remediation through biodegradable reagents. Nowadays, the use of these reagents is a key-factor to ensure a remediation process characterized by operating costs affordability and environmental sustainability. Low-molecular-weight organic acids (LMWOA), chelating agents, and biosurfactants can represent suitable extractant agents for the achievement of both high treatment efficiencies and minimized soil characteristics alteration. In this perspective, the characteristics of the main reagents involved in the washing process and the related mechanisms influencing the removal of Potentially Toxic Elements (PTEs) from soils are thoroughly analyzed. Indeed, the findings from previous studies highlight the need of preliminary investigations at lab scale to identify the soil properties and consequently select the best process operating conditions in order to perform feasible and effective treatments. Moreover, the literature review identifies the chelating agents as the most used extractants to date. Nonetheless, several research aimed at further deepening this topic also indicate the LMWOA and biosurfactants as promising and less impacting alternatives in the near future also due to their possible low-cost production through biological processes.

Also, this thesis proposes the surgical mask as an affordable and sustainable adsorbent for the remediation of diesel–contaminated seawater to cope with the polymeric waste generated monthly in hospital facilities. This approach can also be helpful considering a possible future pandemic, alleviating the pressure on the waste management system by avoiding improper mask incineration and landfilling, as instead occurred during the previous COVID–19. Batch adsorption–desorption

experiments revealed a complete diesel removal from seawater after 120 min with the intact laceless mask, which showed an adsorption capacity of up to 3.43 g/g. The adsorption curve was better predicted via Weber and Morris's kinetic ($R^2 = 0.876$) and, in general, with Temkin isotherm ($R^2 = 0.965 – 0.996$) probably due to the occurrence of chemisorption with intraparticle diffusion as one of the rates–determining steps. A hysteresis index of 0.23 – 0.36 was obtained from the desorption isotherms, suggesting that diesel adsorption onto surgical masks was faster than the desorption mechanism. Also, the effect of pH, ionic strength and temperature on diesel adsorption was examined. The results from the reusability tests indicated that the surgical mask can be regenerated for 5 consecutive cycles while decreasing the adsorption capacity by only approximately 11%.

Finally, this thesis aims to investigate, the effect of MIT on the nitrification-denitrification process in a moving-bed biofilm reactor (MBBR). After a preliminary study performed in a fed-batch reactor, two MBBRs were simultaneously operated in semi-continuous mode for 136 days evaluating a concentration of MIT in the influent of 0.1 and 1.0 mg/L. A parallel study was also conducted under anaerobic conditions to evaluate the effect of MIT on methane production and volatile fatty acids accumulation. At a mere concentration of 0.1 mg MIT/L, the nitrification process experienced an initial complete inhibition. Subsequently, nitrifying bacteria gradually recovered, reaching approximately 49% oxidation of ammonia nitrogen, a removal improved up to 64% at 1.0 mg MIT/L. Although the denitrification process faced temporary inhibition, ultimately achieved a 100% reduction in nitrite and nitrate concentrations when the MIT concentration was increased from 0.1 to 1.0 mg/L. The cumulative methane yield reached approximately 134 mL CH4/g VS for the control group and was similar to the methane production obtained in the presence of MIT. A MIT removal of 100% was achieved under aerobic, anoxic, and anaerobic conditions.

TABLE OF CONTENTS

ABSTRACT I
LIST OF FIGURES V
LIST OF TABLES VII
INTRODUCTION 1
CHAPTER 1. Remediation of PTEs contaminated soils by washing treatment with biodegradable reagents 4
1.1 Introduction 4
1.2 Biodegradable reagents 6
1.2.1 Low-molecular-weight organic acids 6
1.2.2 Aminopolycarboxylic Acids 9
1.2.3 Biosurfactants 9
1.3 Washing Treatments 10
1.3.1 Soil Washing 10
1.3.2 Soil flushing 11
1.4 PTEs-Reagents interactions 12
1.4.1 PTEs interaction mechanisms with low-molecular-weight organic acids (LMWOAs) 12
1.4.2 Aminopolycarboxylic Acids 22
1.4.3 Biosurfactant 22
1.5 Conclusions and future perspectives 23
1.6 References 24
CHAPTER 2. Reuse of polymeric waste for the treatment of marine water polluted by diesel 34
2.1 Introduction 34
2.2 Materials and methods 36
2.2.1 Diesel fuel, seawater and the surgical mask 36
2.2.2 Adsorption–desorption experiments 36
2.2.3 The effect of ionic strength, pH and temperature 36
2.2.4 Reusability experiments 37
2.2.5 Analytical methods 37

2.3 Results and discussion 38
2.3.1 Use of the surgical mask for diesel adsorption 38
2.3.2 Adsorption–desorption mechanism 40
2.3.3 Regeneration and reutilization of the surgical mask 47
2.4 Conclusions 48
2.5 References 49
CHAPTER 3. Moving-bed biofilm reactor (MBBR) alleviates the negative effect of methylisothiazolinone on the nitrification-denitrification process 57
3.1 Introduction 57
3.2 Materials and methods 59
3.2.1 Activated sludge, digestate and synthetic influent 59
3.2.2 Experimental setup and bioreactor operations 60
3.2.3 Biochemical methane potential tests 61
3.2.4 Sampling, analytical methods and calculation 62
3.2.5 ANOVA test 63
3.3 Results and discussion 64
3.3.1 The effects of MIT on the nitrification process in fed-batch reactor 64
3.3.2 The impact of MIT on the nitrification-denitrification process in moving-bed biofilm reactors 67
3.3.3 The influence of MIT on biogas production during the AD process in the sludge line 71
3.3.4 Kinetics and mechanism of methylisothiazolinone removal under aerobic, anoxic and anaerobic conditions 74
3.4 Conclusions 79
3.5 References 79
CONCLUSIONS AND FUTURE PERSPECTIVES 92

LIST OF FIGURES

Figure 1.1 – Scheme of the Soil Washing process 11
Figure 1.2 – Scheme of the soil flushing process 11
Figure 2.1 – The effect of initial diesel concentration (Ci, g/L) on total and dissolved diesel removal (%) using non–worn masks in distilled water (NMDW) after 120 min of adsorption experiments. 39
Figure 2.2 – Diesel adsorption (Qt, e) onto surgical masks (g/g) vs time (min) in a solution at 5 g diesel/L for 120 min by fitting the experimental points with the Elovich and Intraparticle Diffusion (ID) kinetic models (a), and vs diesel concentration (g/L) at the equilibrium in the solution phase (Ce) by using the Freundlich and Temkin equilibrium isotherms (b). Diesel desorption (Qe) from surgical masks (g/g) vs initial diesel concentration (Ci, g/L) by employing the Freundlich and Langmuir isotherms (c). 46
Figure 2.3 – The effect of a) ionic strength (M) and b) initial pH on the surgical mask adsorption capacity (Q_e, g/g) after 120 min. 47
Figure 2.4 – Van't Hoff plots for diesel adsorption a) and desorption b) using surgical masks at different temperature–dependent isotherms (i.e., 281.15, 293.15, 303.15 and 313.15 K). 47
Figure 2.5 – Diesel removal (%) after 5 consecutive adsorption–desorption cycles. 48
Figure 3.1 – Evolution of a) ammonia nitrogen (NH_4^+–N, mg/L), b) water soluble organic carbon (WSOC, mg/L), vs time (days) during Phases I, II, and III; and c) NH_4^+–N and WSOC removal efficiencies (%), d) volatile suspended solids (VSS, g/L) thorough 12 cycles of operation of the fed-batch reactor (F-BR). 66
Figure 3.2 – Evolution of a) ammonia (NH_4^+–N, mg/L), b) nitrate (NO_3^-–N, mg/L), c) nitrite (NO_2^-–N, mg/L) vs time (days) in the 1st (enrichment), 2nd (steady phase), 3rd (methyl-4-isothiazolin-3-one) Period during 136 days of moving-bed biofilm reactor (MBBR) operation under nitrification (MBBR-N) and denitrification (MBBR-D) performed in semi-continuous mode. 70
Figure 3.3 – a) Cumulative methane yield (mL CH_4/g VS); b) biogas composition (%) in terms of CH_4 and CO_2; total VFA evolution (mg HAc/L) in c) the control and

d) methyl-4-isothiazolin-3-one (MIT) groups during 109 days of anaerobic digestion. The dissimilar letters (Tukey test) denote significant differences ($p < 0.05$). 76

Figure 3.4 – Methyl-4-isothiazolin-3-one (MIT) degradation ($C_{MIT,i}/C_{MIT,0}$, %) during a) nitrification/denitrification processes and b) anaerobic digestion. The dissimilar letters (Tukey test) denote significant differences ($p < 0.05$). 77

Figure 3.5 – Proposed mechanisms involved during methyl-4-isothiazolin-3-one (MIT) removal. 79

LIST OF TABLES

Table 1.1 – List of the most common biodegradable reagents used for remediation of contaminated sites 7

Table 1.2 – Removal efficiencies for PTEs by varying the operating conditions and the reagents 14

Table 2.1 – Elovich and Intraparticle Diffusion kinetic models of diesel adsorption (Qt) onto surgical masks in aqueous solution (i.e., initial concentration of 5 g/L) after 120 min. Kid and α are the adsorption rate constants, and β and C represent the model constants..... 41

Table 2.2 – Freundlich, Temkin and Langmuir equilibrium isotherms of diesel adsorption–desorption onto surgical masks in water solutions at different diesel equilibrium (C_e, g/L) and initial (C_i, g/L) concentrations. A_t, $K_{f,ads}$ and $K_{f,des}$ represent the adsorption–desorption factors, Q_L is the maximum desorption capacity, and b_t, n_{ads}, n_{des} and K_L are the isotherm constants. 41

Table 2.3 – Thermodynamic parameters for the adsorption–desorption of diesel in water solutions using surgical masks. The values are the thermodynamic equilibrium coefficient (K_d), the free energy of Gibbs (ΔG), the enthalpy (ΔH) and entropy (ΔS). 44

Table 3.1 – Physical-chemical characteristics of activated sludge and digestate. TS = total solids; VS = volatile solids; NO_3^-–N = nitrate; NH_4^+–N = ammonia nitrogen. 60

Table 3.2 – The Gibbs free energy change (ΔG) for nitrification and denitrification processes is calculated as the difference between the standard Gibbs free energy of formation (ΔG°f) of products and reactants, obtained through a summary of each species involved. 73

Table 3.3 – Kinetic model of cumulative methane yield (mL CH_4/g VS) under the control and 2-methyl-4-isothiazolin-3-one (MIT) groups during 109 days of BMP test. 73

Table 3.4 – Kinetic models of methyl-4-isothiazolin-3-one (MIT) degradation under aerobic, anoxic, and anaerobic groups in moving-bed biofilm reactors and biochemical methane potential test. 78

INTRODUCTION

In recent years, there has been increasing attention paid to the water resource, with a greater awareness acquired regarding its potential recycling and hence its potential contamination. Scientific literature has consequently focused on how to optimize water reuse and, consequently, the best way to remove or reduce any impurities, pollutants, or microorganisms below the limits imposed by regulations.

The issue of Potentially Toxic Elements (PTEs) contaminating water, soils and sediments is a well-known problem worldwide, backed up by extensive scientific research conducted over the past thirty years (Li et al., 2022; Reyes et al., 2021). The harmful effect lies not only in the toxicity of PTEs but also in their solubility in lipids, which allows them to accumulate in fatty tissues and move up the food chain, resulting in biological magnification (Murtaza et al., 2022). Since soils are the primary target of PTEs contamination from human activities, they possess high retention capacities for contaminants, leading to persistent environmental pollution (Ferraro et al., 2023; Tarvainen et al., 2020). Unlike organic compounds, PTEs contamination cannot be mitigated through biological degradation. Soil contamination by PTEs has caused significant economic losses for the agricultural sector, hindering optimal land use and disrupting natural ecosystem balances (Abrahams and Thornton, 1994; Dahlin et al., 1997). Environmental factors can further exacerbate PTEs contamination by altering their chemical forms and bioavailability over time, potentially increasing the hazards associated with contamination. The European Environment Agency (EEA) has identified millions of potentially contaminated sites within the EU, necessitating remediation efforts for a significant portion of them (EEA, 2020). Remediating PTEs contaminated soils is a challenging task that requires efficient strategies. Soil washing, which employs biodegradable reagents, is a promising technique for remediation, ensuring minimal alteration to soil properties and the avoidance of toxic by-products (Peters, 1999). This chemical-physical method involves solubilizing contaminants in an aqueous phase through the washing of excavated soils with extracting reagents in closed reactors (Dermont et al., 2008). This would allow to reduce the risk for sensitive environments such as marine compartments when an accidental spill occurs.

The contamination of seawater by oil spills is indeed pressing environmental issue, primarily driven by petroleum-related activities. Millions of tons of crude oil are transported offshore annually, posing risks to aquatic ecosystems and coastal areas (Ben Jmaa and Kallel, 2019; Diraki et al., 2019). To mitigate oil pollution in seawater, the utilization of waste-derived adsorbents, such as biochar, offers a sustainable and effective solution, provided the adsorbents possess hydrophobic and oleophilic properties (Hossain et al., 2019; Lee et al., 2022). On the other hand, the widespread use of disposable face masks during the COVID-19 pandemic has raised concerns about their environmental impact, particularly regarding waste management and pollution. Polymeric materials used in these masks, such as polypropylene and polyethylene, hold promise for organic pollutant removal, but concerns over microplastic release and appropriate reuse strategies persist (Jung et al., 2021; Selvaranjan et al., 2021).

Likewise, the release of microplastics, other emerging pollutants such as 2-methyl-4-isothiazolin-3-one (MIT), has raised significant environmental and health concerns. The scientific community has shown a growing interest in this class of pollutants, often present in wastewater, whose term derives from the union of two key aspects that unite a large and diverse number of substances: the reduced concentrations classify these compounds as micropollutants, while the limited scientific information regarding the negative effects on living organisms makes these substances difficult to place in an appropriate regulatory context, compared to conventional pollutants. MIT, widely used as a biocide and disinfectant, can persist in wastewater and disrupt biological processes in treatment systems, necessitating effective mitigation strategies (Nowak-Lange et al., 2022; Speksnijder et al., 2010). For this purpose, this thesis highlights the need for effective mitigation eco-approaches, as an alternative to the use of adsorbents.

This Ph.D. thesis comprises four chapters, including a literature review and two research chapters, followed by a final section addressed to conclusive remarks and future perspectives. The structure of the present thesis is reported as follows:

- chapter 1 is an overview of the literature, focusing on the application and effectiveness of the remediation of Potentially Toxic Elements (PTEs) through biodegradable reagents for reducing the wastewater toxicity;
- chapter 2 evaluates the use of surgical masks as an affordable and sustainable adsorbent for the remediation of contaminated saline solutions;

- chapter 3 investigates the employment of a Moving-bed biofilm reactor (MBBR) to alleviate the negative effect of methylisothiazolinone on the nitrification-denitrification process of wastewater treatment plants;
- chapter 4 is a conclusion section that highlights the main findings of this doctoral thesis and discusses their relevance to existing literature. Recommendations for future studies are expressed in this chapter.

In the lights of above, it becomes evident that interdisciplinary approaches and innovative solutions are paramount in safeguarding our ecosystems and public health amidst evolving ecological challenges. Through collaborative research efforts and technological advancements, this work pave the way for a more sustainable and resilient future.

CHAPTER 1. REMEDIATION OF PTES CONTAMINATED SOILS BY WASHING TREATMENT WITH BIODEGRADABLE REAGENTS

1.1 Introduction

Contamination of soils and sediments by Potentially Toxic Elements (PTEs) is an ascertained worldwide issue as also highlighted by several scientific studies over the last 30 years (Li et al., 2022; Reyes et al., 2021). This concern is not only due to the PTEs toxicity but also to their solubility in lipids. In fact, PTEs tend to concentrate either in the fatty tissue or in organisms from one trophic level to another along the food chain. Also, the very slow rate of PTEs excretion from fatty tissue is a potential cause for "biological magnification" occurrence (Murtaza et al., 2022).

Soils represent the main target of PTEs contamination from human activities and their high contaminant retention capacity leads to long-lasting pollution conditions in the environment (Ferraro et al., 2023; Tarvainen et al., 2020). Besides this, PTEs contamination cannot be reduced by biological degradation as naturally occurs for organic compounds.

In the agricultural sector, soils contamination by PTEs prevents an optimal use of the land, thus causing serious economic damage (Abrahams and Thornton, 1994) and altering the existing balance of natural components (Dahlin et al., 1997).

Also, influence by environmental factors can change both PTEs chemical form (speciation) and bioavailability with time thus possibly resulting in more hazardous form of contamination. The European Environment Agency (EEA) estimated 2.5 million of potentially contaminated sites in the EU. The 14% of these cases are characterized by an ascertained contamination then requiring the involvement of remediation processes (EEA, 2020).

For contaminated agricultural areas, optimal remediation approaches should be aimed at removing pollutants without affecting the original structure and composition of the soil. Generally, this result can be achieved by phytoremediation, but this technique might not be feasible for high contaminants concentration and very deep contamination in soils (Gabriele et al., 2022). In a contaminated land, anthropogenic activities can be cause of very high PTEs concentrations occurrence in delimited areas. These are identified as hot spots (Goovaerts, 1997) and their remediation requires more specific approaches than that based on treatments for low contamination levels (such as phytoremediation) (Dermont et al., 2008).

According to this, the remediation of PTEs contaminated soils is an important challenge to deal with the involvement of suitable and efficient strategies. In this perspective, soil washing processes represent a promising technical solution if performed with extracting reagents which minimize the soil characteristics alteration and do not result in toxic by-products formation after treatment (Peters, 1999).

The Soil Washing is a well-assessed chemical-physical technique involved for the contaminants removal from the solid matrix through solubilization in an aqueous phase. It is an actual washing of the contaminated soils which are excavated and mixed with water solutions containing an extracting reagent (such as surfactants, biosurfactants, organic solvents, chelating reagents, acids or bases) in closed reactors (Dermont et al., 2008).

This method has been successfully applied to different pollutant classes, such as semi-volatile organic compounds, fuels, PTEs as well as volatile organic compounds and pesticides. The removal efficiencies of inorganic compounds can be very high but vary as a function of the extracting reagent added to the washing solution. Also for PTEs removal, Soil Washing can be performed through different extracting reagents which differ for costs and efficiency. In particular, acid solutions (HCl, H2SO4, HNO3) or complexing reagents such as citric acid, ammonium acetate, Nitrilotriacetic acid (NTA), Ethylenediaminetetraacetic acid (EDTA) and Ethylenediaminedisuccinic acid (EDDS) are most frequently used (Fabbricino et al., 2013). However, suitable reagent selection needs to be carried out by also considering the effect on soil characteristics after the treatment and the possible reuse of the remediated solid matrix. For instance, the soil fertility preservation and prevention of toxic by-products formation should be priority aspects in the treatment of soils for further agricultural reuse (Race et al., 2019). Accordingly, the involvement of biodegradable and non-toxic reagents indeed represents a key-solution for a feasible and environmental friendly contaminated soil remediation processes. This chapter aims at deeply

discussing the Soil Washing technique performed through biodegradable reagents and specifically provides detailed considerations about the chemical, biological, and engineering aspects related to the process.

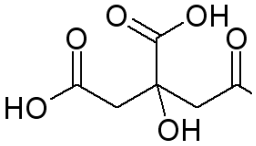
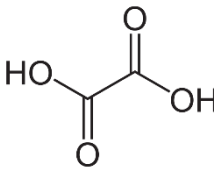
1.2 Biodegradable reagents

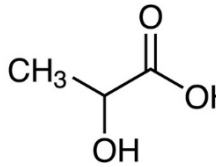
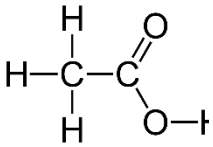
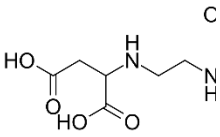
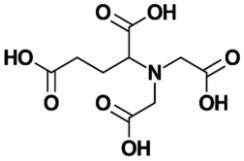
Several literature studies analyzed various reagents applicability in the remediation of contaminated sites. The main one involved in the remediation process are generally: i) inorganic reagents, ii) low-molecular-weight organic acids (LMWOA), iii) chelating reagents. However, only LMWOAs and some synthetic chelating reagents are biodegradable and, therefore, suitable to perform environmentally sustainable treatments.

1.2.1 Low-molecular-weight organic acids

LMWOAs are very widespread since their microbial, plant, or animal origins. In the industrial field, their production is mainly achieved through chemical processes while only in modest quantities through biological ones (Papagianni, 2011). LMWOAs are naturally found in soils due to production by lichens and algae. Moreover, LMWOAs are strongly linked to the carbon cycle, and usually, their concentration does not exceed 100 mM (Adeleke et al., 2017). LMWOAs are characterized by the presence of at least one carboxylic acid group, which enables the formation of complexes with PTEs. For this reason, the number of scientific studies investigating the use of LMWOAs as soil-washing reagents has grown in the last decade (Gzar et al., 2014; Race et al., 2019; Xu et al., 2022). The main advantage of LMWOAs application is their low toxicity and high biodegradability compared to inorganic acids and chemically produced organic acids. Unlike strong mineral acids, organic acids are usually weak and are not completely dissociated in water (Khan and Iqbal, 2016). Furthermore, LMWOAs can be widely used in remediation processes, even at high concentrations, thanks to their high solubility (Tab. 1.1). The supply costs are strongly dependent on the production method and, obviously, on the degree of LMWOAs purity. For instance, biological methods are advantageous for the concurrent production of various LMWOAs facilitating their subsequent use as a mixture. In this case, the supply costs would be very low compared to other biodegradable reagents.

Table 1.1 – List of the most common biodegradable reagents used for remediation of contaminated sites

	pKa	Structure	Solubility [g/L]	Stability Constants (Ks)	Number of manuscripts 2013-2022	References
citric acid (CA)	2.79	$C_6H_8O_7$ or CH_2 COOH-C(OH)COOH-CH_2COOH 	592	Cd : 3.5 Ni : 3.4 Cu : 5.9 Cr(III) : 7.7 Pb : 4.1 Zn : 4.9 Mn : 2.6 Fe(III) : 13.2 Ca : 4.9 Mg: 4.9	86	(Mertens et al., 2018; Mo et al., 2018; Serjeant and Dempsey, 1979)
oxalic acid (OA)	pKa 1: 1.46; pKa 2: 4.40	$C_2H_2O_4$ or $(COOH)_2$ or HOOCCOOH 	220	Cd : 3.0 Ni : 5.2 Cu : 6.3 Cr(III) : 5.3 Pb : 4.0 Zn : 4.9 Mn : 3.9 Fe(III) : 9.4 Mg: 2.6	46	(Clayton and Clayton, 1981; Ostroushko and Russkikh, 2017; Vinokurov and Bondar', 2003)
lactic acid (LA)	3.86	$C_3H_6O_3$ or CH_3 CHOHCOOH or $HC_3H_5O_3$	1000	Cd : 1.3 Ni : 1.6 Cu : 2.5 Cr(III) : 3.3 Pb : 2.0 Zn : 1.6	8	(Hamada et al., 2005; Merck Index, 1996; Portanova et al., 2003)

				Mn : 1.0 Ca : 0.9 Mg : 0.8		
Acetic Acid (AA)	4.76	$C_2H_4O_2$ or CH_3COOH 	1000	Cd : 1.3 Ni : 0.7 Cu : 1.8 Cr(III) : 3.7 Pb : 1.9 Zn : 0.9 Fe(III) : Ca : 0.5 Mg: 0.5	29	(Bunting and Thong, 1970; Serjeant and Dempsey, 1979)
Ethylenediamine-N,N'-disuccinic acid (EDDS)	pKa1 2.4, pKa2 3.9, pKa3 6.8, pKa4 9.8	$C_{10}H_{16}N_2O_8$ 	slightly soluble	Cd : 10.9 Ni : 16.7 Cu : 18.4 Cr(III) : 10.8 Pb : 12.7 Zn : 13.4 Fe(III) : 22 Ca : 4.6 Mg: 6.0	38	(Orama et al., 2002; USDA, 2010)
Glutamic acid-N,N-diacetic acid (GLDA)	pKa1 2.6, pKa2 3.5, pKa3 5.0, pKa4 9.4	$C_9H_{13}NO_8$ 	65	Cd : 10.3 Ni : 12.7 Cu : 13.0 Cr(III) : 12.9 Pb : 11.6 Zn : 11.5 Mn : 7.6	15	(Abdelgawad et al., 2019; Begum et al., 2012a; FEEDAP et al., 2018; Kołodyńska, 2011;

	Fe(III) : 11.7 Ca : 5.2 Mg : 6.1	Zheng et al., 2022)

1.2.2 Aminopolycarboxylic Acids

Aminopolycarboxylic acids (AAs) are produced by both chemical and biological processes (Bucheli-Witschel and Egli, 2001). AAs are characterized by a high tendency to form complexes with PTEs. Therefore, these reagents are widely used in the remediation of PTEs contaminated soils. To date, the most commonly used AAs is the EDTA. However, EDTA is characterized by negligible biodegradability, and previous studies showed the potential toxicity of EDTA-Me complexes (Gusiatin et al., 2020; Sillanpää and Oikari, 1996). Consequently, in recent decades, new AAs with high biodegradability and low toxicity have been investigated. These AAs are characterized by one or more N atoms bound to carboxyl groups by C atoms. Nonetheless, the production of biodegradable AAs is still not common at industrial scale. In fact, EDTA is still one of the AAs mainly used in soil remediation processes thus resulting in high costs for treatments carried out by involving other AAs. A further disadvantage of soil remediation through AAs is represented by the reagents reduced solubility. Then, treatments performed with high reagent concentrations are not feasible (USDA, 2010). Accordingly, AAs application could be recommended for site contaminations not spatially extensive and characterized by modest pollutant concentrations.

1.2.3 Biosurfactants

Biosurfactants (BSs) are produced by the vital activities of bacteria, yeasts, and fungi (i.e., surfactin, sophorolipids etc.) but also by plants and animals (tannic acid) (Paria, 2008). BSs enhance the desorption and solubilization rate of PTEs. Due to their different origins, they can be composed by different chemical compounds (i.e., carboxylic acid with an aliphatic chain, glycolipid, etc.) as well as display different chemical structures.

BSs of natural origin are very suitable for the remediation of contaminated sites as they do not significantly alter the soil characteristics. However, the co-use of several biosurfactants during the chemical washing may be necessary, especially for highly contaminated soils. Their costs are currently relatively high. However, soil

remediation with BSs may become economically feasible in the perspective of an increase of their production through biological processes (Zhang et al., 2022).

1.3 Washing Treatments

Chemical washing on soils can be carried out both in situ and ex-situ (Dermont et al., 2008). In the first case, the soil is not excavated by site of origin and process is defined as Soil Flushing. In the ex-situ remediation, the soil is instead excavated prior the treatment which is as Soil Washing. The reagents involved can be the same for both approaches and dependent on the type of target contaminant. PTEs, radioactive elements and some organic compounds (i.e., PAHs, PCBs etc.) are generally removed by Soil Washing.

1.3.1 Soil Washing

Soil Washing is a remediation treatment based on physical and/or chemical mechanisms (Liu et al., 2021). Physical mechanisms consist of dry (or wet) grading methods to separate the fine fraction (most contaminated) from the coarse material which can be recovered. Instead, the chemical mechanisms allow the pollutant removal through solubilization from the solid matrix to the liquid phase represented by the washing solution (Griffiths, 1995). In this case, the chemical reagents in the washing solution enhance the pollutant removal. The treatment cycle (Fig. 1.1) includes sequential operating units, each of them affected by different factors depending on characteristics of both soils and contaminants. The main steps are as follow:

1) removal of soil from the origin site;

2) granulometric separation: the separation technique can vary according to the soil particle sizes to collect for further treatment; the most common are the drum screening, hydrocyclones, etc.;

3) treatment of the contaminated fraction: the reagent is chosen according to: (i) the selectivity towards the target contaminants, (ii) economy, and (iii) low toxicity; moreover, studies are required to evaluate the best operating conditions (i.e., contact time, pH, soil/solution ratio, reagent dosage);

4) treatment of the exhausted solution: processes aimed at treating industrial process waters are used; however, whenever possible, attempts are conducted to reuse both the aqueous solution and the reagent.

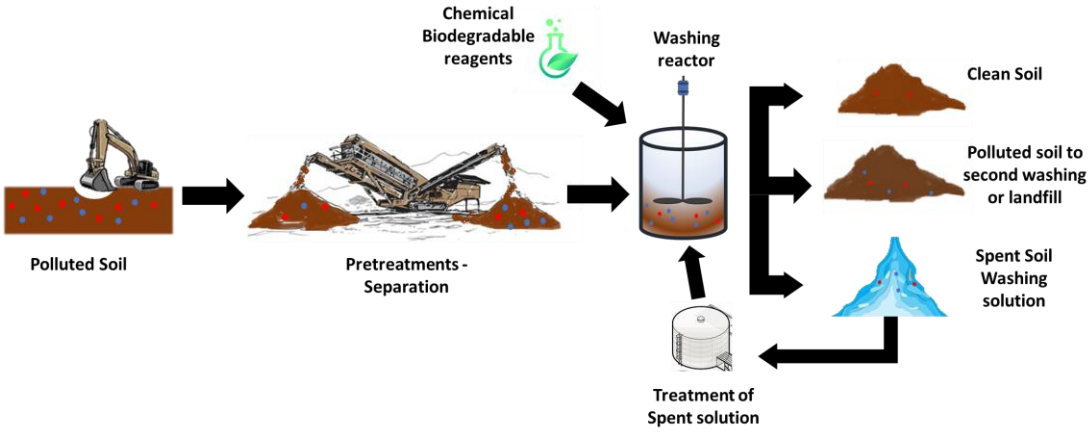


Figure 1.1 – Scheme of the Soil Washing process

1.3.2 Soil flushing

In the Soil Flushing process, being an in-situ approach, the previously discussed steps 1 and 2 are not carried out. Furthermore, in this case, proper selection of the involved reagent is essential to avoid the pollution of the deep layers of soil as well as the aquifer (Martel et al., 1998). Soil Flushing requires the construction of wells (vertical or sloped) for the washing solutions injection within the soil. Moreover, the wells allow the extraction of the solutions containing the dissolved contaminants after the treatment. For the Soil Flushing, soil permeability plays an important role as it affects the flows of the injected washing solution (Atteia et al., 2013). Then, a geological study of the contaminated area before treatment is essential.

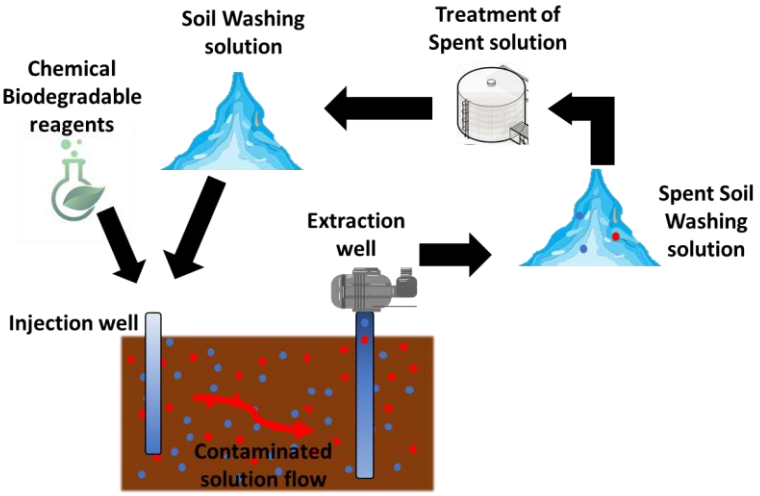


Figure 1.2 – Scheme of the soil flushing process

1.4 PTEs-Reagents interactions

The interactions between PTEs and reagents can differ according to their mutual characteristics. However, the pivotal principle of all successful mechanisms is the solubilization of PTEs. This section describes the individual mechanisms that can occur between reagents and PTEs.

1.4.1 PTEs interaction mechanisms with low-molecular-weight organic acids (LMWOAs)

The LMWOAs mainly studied in previous literature are reported in Tab. 1.1. LMWOAs can dissolve, solubilize and desorb PTEs from the soil particles (Ash et al., 2016). The interaction between PTEs and LMWOAs results in the formation of soluble complexes. LMOWAs have different stability and complexation constants for each single metal (Tab. 1.1). Then, the involvement of LMWOAs for soil remediation should be decided according to the specific contamination detected in the solid matrix.

The use of LMWOAs at high concentrations can change the soil pH resulting in the non-selective dissolution of several elements. The pH variation can affect the balance of the formed complexes by varying the speciation of the single LMWOA and, therefore, altering its capacity to form complexes (Kim et al., 2013).

However, the extraction of the single PTE can also be influenced by its bioavailability, which is generally determined through sequential extraction procedure but not always discussed in scientific studies. More in detail, PTEs can be bound to different fractions of the soil: exchangeable, oxidizable, reducible and residual. The quantity of PTEs contained in the residual fraction cannot be leached in any environmental condition. However, some study also reported the decrease of PTEs in the residual fraction due to the dissolution of inorganic complexes. For instance, Zou et al. (2019) observed vanadium reduction by more than 50%. On the contrary, PTEs dissolution occurs more easily from the mobile fractions represented by the exchangeable, reducible, and oxidizable ones. In general, LMWOAs solubilize elements from these fractions (Yao et al., 2022). PTEs can be released from the first fraction (exchangeable) in slightly acidic conditions. Concerning the reducible fraction, it is basically due to the reduction of the iron/manganese oxides is the main phenomenon which leads to the PTEs release. Finally, for the oxidizable fraction, LMWOAs can dissolve the soil's organic matter thus allowing the PTEs solubilization (Ding et al., 2011). The solubilization effect is not observed with High-molecular-weight organic acids (HMWOAs) which instead are generally effective in the

stabilization of the contaminants within a solid matrix (Yao et al., 2022). Based on the above discussion, it is clear that selection of proper analyses aimed at characterizing the PTEs bioavailability in soils could play a fundamental role for the efficiency of the treatment. Then, single sequential extraction analysis could be unsuitable especially considering the variable chemical speciation possibly displayed by metals.

Remediation process on soils contaminated by different PTEs can be carried out at various operating conditions. Tab. 1.2 shows the main results from scientific literature. The characteristics of both soils and contaminants as well as the washing methods can significantly affect the removal efficiency. High concentration of LMWOA results in high PTEs removal efficiencies. However, concurrent removal of nutrients (i.e. K, P, Ca, Mg, etc.) can also be observed from soil since LMWOA are non-selective extractants. According to this, a previous ecotoxicological study suggested the addition of nutrient-rich salts after the treatment process in order to restore the soil initial characteristics (Race et al., 2019). Due to the strong selectivity of LMWOAs toward specific pollutants (Tab. 1.1), the use of a low reagent dosage could be very effective for the removal of target contaminants. In fact, for citric acid, the Cu removal efficiency is usually more significant than that of the other PTEs such as Cd and Zn. Among the LMOWAs, oxalic acid (OA) showed effective applicability especially at high concentrations. OA forms insoluble complexes with PTEs (i.e., Pb) and other elements in the soil. Nonetheless the formed OA complex can easily resolubilize at slightly acidic pH thus increasing the fraction of potentially releasable metals. Sun et al. (2001), observed a concentration increase of Cu and Pb in the exchangeable fraction due to the formation of oxalates. Accounting for Tartaric Acid and Lactic Acid, their use in the washing process is less frequent despite the high removal efficiencies achievable. Currently, scientific studies on washing process performed through LMOWA mixtures are lacking in literature. Indeed, this aspect could be worth of future investigations by also studying the effects on the soil remediation process through washing solution characterized by combination of LMOWAs from biological treatments carried out different application fields (such as wastewater treatment).

The solid/liquid (S/L) ratio (v/v) indirectly affects the PTEs-LMOWA molar ratio. High values of the S/L ratio lead to enhanced diffusion phenomena (Ferraro et al., 2016). As reported in Tab. 1.2, treatment efficiency increase can be observed at increasing S/L ratio values. However, in full-scale applications, too high S/L ratio could hinder the process feasibility due to the consequent requirement of large washing solution volumes and their subsequent treatment. According to the results observed in Tab. 1.2, S/L ratio of 1/10 seems in most of the case an optimal operating condition.

LMOWAs are readily biodegradable but after their complexation with PTEs, the biodegradability rate slows down (Nowak and Nowak, 1990). Francis et al. (1992) observed that the citric acid is not biodegradable after complex formation with Cu at CA/Cu molar ratio equal to 1/1. On the contrary, CA is still totally biodegradable if the CA/Cu molar ratio increases to 2/1. The biodegradation of LMOWAs can also occur due to microorganisms present in the soil. Nonetheless, monitoring of potential changes occurring in the distribution of microorganisms community within soil after treatment with LMOWAs would be strongly recommended (Renella et al., 2004). Therefore, based on the above reported discussion, the selection of a proper LMWOA (and its concentration) for the soil treatment should be done by also evaluating the biodegradability and toxicity of the formed complexes besides the PTEs removal efficiencies potentially achievable.

Table 1.2 – Removal efficiencies for PTEs by varying the operating conditions and the reagents

Soil	PTE	Concentration (mg kg^{-1})	Parameter	Removal efficiences [%]	References
pH 7.4; CEC:3.6 meq/100g; Sand(%): 97; Silt(%):3; Clay(%) 0; OM(%): 0.2	Cd	500 (Artificially contaminated)	0.001 – 0.1 mol l-1 S/L=1/10 T=3hr	AA : 5.2-31.1	(Gzar et al., 2014)
	Pb	500 (artificially contaminated)		AA : 42.2-100	
	Ni	500 (artificially contaminated)		AA : <1	
pH 6.1; CEC:1.6 %; Sand(%): 78; Silt(%):13; Clay(%) 9; OM(%): 0.2	Ni	438 (Artificially contaminated)	0.05 mol l-1 S/L=1/25 T=6hr	CA: 46 TA: 28	(Wuana et al., 2010)
	Cu	498 (Artificially contaminated)		CA: 50 TA: 30	
	Zn	376 (Artificially contaminated)		CA: 44 TA: 27	
	Cd	340 (Artificially contaminated)		CA: 38 TA: 19	

	Pb	293 (Artificially contaminated)		CA: 31 TA: 16	
pH 5.1; CEC:1.6 %; Sand(%): 49; Silt(%):30; Clay(%) 21; OM(%): 5.4	Pb	2797	0.03-0.16 mol l-1 S/L=1/25 T=6-9hr	CA: 83 TA: 88	
	Cd	1821		CA: 96 TA: 97	
pH 6.3; CEC:12.2 %; Sand(%): 53; Silt(%):24; Clay(%) 23; OM(%): 7.1	Pb	1036	0.03-0.40 mol l-1 S/L=1/25 T=12-24hr	CA : 80 TA : 87 CA + OA : 70	(Wasay et al., 1998)
	Cd	794		CA : 100 TA : 99.9 CA + OA :82	
	Cu	926		CA : 88 TA : 97 CA + OA : 99.9	
	Zn	1029		CA : 96 TA : 98 CA + OA : 99.9	
pH 7.5-8.4; CEC: 1.2–4.0 meq/100 g; Sand(%): 60;	Cd	7	0.05 mol l-1 S/L=1/10 T=3hr	CA : 40 OA : 9	(Peters, 1999)
	Cr	238		CA : 2 OA : 2	
	Cu	1241		CA : 24 OA : 15	
	Hg	2		CA : 18	

Silt(%):30 ; Clay(%) 10; OM(%): 7.1	Pb	21560		OA : 14 CA : 5 OA : <1	
	Zn	3729		CA : 22 OA : 5	
	As	18		CA : 5 OA : 5	
pH 8; CEC: -; Sand(%): 100; Silt(%):0; Clay(%) 0; OM(%): 0	U	0.006 (Artificially contaminated)	0.01Na Cl + 0.001 mol l-1 S/L=1/5 T=1hr	NaCl + CA : 95	(Kantar and Honeyman, 2006)
pH 6.25; CEC: 12.40 cmol kg −1; Sand(%): 52; Silt(%):8; Clay(%) 40; OM(%): 1.9	Cd	17	0.070 mol l-1 S/L=1/10 T=2hr	CA : 24 EDDS : 24 GLDA : 61	(Wang et al., 2016)
	Pb	1640		CA : 35 EDDS : 44 GLDA : 89	
	Zn	2589		CA : 40 EDDS : 83 GLDA : 38	
pH 7.0; CEC: 18 cmol kg −1; Sand(%): 65; Silt(%):17 ; Clay(%)	Cd	33	0.070 mol l-1 S/L=1/10 T=2hr	CA : 46 EDDS : 43 GLDA : 67	
	Pb	681		CA : 32 EDDS : 72 GLDA : 85	
	Zn	368		CA : 43 EDDS : 34	

18; OM(%): 2.4				GLDA : 40	
pH: 8.5 CEC : 6 (meq/100 g); Sand (%): 19 Silt (%): 47 Clay (%): 34	Cr	769	0.2 $Na_3C_6H_5O_7$ + 0.2 mol l-1 S/L=1/2 T=20hr	CA : 49	(Li et al., 2017)
pH: 8.0 CEC : - Sand (%): 99 Silt (%): <1 Clay (%): <1; TOC 23: g kg-1	As	49	25 %v/v S/L=1/10 T=1hr	LA : 79	(Reynier et al., 2013)
	Cu	80		LA : 74	
	Cr	35		LA : 71	
pH: 7.4 - CEC : - Sand (%): 60; Silt (%): 28; Clay (%): 12; OM (%): 27	Cr	3051	0.8 - 1 mol l-1 S/L=1/10 T=48hr	LA : 85 MA: 67 OA : 74	(Race et al., 2019)
			0.1 mol l-1 S/L=1/10 T=48hr	LA :2 MA : 5 OA : 3 CA : 6	
pH: 5.2 - CEC : 15.82 cmol kg-1; OM (%): 2.9	Cd	27	0.1 mol l-1 S/L=1/25 T=48hr	MA : 53 TA: 33 CA : 69 NTA : 58 EDDS : 44 CTAB: 1	(Xu et al., 2022)
			10 %v/v S/L=1/25	LA :62 GLDA: 14	

			T=48hr		
	Pb	619	0.1 mol l-1 S/L=1/25 T=48hr	MA: 35 TA: 3 CA: 49 NTA: 31 EDDS: 21 CTAB: 1	
			10 %v/v S/L=1/25 T=48hr	LA: 60 GLDA: 4	
	As	290	0.1 mol l-1 S/L=1/25 T=48hr	MA: 7 TA: 7 CA: 10 NTA: 0 EDDS: 10 CTAB: 0	
			10 %v/v S/L=1/25 T=48hr	LA: 17 GLDA: 6	
pH: 6.3 - CEC: 19 cmol kg-1; OC (%): 19	Zn	1037	10 g l-1 S/L=1/10 T=4hr	OA: 59 TA: 57 CA: 54	(Chen et al., 2016)
pH: 7.8 - CEC: 2.8 cmol kg-1; Sand (%): 78; Silt (%): 10; Clay (%): 12; OM (%): 10	Cu	6511	0.10 g l-1 S/L=1/25 T=24-72hr	Surfactin: 17	(Maity et al., 2013)
	Pb	4955		Surfactin: <1	
	Zn	15090		Surfactin: 24	
	Cu	6511	0.015 g l-1 S/L=1/25	Saponin: 36	
	Pb	4955		Saponin: 47	
	Zn	15090		Saponin: 18	

			T=24-72hr		
pH: 6.3; Sand (%): 40; Silt (%): 8; Clay (%): 52; OC (%): 2	Cd	18	0.05mol l-1 S/L=1/10 T=1hr	GLDA: 39 ISA: 12	(Wang et al., 2020)
	Pb	1222		GLDA: 58 ISA: 34	
	Zn	2648		GLDA: 22 ISA: 13	
pH: 7.1; Sand (%): 18; Silt (%): 17; Clay (%): 65; OC (%): 2.4	Cd	43	0.05mol l-1 S/L=1/10 T=1hr	GLDA: 81 ISA: 40	
	Pb	232		GLDA: 79 ISA: 45	
	Zn	1286		GLDA: 64 ISA: 61	
pH: 4.8 - CEC: 13 cmol kg-1; Sand (%): 40; Silt (%): 40; Clay (%): 20; OM (%): 4	Cd	5	0.06mol l-1 S/L=1/2 T=18hr	GLDA: 76 EDDS: 20 IDS: 31	(Gluhar et al., 2020)
	Pb	809		GLDA: 58 EDDS: 7 IDS: 25	
	Zn	448		GLDA: 29 EDDS: 23 IDS: 22	
organic-rich soil reference material BCR 700 from EC-JRCIRMM	Cd	132	0.05mol l-1 S/L=1/10 T=1hr	GLDA: 62 MGDA: 49 EDDS: 36 IDSA: 35	(Begum et al., 2012b)
	Cu	169		GLDA: 44 MGDA: 35 EDDS: 37 IDSA: 36	
	Ni	373		GLDA: 18 MGDA: 13	

				EDDS: 14 IDSA: 14	
	Pb	288		GLDA: 17 MGDA: 10 EDDS: 9 IDSA: 11	
	Zn	1584		GLDA: 32 MGDA: 25 EDDS: 23 IDSA: 23	
smelter site, no other information is available	Cr	1060	0.1 mol l-1 S/L=1/10 T=24hr	AA: <1 TA: 4 CA: 5 MA: 5 OA: 6	(Zou et al., 2019)
	V	2015		AA: 27 TA: 48 CA: 48 MA: 48 OA: 52	
pH: 6.6 - CEC: 11.7 cmol kg-1; Sand (%): 86; Silt (%): 6; Clay (%): 8; OM (%): 0.5	Pb	842	0.5 mol l-1 S/L=1/10 T=1hr	TA: 63	(Moon et al., 2016)
	Cu	438		TA: 42	
	Zn	375		TA: 49	
pH: 7.8 - CEC: 2.4 cmol dm-3; Silt-	As	114 (Artificially contaminated)	2% S/L=1/20 T=48hr	Rhamnolipid: 53	(Dahrazma and Mulligan, 2007)
	Cd	122 (Artificially contaminated)		Rhamnolipid: 90	

loam; C(%): 1.2	Zn	3339 (Artificially contaminated)		Rhamnolipid: 80	
pH: 6.4 - CEC: 14.6 meq per 100g; Sand (%): 15; Silt(%): 65; Clay(%): 20; OM(%): 20	Cu	140	Soil flushing 10g 0.05 ml g-1 min-1	Rhamnolipid: 17	(Lopes et al., 2021)
	Zn	4854		Rhamnolipid: 6	
	Ni	76		Rhamnolipid: 16	
pH: 7.7 - CEC: 73 meq per 100g; Sand (%): 27; Silt(%): 26; Clay(%): 47; C(%): 0.45	Cd	16	Soil flushing 50g 0.2 ml min-1 T: 36	Rhamnolipid: 19	(Juwarkar et al., 2007)
	Pb	19		Rhamnolipid: 8	
pH: 6.3 - CEC: 66 meq per 100g; Sand (%): 30; Silt(%): 28; Clay(%):	Cd	435 (Artificially contaminated)		Rhamnolipid: 91	
	Pb	905 (Artificially contaminated)		Rhamnolipid: 87	

42; C(%): 0.38

1.4.2 Aminopolycarboxylic Acids

Aminopolycarboxylic Acids (AAs) are synthetic chelating substances. AAs can form complexes with very stable and water-soluble PTEs, thus avoiding PTEs precipitation (Lestan et al., 2008). To date, the most used AAs at full scale are scarcely biodegradable (i.e., EDTA) but many scientific studies investigated the possible application of biodegradable AAs in the remediation of contaminated sites. The removal mechanisms of PTEs from soils are similar to those discussed for LMWOAs. Compared to a LMWOA washing, the removal efficiencies achievable in the AAs washing at same reagent concentration are higher due to the high stability constants values of the formed complexes (Tab. 1.1) (Xu et al., 2022). However, unlike LMWOAs, the pH variation plays a minor role with AAs since no soil pH alteration are significantly observed. In general, the efficiency of AAs washing is affected by: i) physicochemical characteristics of the soil, ii) process parameters, and iii) characteristics of PTEs contamination.

Despite the very high removal efficiencies which can be generally achieved with AAs, selection of the most suitable reagent is done by evaluating the stability constants of the complexes that they could form from the interaction with the target PTE (Bari et al., 2022; Tsang and Hartley, 2014).

After the AAs washing, possible consequences observable in the treated soil are: i) removal of some nutritional elements (i.e., Ca and Mg) in addition to the PTEs and ii) partial adsorption of the formed PTEs-AAs on the soil particles. The AAs biodegradability after the complex formation with the PTE as well as the toxicity of biodegradable PTEs-AAs complexes are not thoroughly reported in scientific literature. Nonetheless, an exemplifying study showed the reduction of both overall biodegradability and biodegradation rate of EDDS after complexation with Cu (Vandevivere et al., 2001).

1.4.3 Biosurfactant

According to their definition, surfactants are a mixture of surface active agents created by Antara products in 1950. Surfactants are usually amphiphilic organic compounds (they contain both hydrophobic and hydrophilic groups). Therefore, surfactants are soluble in both organic solvents and water (Jene et al., 1997). Surfactants reduce the surface tension of water by adsorbing at the liquid-gas interface, and reduce the interfacial tension between oil and water by adsorbing at the liquid-

liquid interface. Surfactants can be either anionic or cationic and both are successfully used to remediate sites contaminated by PTEs (Jiménez-Castañeda and Medina, 2017). Usually, anionic surfactants are preferred to the cationic ones because they are more soluble in water and form complexes with positively charged PTEs (i.e., Cd, Pb, Cu, etc.). Instead, the remediation of soils with PTEs in oxyanions form (i.e., Cr and As) requires cationic surfactants. Surfactants are generally produced through chemical processes. However, in recent years, research has increasingly moved toward the BSs production. These are generated by microorganisms, animals, or plants (i.e., rhamnolipids can come from Pseudomonas aeruginosa) (Zheng et al., 2022).

The most common BSs used to remediate contaminant sites are rhamnolipids (glycolipids) and saponin. Rhamnolipids reduces the solution's surface tension and are characterized by the presence of carboxyl groups that complex the PTEs with stability constants greater than those between PTEs and soil particles. Tab. 1.2 shows the results obtained by using rhamnolipids highlighting the achievement of very high removal efficiencies (about 90%). Moreover, with the use of rhamnolipids, no alterations of the treated soils characteristics (i.e., pH variations) are observed. On the contrary, an increase in the microbial population was reported (Juwarkar et al., 2007). Accounting for the PTEs removal based on their bioavailability in soil, Lopes et al. (2021) observed As, Cd, and Zn solubilization from both exchangeable and carbonate-bound fractions.

Another BS widely used in the soil remediation treatment is saponin, which can display PTEs removal efficiencies comparable to rhamnolipids. In general, BSs have a high biodegradability. However, when BSs are complexed to PTEs are more slowly biodegradable than CA (Wen et al., 2009).

1.5 Conclusions and future perspectives

The remediation of contaminated sites is a relevant topic and its significance is constantly increasing: the fertile soil resource is becoming rare and proper agricultural soils preservation/reclamation strategies are nowadays required. Remediation treatments can be useful for PTEs removal, but at the same time, can reduce the soil fertility up to the occurrence of very adverse environmental conditions. The use of LMWOAs, AAs, and BSs could represent a feasible approach because of the high extraction rates achievable, compared to inorganic acids, and the lack of soil characteristics alteration if properly used.

However, further studies are needed to evaluate their applicability at full-scale and to evaluate any long-term ecotoxicity effects as well. In this perspective, it also worth noticing that laboratory scale tests can still represent a fundamental source for preliminary identification of optimal washing reagent and operating conditions to perform an efficient and environmentally sustainable soil washing process.

1.6 References

Abdelgawad, K.Z., Mahmoud, M., Elkatatny, S., Abdulraheem, A., Patil, S., 2019. Reaction kinetics and coreflooding study of high-temperature carbonate reservoir stimulation using GLDA in seawater. Energies 12, 3407.

Abrahams, P.W., Thornton, I., 1994. The contamination of agricultural land in the metalliferous province of southwest England: implications to livestock. Agric. Ecosyst. Environ. 48, 125–137.

Adeleke, R., Nwangburuka, C., Oboirien, B., 2017. Origins, roles and fate of organic acids in soils: A review. South African J. Bot. 108, 393–406.

Ash, C., Tejnecký, V., Borůvka, L., Drábek, O., 2016. Different low-molecular-mass organic acids specifically control leaching of arsenic and lead from contaminated soil. J. Contam. Hydrol. 187, 18–30.

Atteia, O., Del Campo Estrada, E., Bertin, H., 2013. Soil flushing: a review of the origin of efficiency variability. Rev. Environ. Sci. Bio/Technology 12, 379–389.

Bari, A.S.M.F., Lamb, D., MacFarlane, G.R., Rahman, M.M., 2022. Soil washing of arsenic from mixed contaminated abandoned mine soils and fate of arsenic after washing. Chemosphere 296, 134053.

Begum, Z.A., Rahman, I.M.M., Sawai, H., Tate, Y., Maki, T., Hasegawa, H., 2012a. Stability constants of Fe (III) and Cr (III) complexes with dl-2-(2-carboxymethyl) nitrilotriacetic acid (GLDA) and 3-hydroxy-2, 2′-iminodisuccinic acid (HIDS) in

aqueous solution. J. Chem. Eng. Data 57, 2723–2732.

Begum, Z.A., Rahman, I.M.M., Tate, Y., Sawai, H., Maki, T., Hasegawa, H., 2012b. Remediation of toxic metal contaminated soil by washing with biodegradable aminopolycarboxylate chelants. Chemosphere 87, 1161–1170.

Bucheli-Witschel, M., Egli, T., 2001. Environmental fate and microbial degradation of aminopolycarboxylic acids. FEMS Microbiol. Rev. 25, 69–106.

Bunting, J.W., Thong, K.M., 1970. Stability constants for some 1: 1 metal–carboxylate complexes. Can. J. Chem. 48, 1654–1656.

Chen, Y., Zhang, S., Xu, X., Yao, P., Li, T., Wang, G., Gong, G., Li, Y., Deng, O., 2016. Effects of surfactants on low-molecular-weight organic acids to wash soil zinc. Environ. Sci. Pollut. Res. 23, 4629–4638.

Clayton, G.D., Clayton, F.E., 1981. Patty's industrial hygiene and toxicology. Vol. 2A. Toxicology. John Wiley & Sons, Inc., Baffins Lane, Chichester, Sussex PO19 1DU.

Dahlin, S., Witter, E., Mårtensson, A., Turner, A., Bååth, E., 1997. Where's the limit? Changes in the microbiological properties of agricultural soils at low levels of metal contamination. Soil Biol. Biochem. 29, 1405–1415.

Dahrazma, B., Mulligan, C.N., 2007. Investigation of the removal of heavy metals from sediments using rhamnolipid in a continuous flow configuration. Chemosphere 69, 705–711.

Dermont, G., Bergeron, M., Mercier, G., Richer-Laflèche, M., 2008. Soil washing for metal removal: a review of physical/chemical technologies and field applications. J. Hazard. Mater. 152, 1–31. https://doi.org/10.1016/j.jhazmat.2007.10.043

Ding, Q., Wu, H.L., Xu, Y., Guo, L.J., Liu, K., Gao, H.M., Yang, H., 2011. Impact of low molecular weight organic acids and dissolved organic matter on sorption and mobility of isoproturon in two soils. J. Hazard. Mater. 190, 823–832.

EEA, E.E.A., 2020. Soil Contamination Widespread in Europe.

Fabbricino, M., Ferraro, A., Del Giudice, G., D'Antonio, L., 2013. Current views on EDDS use for ex situ washing of potentially toxic metal contaminated soils. Rev. Environ. Sci. Bio/Technology Volume 12, pp 391-398.

FEEDAP, E.P. on A. and P. or S. used in A.F., Rychen, G., Aquilina, G., Azimonti, G., Bampidis, V., Bastos, M. de L., Bories, G., Chesson, A., Cocconcelli, P.S., Flachowsky, G., 2018. Safety and efficacy of Kelforce®(l-glutamic acid, N, N-diacetic acid, tetrasodium salt (GLDA-Na4)) as a feed additive for chickens for fattening. EFSA J. 16, e05279.

Ferraro, A., Fabbricino, M., van Hullebusch, E.D., Esposito, G., Pirozzi, F., 2016. Effect of soil/contamination characteristics and process operational conditions on aminopolycarboxylates enhanced soil washing for heavy metals removal: a review. Rev. Environ. Sci. Bio/technology 15, 111–145.

Ferraro, A., Parisi, A., Barbone, E., Race, M., Mali, M., Spasiano, D., Fratino, U., 2023. Characterising contaminants distribution in marine-coastal sediments through multivariate and nonparametric statistical analyses: a complementary strategy supporting environmental monitoring and control. Environ. Monit. Assess. 195, 1–19.

Francis, A.J., Dodge, C.J., Gillow, J.B., 1992. Biodegradation of metal citrate complexes and implications for toxic-metal mobility. Nature 356, 140–142.

Gabriele, I., Race, M., Papirio, S., Papetti, P., Esposito, G., 2022. Phytoremediation of a pyrene-contaminated soil by Cannabis sativa L. at different initial pyrene concentrations. Chemosphere 300, 134578.

Gluhar, S., Kaurin, A., Lestan, D., 2020. Soil washing with biodegradable chelating agents and EDTA: Technological feasibility, remediation efficiency and environmental sustainability. Chemosphere 257, 127226.

Goovaerts, P., 1997. Geostatistics for natural resources evaluation. Oxford university press.

Griffiths, R.A., 1995. Soil-washing technology and practice. J. Hazard. Mater. 40, 175–189.

Gusiatin, Z.M., Kulikowska, D., Klik, B., 2020. New-generation washing agents in remediation of metal-polluted soils and methods for washing effluent treatment: A review. Int. J. Environ. Res. Public Health 17, 6220.

Gzar, H.A., Abdul-Hameed, A.S., Al-Taie, A., 2014. Extraction of lead, cadmium and nickel from contaminated soil using acetic acid. Open J. soil Sci. 4, 207–214.

Hamada, Y.Z., Carlson, B., Dangberg, J., 2005. Interaction of malate and lactate with chromium (III) and iron (III) in aqueous solutions. Synth. React. Inorg. Met. Chem. 35, 515–522.

Jene, Q., Pearson, J.C., Lowe, C.R., 1997. Surfactant modified enzymes: solubility and activity of surfactant-modified catalase in organic solvents. Enzyme Microb. Technol. 20, 69–74.

Jiménez-Castañeda, M.E., Medina, D.I., 2017. Use of surfactant-modified zeolites and clays for the removal of heavy metals from water. Water 9, 235.

Juwarkar, A.A., Nair, A., Dubey, K. V, Singh, S.K., Devotta, S., 2007. Biosurfactant technology for remediation of cadmium and lead contaminated soils. Chemosphere 68, 1996–2002.

Kantar, C., Honeyman, B.D., 2006. Citric acid enhanced remediation of soils contaminated with uranium by soil flushing and soil washing. J. Environ. Eng. 132, 247–255.

Khan, S.H., Iqbal, J., 2016. Recent advances in the role of organic acids in poultry nutrition. J. Appl. Anim. Res. 44, 359–369.

Kim, J.-O., Lee, Y.-W., Chung, J., 2013. The role of organic acids in the mobilization of heavy metals from soil. KSCE J. Civ. Eng. 17, 1596–1602.

Kołodyńska, D., 2011. Chelating agents of a new generation as an alternative to conventional chelators for heavy metal ions removal from different waste waters. Expand. issues Desalin. 339–370.

Lestan, D., Luo, C., Li, X., 2008. The use of chelating agents in the remediation of metal-contaminated soils: a review. Environ. Pollut. 153, 3–13. https://doi.org/10.1016/j.envpol.2007.11.015

Li, C., Wang, H., Liao, X., Xiao, R., Liu, K., Bai, J., Li, B., He, Q., 2022. Heavy metal pollution in coastal wetlands: A systematic review of studies globally over the past three decades. J. Hazard. Mater. 424, 127312.

Li, G., Yang, X., Liang, L., Guo, S., 2017. Evaluation of the potential redistribution of chromium fractionation in contaminated soil by citric acid/sodium citrate washing. Arab. J. Chem. 10, S539–S545.

Liu, J., Zhao, L., Liu, Q., Li, J., Qiao, Z., Sun, P., Yang, Y., 2021. A critical review on

soil washing during soil remediation for heavy metals and organic pollutants. Int. J. Environ. Sci. Technol. 1–24.

Lopes, C.S.C., Teixeira, D.B., Braz, B.F., Santelli, R.E., de Castilho, L.V.A., Gomez, J.G.C., PV Castro, R., Seldin, L., Freire, D.M.G., 2021. Application of rhamnolipid surfactant for remediation of toxic metals of long-and short-term contamination sites. Int. J. Environ. Sci. Technol. 18, 575–588.

Maity, J.P., Huang, Y.M., Hsu, C.-M., Wu, C.-I., Chen, C.-C., Li, C.-Y., Jean, J.-S., Chang, Y.-F., Chen, C.-Y., 2013. Removal of Cu, Pb and Zn by foam fractionation and a soil washing process from contaminated industrial soils using soapberry-derived saponin: a comparative effectiveness assessment. Chemosphere 92, 1286–1293.

Martel, R., Gélinas, P.J., Saumure, L., 1998. Aquifer washing by micellar solutions:: 3 Field test at the Thouin Sand Pit (L'Assomption, Quebec, Canada). J. Contam. Hydrol. 30, 33–48.

Merck Index, M., 1996. 7943 and 9877, Merck & Co.

Mertens, M., Höss, S., Neumann, G., Afzal, J., Reichenbecher, W., 2018. Glyphosate, a chelating agent—relevant for ecological risk assessment? Environ. Sci. Pollut. Res. 25, 5298–5317.

Mo, A., Wang, Y., Liu, Y., Zhou, W., Zhou, Q., Yasin, A., Yang, H., 2018. Enhanced viscosity of poly (acrylamide) solution in the presence of chromium citrate triggered by release of CO2. Chinese J. Chem. Phys. 31, 117–122.

Moon, D.H., Park, J.-W., Koutsospyros, A., Cheong, K.H., Chang, Y.-Y., Baek, K., Jo, R., Park, J.-H., 2016. Assessment of soil washing for simultaneous removal

of heavy metals and low-level petroleum hydrocarbons using various washing solutions. Environ. Earth Sci. 75, 1–8.

Murtaza, G., Shehzad, M.T., Kanwal, S., Farooqi, Z.U.R., Owens, G., 2022. Biomagnification of potentially toxic elements in animals consuming fodder irrigated with sewage water. Environ. Geochem. Health 44, 4523–4538.

Nowak, G., Nowak, J., 1990. Turnover of 14 C-labelled oat residues and small molecular organic compounds in two soils under different levels of mineral nutrition. Plant Soil 122, 67–77.

Orama, M., Hyvönen, H., Saarinen, H., Aksela, R., 2002. Complexation of [S, S] and mixed stereoisomers of N, N′-ethylenediaminedisuccinic acid (EDDS) with Fe (III), Cu (II), Zn (II) and Mn (II) ions in aqueous solution. J. Chem. Soc. Dalt. Trans. 4644–4648.

Ostroushko, A.A., Russkikh, O.V., 2017. Oxide material synthesis by combustion of organicinorganic compositions. Наносистемы: физика, химия, математика 8, 476–502.

Papagianni, M., 2011. 1.09 - Organic Acids, in: Moo-Young, M.B.T.-C.B. (Second E. (Ed.), . Academic Press, Burlington, pp. 109–120. https://doi.org/https://doi.org/10.1016/B978-0-08-088504-9.00011-8

Paria, S., 2008. Surfactant-enhanced remediation of organic contaminated soil and water. Adv. Colloid Interface Sci. 138, 24–58.

Peters, R.W., 1999. Chelant extraction of heavy metals from contaminated soils. J. Hazard. Mater. 66, 151–210.

Portanova, R., Lajunen, L.H.J., Tolazzi, M., Piispanen, J., 2003. Critical evaluation of

stability constants for alpha-hydroxycarboxylic acid complexes with protons and metal ions and the accompanying enthalpy changes. Part II. Aliphatic 2-hydroxycarboxylic acids (IUPAC Technical Report). Pure Appl. Chem. 75, 495–540.

Race, M., Marotta, R., Fabbricino, M., Pirozzi, F., Andreozzi, R., Guida, M., Siciliano, A., 2019. Assessment of optimal conditions for the restoration and recovery of agricultural soil. J. Hazard. Mater. 373, 801–809. https://doi.org/https://doi.org/10.1016/j.jhazmat.2019.04.007

Renella, G., Landi, L., Nannipieri, P., 2004. Degradation of low molecular weight organic acids complexed with heavy metals in soil. Geoderma 122, 311–315.

Reyes, A., Cuevas, J., Fuentes, B., Fernández, E., Arce, W., Guerrero, M., Letelier, M.V., 2021. Distribution of potentially toxic elements in soils surrounding abandoned mining waste located in Taltal, Northern Chile. J. Geochemical Explor. 220, 106653.

Reynier, N., Blais, J.-F., Mercier, G., Besner, S., 2013. Treatment of arsenic-, chromium-, copper-and pentachlorophenol-polluted soil using flotation. Water, Air, Soil Pollut. 224, 1514.

Serjeant, E.P., Dempsey, B., 1979. Ionisation constants of organic acids in aqueous solution. IUPAC Chem. data Ser. 23, 160–190.

Sillanpää, M., Oikari, A., 1996. Assessing the impact of complexation by EDTA and DTPA on heavy metal toxicity using microtox bioassay. Chemosphere 32, 1485–1497.

Sun, B., Zhao, F.J., Lombi, E., McGrath, S.P., 2001. Leaching of heavy metals from

contaminated soils using EDTA. Environ. Pollut. 113, 111–120.

Tarvainen, T., Reyes, A., Sapon, S., 2020. Acceptable soil baseline levels in Taltal, Chile, and in Tampere, Finland. Appl. Geochemistry 123, 104813.

Tsang, D.C.W., Hartley, N.R., 2014. Metal distribution and spectroscopic analysis after soil washing with chelating agents and humic substances. Environ. Sci. Pollut. Res. 21, 3987–3995.

USDA, 2010. Technical Evaluation Report. Tech. Eval. Rep. (S, S)-Ethylenediaminedisuccinic Acid (free acid) Crop Prod.

Vandevivere, P.C., Saveyn, H., Verstraete, W., Feijtel, T.C.J., Schowanek, D.R., 2001. Biodegradation of metal−[S, S]-EDDS complexes. Environ. Sci. Technol. 35, 1765–1770.

Vinokurov, E.G., Bondar', V. V, 2003. Prediction of stability constants for Cr (III) and Cr (II) complexes. Russ. J. Coord. Chem. 29, 66–72.

Wang, G., Pan, X., Zhang, S., Zhong, Q., Zhou, W., Zhang, X., Wu, J., Vijver, M.G., Peijnenburg, W.J.G.M., 2020. Remediation of heavy metal contaminated soil by biodegradable chelator–induced washing: Efficiencies and mechanisms. Environ. Res. 186, 109554.

Wang, G., Zhang, S., Xu, X., Zhong, Q., Zhang, C., Jia, Y., Li, T., Deng, O., Li, Y., 2016. Heavy metal removal by GLDA washing: Optimization, redistribution, recycling, and changes in soil fertility. Sci. Total Environ. 569–570, 557–568. https://doi.org/10.1016/J.SCITOTENV.2016.06.155

Wasay, S.A., Barrington, S.F., Tokunaga, S., 1998. Remediation of soils polluted by heavy metals using salts of organic acids and chelating agents. Environ. Technol.

19, 369–379.

Wen, J., Stacey, S.P., McLaughlin, M.J., Kirby, J.K., 2009. Biodegradation of rhamnolipid, EDTA and citric acid in cadmium and zinc contaminated soils. Soil Biol. Biochem. 41, 2214–2221.

Wuana, R.A., Okieimen, F.E., Imborvungu, J.A., 2010. Removal of heavy metals from a contaminated soil using organic chelating acids. Int. J. Environ. Sci. Technol. 7, 485–496.

Xu, L., Dai, H., Skuza, L., Xu, J., Shi, J., Wei, S., 2022. Co-high-efficiency washing agents for simultaneous removal of Cd, Pb and As from smelting soil with risk assessment. Chemosphere 300, 134581.

Yao, W., Huang, L., Yang, Z., Zhao, F., 2022. Effects of organic acids on heavy metal release or immobilization in contaminated soil. Trans. Nonferrous Met. Soc. China 32, 1277–1289.

Zhang, H., Xu, Y., Kanyerere, T., Wang, Y., Sun, M., 2022. Washing Reagents for Remediating Heavy-Metal-Contaminated Soil: A Review . Front. Earth Sci. .

Zheng, X.-J., Li, Q., Peng, H., Zhang, J.-X., Chen, W.-J., Zhou, B.-C., Chen, M., 2022. Remediation of heavy metal-contaminated soils with soil washing: a review. Sustainability 14, 13058.

Zou, Q., Gao, Y., Yi, S., Jiang, J., Aihemaiti, A., Li, D., Yang, M., 2019. Multi-step column leaching using low-molecular-weight organic acids for remediating vanadium- and chromium-contaminated soil. Environ. Sci. Pollut. Res. 26, 15406–15413.

CHAPTER 2. REUSE OF POLYMERIC WASTE FOR THE TREATMENT OF MARINE WATER POLLUTED BY DIESEL

2.1 Introduction

The contamination of seawater by the oil spill is an environmental issue mainly due to petroleum extraction, transportation and refining processes, which are still essential to tackle non–renewable energy demand and for chemical and synthetic polymer manufacturing (Ben Jmaa and Kallel, 2019; Diraki et al., 2019). Indeed, millions of tons of crude oil are shipped offshore yearly, which poses a risk to the aquatic environment due to the accidental release of toxic and carcinogenic compounds (e.g., n–alkanes, aromatic hydrocarbons) (Bao et al., 2012; Gurav et al., 2021). These accidents are of particular interest also for harbor areas where boats are involved in human activities such as trade and fishery (Grant et al., 2021). For instance, approximately 180000 L of diesel were spilled in the Skjervøy harbor (Norway) in 2013 (Breitwieser et al., 2018). Therefore, since the released organic pollutants are particularly recalcitrant to natural attenuation, a remediation technique is needed to alleviate the seawater contamination (Louati et al., 2014).

Among the remediation techniques, the employment of waste–derived adsorbents (e.g., biochar) can represent a sustainable, effective, and affordable solution to treat oil–polluted seawater (Hossain et al., 2019; Lee et al., 2022; Yang et al., 2021). An ideal adsorbent should be generally characterized by a great surface area, low toxicity, high recoverability, cost–effectiveness, and quick availability at a large scale (Ge et al., 2016; Oliveira et al., 2021). In addition, the used adsorbent should be also hydrophobic and oleophilic to avoid sinking phenomena and efficiently remove oil floating on the seawater surface (Saharan et al., 2022; Sidik et al., 2012). Therefore, modification procedures employing chemicals (e.g., ethanol, organic acids) have been proposed for treating the adsorbent surface (Gurav et al., 2021; Sun et al., 2022). Notwithstanding, the adsorbent further requires nanoparticle addition (e.g., magnetic

biochar) to be easily recovered, and this operation can be costly and lead to a decrease of the adsorption capacity (Bianco et al., 2023). Thus, adsorbents deriving from polymer waste (e.g., polypropylene, polyethylene) can represent a suitable solution, since polymeric adsorbents are known to be effective for oil remediation but their application is still limited due to high costs (Oliveira et al., 2021).

The previous COVID–19 pandemic led to extensive use of disposable face masks (e.g., surgical masks, KN95), especially in hospital facilities, which practice is still in use to contain the spread of viruses and bacteria through aerosols and droplets (Tang et al., 2021). The latest SARS–CoV–2 BA.2.86 variant (Uriu et al., 2023), as well as a possible future pandemic, can cause an increase of face masks discarded weekly (i.e., above 5 billion during COVID–19) that should be incinerated or landfilled by adding further pressure on the waste management system (Jung et al., 2021; Selvaranjan et al., 2021). Also, improper management practices can pose risks to the environment and human health due to the release of greenhouse gases, pathogenic agents and pollutants (Bianco et al., 2022b; Kathambi and Obiero, 2022). Therefore, more effort is required to find a sustainable approach that can provide valorization through the employment of these polymeric wastes for more virtuous applications rather than their reuse after sterilization (e.g., with UV lights) (Weaver et al., 2021).

Indeed, medical face masks are constituted of polymers such as polypropylene and polyethylene (Jung et al., 2021), which make this waste a suitable candidate for organic pollutant removal (Huang et al., 2021). So far, MAF6–coated polypropylene waste and heptane–treated KN94 mask have been proposed to remove various organic pollutants (e.g., crude oil, chloroform, toluene) from fresh water (Guselnikova et al., 2022; Park et al., 2022). However, the potential release of microplastics due to the preliminary cutting procedure used to reduce the size of polypropylene waste (e.g., 2 x 2 cm) was not considered (Shen et al., 2021). This issue can be avoided using an intact laceless mask, which to our best knowledge, was examined only for the treatment of dye–polluted distilled water (Anastopoulos and Pashalidis, 2021) and therefore requires further investigation for oil adsorption.

Thus, in this thesis, the employment of the laceless surgical mask aimed at diesel oil removal from polluted seawater has been proposed for the first time. For this purpose, adsorption–desorption experiments have been conducted in batch mode by varying the adsorbent type (i.e., new and used masks), background solution (i.e., distilled and seawater), adsorption time and diesel concentration. The obtained experimental points have been fitted with the most common kinetic and isotherm models to clarify the involved adsorption mechanisms. In addition, the effect of

operating parameters on diesel adsorption, i.e., ionic strength, pH, and adsorption temperature, has been examined. Finally, the regeneration of the proposed adsorbent has been considered.

2.2 Materials and methods

2.2.1 Diesel fuel, seawater and the surgical mask

Diesel oil and seawater were obtained from a fuel station located in Cassino (Italy) and the seaside of Scauri (Italy), respectively, then placed in sealed glass vessels before being transferred to the laboratory and finally stored at 277.15 K for further use. Medical face masks were provided by Jiangxi Golden Land Biotechnology Co., Ltd (China) and worn by laboratory users for at least 4 hours when scheduled. Afterwards, the used masks were sterilized in a biological safety cabinet (Clean Air Techniek B.V., The Netherlands) under UV lights for 15 min per side (Weaver et al., 2021) prior to the experiments.

2.2.2 Adsorption–desorption experiments

Batch adsorption–desorption experiments were performed in 250 mL glass jars (Sun et al., 2022) by introducing a non−worn laceless mask (approximately 2.6 ± 1 g) with either 200 mL of diesel−containing distilled water (NMDW) or seawater (NMSW). Prior to mask addition, diesel was placed into water solutions to achieve an initial concentration (C_i) of approximately 5 – 120 g/L since these values were detected in seawater polluted by diesel spills (Gurav et al., 2021). The glass jars were subsequently sealed and placed at 293.15 K till reaching equilibrium before evaluating adsorption isotherms. The experiments were also conducted in seawater by employing used masks (UMDW) to validate the previous results. In addition, adsorption kinetics were examined at a C_i of 5 g/L by sacrificing a jar after 1, 5, 10, 20, 30, 45, 60, 90 and 120 min. After the adsorption tests, the surgical masks were removed from each jar and immediately used for desorption experiments by the established single−step decant–refill batch reactor procedure (Bianco et al., 2022a). All the adsorption−desorption curves were modeled via the kinetic and isotherm models (Al-Ghouti and Da'ana, 2020; Wang and Guo, 2020). The abovementioned adsorption–desorption tests were performed in triplicate using the intrinsic pH (i.e., about 5.5).

2.2.3 The effect of ionic strength, pH and temperature

The effect of initial ionic strength, pH and adsorption−desorption temperature on diesel removal from spiked water was examined. Prior to adsorption experiments, the

ionic strength of the solution phase was modified in the range of 0.04 – 1.37 M with different amounts of NaCl (Wu et al., 2015) by maintaining a constant pH of 5.5. Regarding the experiments at different pH values, diesel–containing solutions were adjusted to a pH of 1, 3, 5, 7, 9, 11, and 13 by adding either 1 M of NaOH or HCl drop–by–drop (Liu et al., 2020). For the thermodynamic study, the vessels were positioned in a controlled temperature chamber at several temperatures (i.e., 281.15, 293.15, 303.15 and 313.15 K) and the free energy of Gibbs (ΔG) was evaluated through temperature–dependent isotherms (Al-Ghouti and Da'ana, 2020). All the mentioned tests were performed in triplicate.

2.2.4 Reusability experiments

The possibility to reuse the adsorbents for further adsorption cycles was evaluated. After the adsorption tests, the adsorbents were regenerated with hexane, as previously described by Gurav et al. (2021). In brief, the adsorbents were removed from the glass jars, manually squeezed and subsequently placed in an n–hexane bath for 5 h to extract the adsorbed diesel. Afterwards, the treated adsorbents were dried overnight and finally employed for a subsequent adsorption cycle. This procedure was repeated for 5 consecutive adsorption–desorption cycles in order to assess any decrease in the removal efficiency (Golnari et al., 2022).

2.2.5 Analytical methods

The residual total diesel content in the aqueous samples was determined based on the Beer–Lambert law by using an 8453 UV–visible spectrophotometer (Agilent, USA) set at 303 nm according to the procedure reported elsewhere (Diraki et al., 2019; Jin et al., 2020). The concentration of dissolved diesel oil in water was assessed via a total organic carbon (TOC)–L Series (Shimadzu, Japan) analyzer (Diraki et al., 2019).

2.3 Results and discussion

2.3.1 Use of the surgical mask for diesel adsorption

The removal efficiencies of total diesel in NMDW, NMSW, and UMSW after 120 min are presented in Fig. 2.1a. Complete removal of total diesel from aqueous solutions was achieved for C_i up to 20 g/L (Fig. 2.1a), and the removal efficiency was not significantly different ($p > 0.05$) among the tested conditions. The mentioned diesel removal was higher than those shown by using microplastic waste for crude oil adsorption (i.e., up to 68%) (Martins et al., 2021). This is most likely due to the porous structure of polyethylene in disposable masks and its hydrogen bonding ability which can improve organic contaminant adsorption (Yu et al., 2020). Also, the calculated solid–water distribution coefficients (K_{dc}) of about 168 – 301 L/kg confirm a similar affinity between the adsorbate and adsorbent in NMDW, NMSW and UMSW (Hörsing et al., 2011).

The dissolved diesel removal (i.e., above 93%, Fig. 2.1b) was not significantly different ($p > 0.05$) among the investigated C_i suggesting that the soluble fraction of diesel was firstly adsorbed onto mask layers. This can be attributed to a low wettability of the adsorbent (data not shown) that forced the migration of the dissolved diesel towards the non–woven layer (Zhou et al., 2016) of the mask by repelling water. Similarly, Mitra et al. (2021) recently reported an oil removal of approximately 79 – 99% in oil–in–water emulsions using waste–derived polyethylene as an adsorbent.

Therefore, the adsorption capacity (Q_e) here achieved was up to approximately 3.43 g/g (Fig. 2.2b), which can be compared to those shown by other waste–derived adsorbents (e.g., biochar, polyethylene granules) when employed for oil adsorption (i.e., 1.73 – 4.50 g/g) (Gurav et al., 2021; Martins et al., 2021; Shojaei et al., 2021). This would indicate a great hydrophobicity and lipophilicity of the surgical mask towards diesel adsorption, as also suggested by the WCA (i.e., about 141°, data not shown) (Navarathna et al., 2020). This is further corroborated by the low adsorption capacity (i.e., only up to 153 mg/kg) of the intact surgical mask aimed at hydrophilic dye removal such as malachite green (Anastopoulos and Pashalidis, 2021). However, the Q_e in UMSW was slightly lower ($p > 0.05$) than that obtained in NMDW and NMSW since worn masks likely contained particles due to air filtration (Mueller et al., 2020). Also, the WCA of the used surgical mask was approximately 122° (data not shown), which was slightly lower compared to that shown by the non–worn disposable mask (i.e., 141°, data not shown). In this case, the mask can be chemically treated to

enhance the adsorption capacity 1.31–fold, as recently shown by Park et al. (2022) using KF94 masks.

These results suggest that the surgical mask represents a suitable adsorbent for removing diesel in both fresh water and seawater and can also be employed for this purpose after being worn.

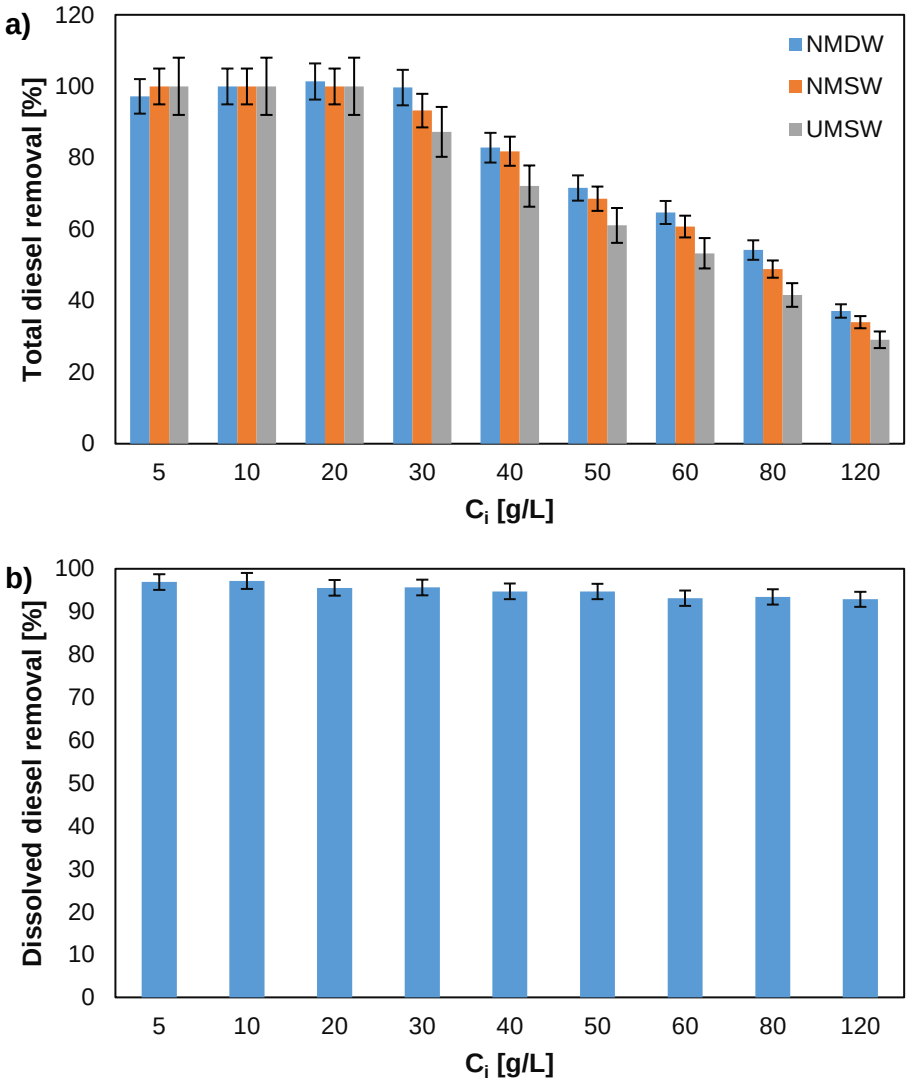


Figure 2.1 – The effect of initial diesel concentration (Ci, g/L) on total and dissolved diesel removal (%) using non–worn masks in distilled water (NMDW) after 120 min of adsorption experiments.

The averages and standard deviations are based on triplicates.

2.3.2 Adsorption–desorption mechanism

2.3.2.1 Kinetic study

The diesel adsorption curve in the presence of the surgical mask is illustrated in Fig. 2.2a. The diesel showed fast two−stage adsorption kinetic onto the surgical mask, which removed approximately 50% of the pollutant from the aqueous solution after only 1 min until reaching the plateau and a complete diesel removal after 120 min (Fig. 2.2a). Therefore, diesel was probably attracted onto the available sites of the surgical mask (i), and after the boundary layer diffusion (ii), a slower intraparticle diffusion (iii) likely took place (Bianco et al., 2022a). The phase (i) is too rapid to be the rate−limiting step, which can be instead represented by both the stages (ii) and (iii). Therefore, to better understand the adsorption mechanism that occurred during the shift of diesel fuel from the water to the surgical mask, the most used kinetics (see Section S1) were employed to fit the experimental data (Fig. 2.2a and Tab. 2.1). The Weber and Morris's intraparticle diffusion model slightly deviated from the origin due to a kinetic constant (C) of 0.169 g/g (Tab. 2.1), suggesting that the adsorption mechanism was likely controlled by both boundary layer and intraparticle diffusion (Zheng et al., 2018), as also reported by Jiang et al. (2016) using biochar for diesel adsorption. Also, the obtained determination coefficient (R^2) was higher for the intraparticle diffusion model (i.e., 0.876, Tab. 2.1) compared to that shown by the Elovich model (i.e., 0.680, Tab. 2.1) by indicating the absence of various activation energies (Alkan et al., 2008).

2.3.2.2 Adsorption isotherms

The adsorption equilibrium isotherms of diesel fuel in NMDW, NMSW and NMSW are presented in Fig. 2.2b. The adsorption (Q_e) improved with the increase of adsorbate concentration at the equilibrium (C_e), and the shape of the adsorption isotherms was similar between the experimental conditions, indicating that a similar adsorption interaction was involved (Krasucka et al., 2022). Therefore, Freundlich and Temkin isotherm models (Section S1) were used to fit the experimental data and further clarify the adsorption mechanism that occurred between diesel and the surgical mask. The Temkin isotherm can be employed to generally predict the diesel adsorption in NMSW and UMSW due to a greater R^2 of 0.986 and 0.996 (Fig. 2.2b and Tab. 2.2), respectively, compared to the Freundlich model, which instead showed a similar determination coefficient in NMDW (Tab. 2.2). The Temkin isotherm model considers that the adsorption heats (Tab. 2.2) of all molecules coating the layer is affected by the temperature and declines linearly instead of logarithmically due to the increase of

surface coverage (Al-Ghouti and Da'ana, 2020), as also suggested by the Freundlich equation in NMDW (Tab. 2.2) (Inam et al., 2017). This model also implies that the binding energies are homogeneous up to a certain value (Tab. 2.2) (Senthil Kumar et al., 2010). The Temkin isotherm also described the occurrence of chemisorption with the increase of C_e as suggested by the linear form (R^2 = 0.952 – 0.997) of the Temkin plot (data not shown) (Al-Ghouti and Da'ana, 2020). In this study, the C–H stretching and CH_2 wagging vibrations generally present at a transmittance of 2840 – 2950 and 2800 – 3000 1/cm in surgical masks due to polyethylene and polypropylene (Erjavec et al., 2022), respectively, could have enhanced the adsorption interactions at this stage. This adsorption mechanism was also reported in other studies investigating diesel adsorption (Ali et al., 2021; Inam et al., 2017; Vannarath and Thalla, 2021).

Table 2.1 – Elovich and Intraparticle Diffusion kinetic models of diesel adsorption (Qt) onto surgical masks in aqueous solution (i.e., initial concentration of 5 g/L) after 120 min. Kid and α are the adsorption rate constants, and β and C represent the model constants.

Kinetics	Equations	Parameters	NMDW
Elovich	$q_t = \frac{1}{\beta} ln(\alpha\beta) + \frac{1}{\beta} ln(t)$	α [g/g/min]	2.686
		β [g/g]	25.990
		R^2	0.680
Intraparticle diffusion	$q_t = K_{id} t^{\frac{1}{2}} + C$	K_{id} [g/g/min$^{1/2}$]	0.020
		C [g/g]	0.169
		R^2	0.876

Table 2.2 – Freundlich, Temkin and Langmuir equilibrium isotherms of diesel adsorption–desorption onto surgical masks in water solutions at different diesel equilibrium (C_e, g/L) and initial (C_i, g/L) concentrations. A_t, $K_{f,ads}$ and $K_{f,des}$ represent the adsorption–desorption factors, Q_L is the maximum desorption capacity, and b_t, n_{ads}, n_{des} and K_L are the isotherm constants.

	Isotherms	Equations	Parameters	NMDW	NMSW	UMSW
Adsorption	Freundlich	$q_e = K_{f,ads} \cdot C_e^{\frac{1}{n_{ads}}}$	$K_{f,ads}$ [(g/g)/(g/L)^n]	2.478	2.019	1.777
			n_{ads}	15.251	9.694	10.602
			R^2	0.970	0.985	0.995

Desorption	Temkin	$q_e = \frac{R \cdot T}{b_t} ln(A_t) + \frac{R \cdot T}{b_t} ln(C_e)$	A_t [L/g]	5.819 E6	0.427	2229.601
			b_t [J/mol]	14986.218	1294.693	11018.417
			R^2	0.965	0.986	0.996
	Freundlich	$q_e = K_{f,des} \cdot C_e^{\frac{1}{n_{des}}}$	$K_{f,des}$ [(g/g)/(g/L)^n]	6.24E–05	–[a]	–
			n_{des}	3.507	–	–
			R^2	0.950	–	–
	Langmuir	$q_e = \frac{C_e \cdot Q_L \cdot K_L}{(1 + C_e \cdot K_L)}$	Q_L [g/g]	2.57E–04	–	–
			K_L [L/g]	0.075	–	–
			R^2	0.989	–	–

a = not available

2.3.2.3 Desorption isotherms and hysteresis

The single–step desorption of diesel adsorbed onto the surgical mask is shown in Fig. 2.2c. Diesel desorption was very low (i.e., < 0.007%, Fig. 2.2c) and the desorption curve can be described through both the Langmuir and Freundlich isotherms ($R^2 \geq$ 0.950, Tab. 2.2), as recently reported by Song et al. (2021) for predicting hydrocarbon desorption from microplastics. Therefore, the hysteretic index (HI) was retrieved to examine the degree of reversibility of adsorption (Zhang et al., 2010). The obtained HI (i.e., 0.23 – 0.36) was not 1, neither 0 nor negative for the surgical mask (Tab. 2.3), thus suggesting that diesel behavior was invariably hysteretic (Akinpelu et al., 2021). This implies the impossibility of recontamination of the water solution after or during the adsorption and was never reported for organic contaminants (e.g., PCB, triclosan) in the presence of microplastics as adsorbents (Mohamed Nor and Koelmans, 2019; Tong et al., 2021).

2.3.2.4 Effect of ionic strength and initial pH

Fig. 2.3 shows the effect of ionic strength (i.e., 0.04 – 1.37 M) and pH (i.e., 1 – 13) on the Q_e of the surgical mask aimed at diesel removal.

The increase of ionic strength from 0.04 to 1.4 M slightly affected ($p > 0.05$) the adsorption of diesel onto the disposable face mask (Fig. 2.3a), thus confirming that this adsorbent can be employed in both fresh and seawater (see Section 3.1). Therefore,

the “salting–out” effect, i.e., a more organized water structure surrounding the cations, was not so obvious (Qian et al., 2011) and the Van der Waals interactions were not likely involved between the adsorbate and adsorbent (Hilner et al., 2015). This can be attributed to the reduction of the interfacial tension between oil and water at a higher of ionic strength, which led to the improvement of particle number at the interface instead of being adsorbed (Ferdous et al., 2012). Similarly, Yang et al. (2017) demonstrated no significant differences in naphthalene adsorption onto biochar by increasing the ionic strength (i.e., up to 25 mM).

The pH of the background solution can play a major role during adsorption and can affect the surface charge of the adsorbent as well as the speciation of the adsorbate (Huang et al., 2019; Muscetta et al., 2021). In this study, the Q_e of the surgical mask was quite stable in the pH range comprised between 3 and 9 (Fig. 2.3b), indicating that diesel removal was not significantly affected ($p > 0.05$) by the solution pH. This is most likely due to the not involvement of acid–basic interactions with the mentioned pH values during diesel adsorption (Guselnikova et al., 2022), which was probably driven by hydrophobic interactions (Navarathna et al., 2020). Notwithstanding, when the pH was either below 3 or above 9, the Q_e was slightly improved ($p > 0.05$) up to 3.6 g/g (Fig. 2.3b), suggesting that diesel adsorption can be affected by the pH_{PZC} of the surgical mask (i.e., 7.5, data not shown), which value can be anywhere in the pH scale as a function of adsorbent nature (Bakatula et al., 2018). Thus, when pH was lower or higher than pH_{PZC} (data not shown), the surface can be positively or negatively charged, respectively, resulting in a protonation and deprotonation of functional groups (Luo et al., 2011) in the surgical mask. This could have led to the generation of hydrogen bonds and/or electrostatic attractions (Adeola and Forbes, 2021) at extremely acidic and alkaline conditions. Interestingly, the stability of oil emulsion and oil coalescence phenomenon cannot be here involved under strong alkalinity and acidity, respectively, since the adsorption capacity was not reduced (Cai et al., 2019).

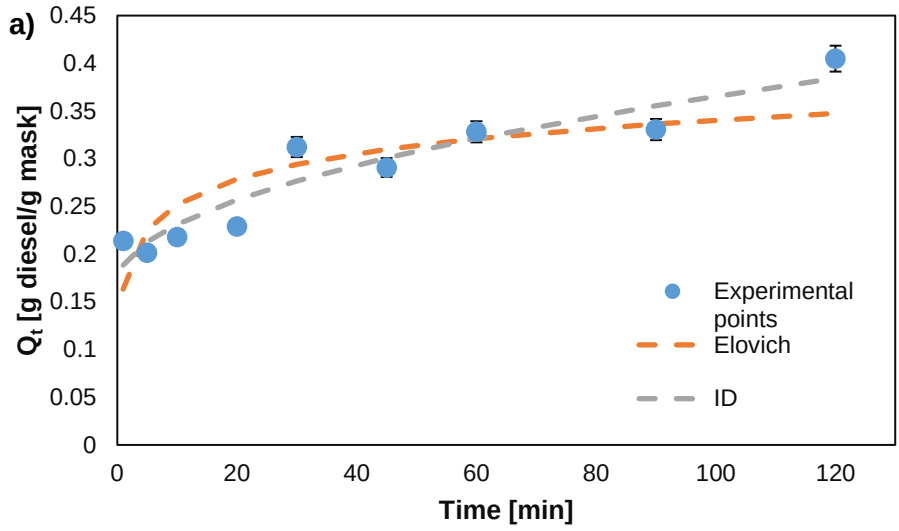
2.3.2.5 Thermodynamic study of adsorption–desorption isotherms

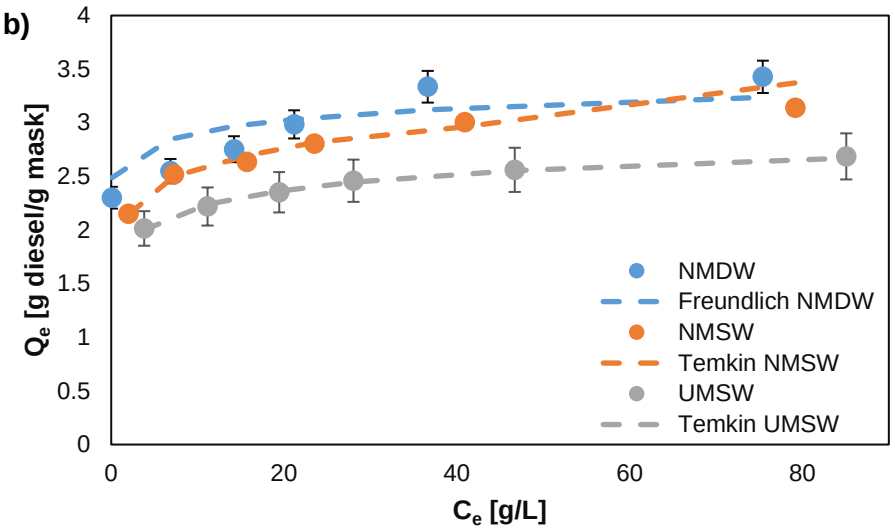
The thermodynamic study plays a key role to comprehend the nature and spontaneity of diesel adsorption (Bera et al., 2013) onto the surgical mask. The obtained thermodynamic equilibrium coefficients ($\ln K_d$) (Fig. 2.4 and Tab. 2.3), may suggest that the adsorption and desorption capacity of the surgical mask decreased and improved, respectively, with the increase of the temperature (Adeola and Forbes,

2021). The negative and positive values of the enthalpy (ΔH) (Tab. 2.3) also indicated that the adsorption and desorption mechanisms were exothermic and endothermic (Bianco et al., 2022a), respectively, suggesting that the decrease of temperature improved the diesel adsorption (Krasucka et al., 2022). This is further supported by the fact that ΔG was greater at higher temperatures, which can indicate reduced feasibility and spontaneity of diesel adsorption by increasing the temperature (Sidik et al., 2012). Also, for the adsorption mechanism, the ΔH was comprised between −2100 and −20900 J/mol, and therefore, the heat developed during physisorption was in the same magnitude order as the condensation heat (Liu and Liu, 2008). The negative values of entropy (ΔS, Tab. 2.3) indicate that diesel adsorption was likely coupled with ΔH with reduced randomness at the mask–aqueous solution interface (Bera et al., 2004). In addition, no substantial modifications in the inner structure of the adsorbent likely occurred during adsorption (Krasucka et al., 2022). This would suggest that the hysteresis here observed was not driven by the "conditioning effect" (see Section 3.2.3).

Table 2.3 – Thermodynamic parameters for the adsorption–desorption of diesel in water solutions using surgical masks. The values are the thermodynamic equilibrium coefficient (K_d), the free energy of Gibbs (ΔG), the enthalpy (ΔH) and entropy (ΔS).

	Temperature		**Thermodynamic parameters**			
	T (K)	**1/T**	**ln(Kd)**	**ΔG (J/mol)**	**ΔS (J/K)**	**ΔH (J)**
Adsorption	281.15	0.004	1.143	–2671.703	–16.733	–7326.047
	293.15	0.003	0.949	–2313.133		
	303.15	0.003	0.912	–2299.059		
	313.15	0.003	0.806	–2099.293		
Desorption	281.15	0.004	–9.234	21585.223	–54.771	6402.024
	293.15	0.003	–9.297	22658.094		
	303.15	0.003	–9.285	23401.339		
	313.15	0.003	–8.905	23184.408		


a)
0.45
0.4
0.35
0.3
0.25
0.2
0.15
0.1
0.05
0
Qt [g diesel/g mask]
0
20
40
60
80
100
120
Time [min]
Experimental points
Elovich
ID


b)
4
3.5
3
2.5
2
1.5
1
0.5
0
Qe [g diesel/g mask]
0
20
40
60
80
Ce [g/L]
NMDW
Freundlich NMDW
NMSW
Temkin NMSW
UMSW
Temkin UMSW

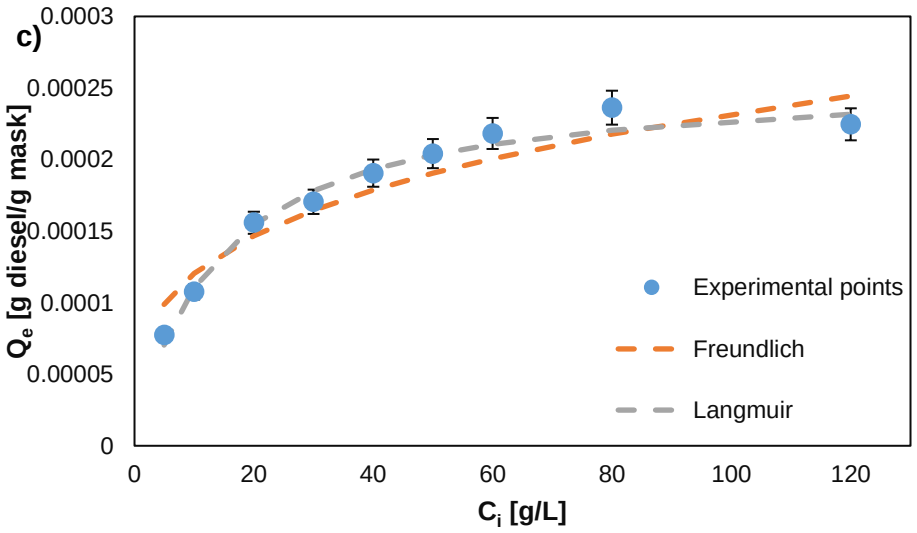

c)
0.0003
0.00025
0.0002
0.00015
0.0001
0.00005
0
Qe [g diesel/g mask]
0
20
40
60
80
100
120
Ci [g/L]
Experimental points
Freundlich
Langmuir

Figure 2.2 – Diesel adsorption (Qt, e) onto surgical masks (g/g) vs time (min) in a solution at 5 g diesel/L for 120 min by fitting the experimental points with the Elovich and Intraparticle Diffusion (ID) kinetic models (a), and vs diesel concentration (g/L) at the equilibrium in the solution phase (Ce) by using the Freundlich and Temkin equilibrium isotherms (b). Diesel desorption (Qe) from surgical masks (g/g) vs initial diesel concentration (Ci, g/L) by employing the Freundlich and Langmuir isotherms (c).

The averages and standard deviations are based on triplicates. NMDW = non–worn mask in distilled water; NMSW = non–worn mask in seawater; UMSW = used mask in seawater.

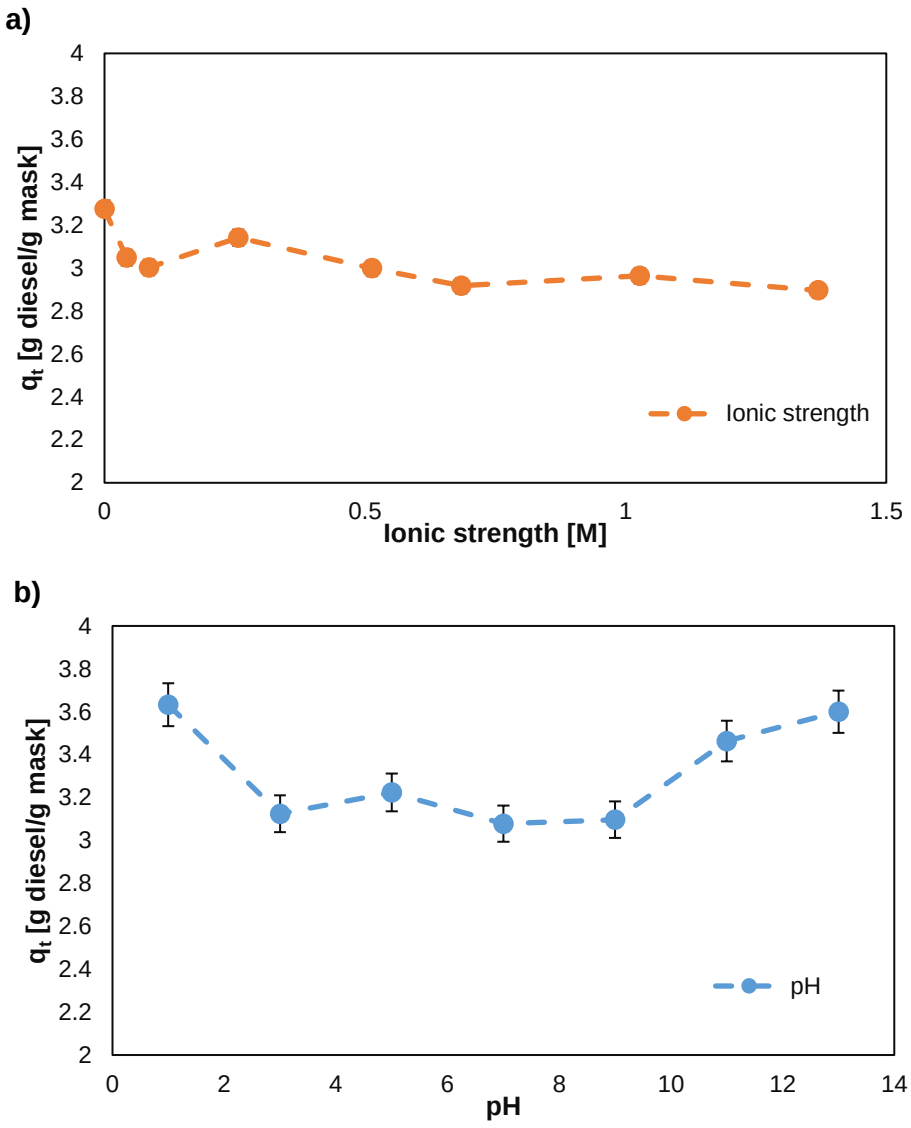


Figure 2.3 – The effect of a) ionic strength (M) and b) initial pH on the surgical mask adsorption capacity (Q_e, g/g) after 120 min.

Error bars indicate deviation standard values of analyses in triplicate.

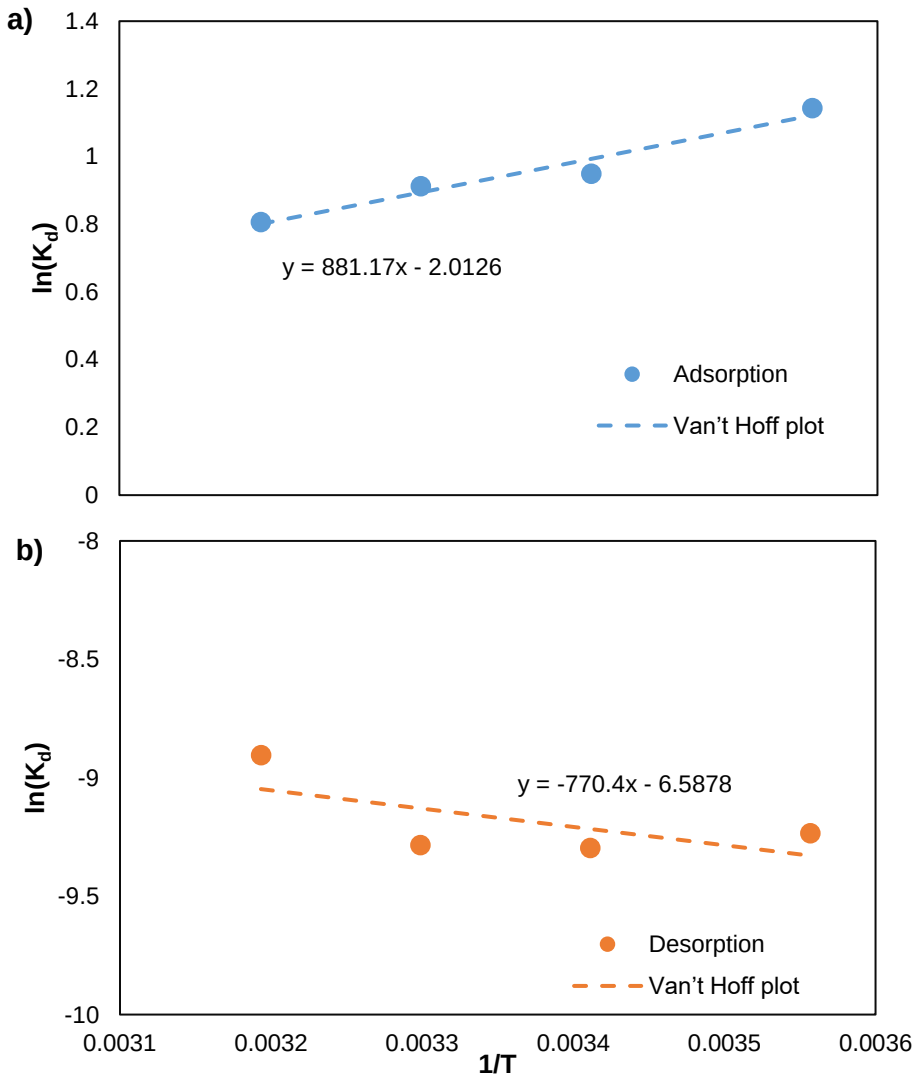


Figure 2.4 – Van't Hoff plots for diesel adsorption a) and desorption b) using surgical masks at different temperature–dependent isotherms (i.e., 281.15, 293.15, 303.15 and 313.15 K).

2.3.3 Regeneration and reutilization of the surgical mask

The reusability test for the surgical mask used as an adsorbent is crucial for deploying affordable technology to prevent secondary pollution due to the landfilling of spent masks. Fig. 2.5 shows that the treated surgical mask can be regenerated for five consecutive cycles while maintaining stability after each adsorption–desorption

round, as suggested by a similar WCA before and after the reusability test (data not shown). Indeed, the diesel removal slightly decreased ($p > 0.05$) from 100% to 89% (Fig. 2.5) after cycle V likely due to an improvement of surface roughness in the solvent–treated adsorbent (Park et al., 2022). Similarly, Guselnikova et al. (2022) obtained a slight reduction of the adsorption capacity of hexane–treated polypropylene waste coated with MAF–6 after 5 adsorption–desorption cycles. This implies that hexane represents a suitable solvent for the desorption of diesel fuel from surgical masks, considering that the presence of the adsorbate onto the adsorbent can hinder diesel removal (Gurav et al., 2021). Also, other adsorbents, such as biochar, can be affected by the loss of key components (e.g., metals, carboxylic acids) during regeneration, thus determining a diesel removal decrease below 50% after 5 adsorption–cycles (Golnari et al., 2022; Kim et al., 2020; Muscetta and Russo, 2021).

Thus, the surgical mask can be considered a promising adsorbent for the continuous removal of diesel from polluted seawater (e.g., 5 cycles).

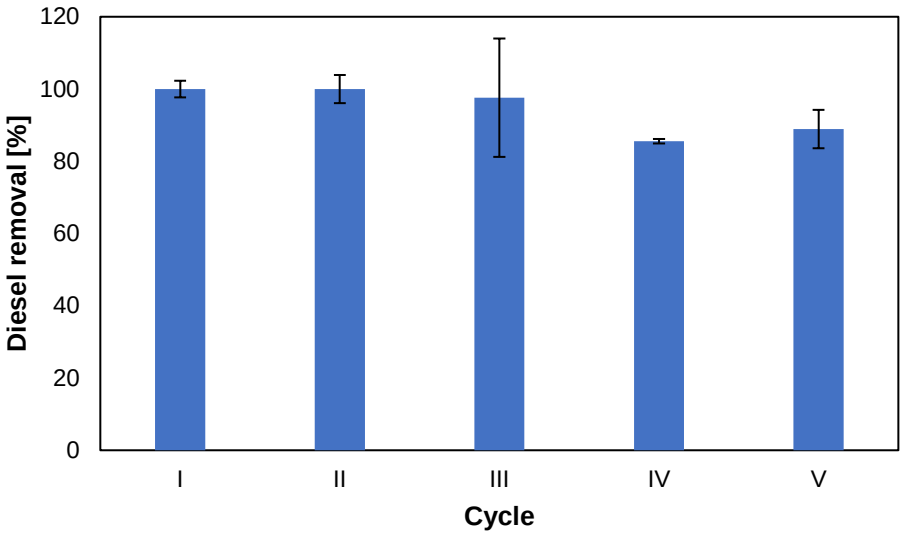


Figure 2.5 – Diesel removal (%) after 5 consecutive adsorption–desorption cycles.

2.4 Conclusions

In this thesis, the surgical mask has proven to be an effective and sustainable adsorbent for complete diesel removal from contaminated seawater. The adsorbent demonstrated a Q_e of up to 3.43 g/g after 120 minutes in fresh and seawater. The boundary layer and intraparticle diffusion (R^2 = 0.876) mechanisms were likely

associated with diesel adsorption, which was also governed by chemisorption with the increase of C_e, as suggested by the Temkin plot (R^2 = 0.952 – 0.997). The reusability test of the surgical mask showed that the adsorption efficiency decreased from 100 to 89% at the fifth adsorption–desorption cycle, thus indicating that secondary pollution can be avoided for real–scale applications. Future studies should evaluate the use of surgical masks for the adsorption of other organic pollutants and the toxicity of the treated water towards aquatic organisms.

2.5 References

Adeola, A.O., Forbes, P.B.C., 2021. Influence of natural organic matter fractions on PAH sorption by stream sediments and a synthetic graphene wool adsorbent. Environ. Technol. Innov. 21, 101202. https://doi.org/10.1016/j.eti.2020.101202

Akinpelu, A.A., Nazal, M.K., Abuzaid, N., 2021. Adsorptive removal of polycyclic aromatic hydrocarbons from contaminated water by biomass from dead leaves of Halodule uninervis: kinetic and thermodynamic studies. Biomass Convers. Biorefinery 1, 1–13. https://doi.org/10.1007/s13399-021-01718-0

Al-Ghouti, M.A., Da'ana, D.A., 2020. Guidelines for the use and interpretation of adsorption isotherm models: A review. J. Hazard. Mater. 393, 122383. https://doi.org/10.1016/j.jhazmat.2020.122383

Ali, M.A., Shaaban-Dessuuki, S.A., El-Wassefy, N.A., Mostafa, S.I., Hussein, M.H., 2021. Adsorption of crude and waste diesel oil onto agar-carboxymethylcellulose-silver nanocomposite in aqueous media. Inorg. Chem. Commun. 133, 108915. https://doi.org/10.1016/j.inoche.2021.108915

Alkan, M., Doğan, M., Turhan, Y., Demirbaş, Ö., Turan, P., 2008. Adsorption kinetics and mechanism of maxilon blue 5G dye on sepiolite from aqueous solutions. Chem. Eng. J. 139, 213–223. https://doi.org/10.1016/j.cej.2007.07.080

Anastopoulos, I., Pashalidis, I., 2021. Single-use surgical face masks, as a potential source of microplastics: Do they act as pollutant carriers? J. Mol. Liq. 326, 115247. https://doi.org/10.1016/j.molliq.2020.115247

Bakatula, E.N., Richard, D., Neculita, C.M., Zagury, G.J., 2018. Determination of point of zero charge of natural organic materials. Environ. Sci. Pollut. Res. 25, 7823–7833. https://doi.org/10.1007/s11356-017-1115-7

Bao, M., Wang, L., Sun, P., Cao, L., Zou, J., Li, Y., 2012. Biodegradation of crude oil using an efficient microbial consortium in a simulated marine environment. Mar.

Pollut. Bull. 64, 1177–1185. https://doi.org/10.1016/j.marpolbul.2012.03.020

Ben Jmaa, S., Kallel, A., 2019. Assessment of Performance of Posidona oceanica (L.) as Biosorbent for Crude Oil-Spill Cleanup in Seawater. Biomed Res. Int. 2019, 1–9. https://doi.org/10.1155/2019/6029654

Bera, A., Kumar, T., Ojha, K., Mandal, A., 2013. Adsorption of surfactants on sand surface in enhanced oil recovery: Isotherms, kinetics and thermodynamic studies. Appl. Surf. Sci. 284, 87–99. https://doi.org/10.1016/j.apsusc.2013.07.029

Bera, D., Lahiri, D., Nag, A., 2004. Kinetic studies on bleaching of edible oil using charred sawdust as a new adsorbent. J. Food Eng. 65, 33–36. https://doi.org/10.1016/j.jfoodeng.2003.11.020

Bianco, F., Marcińczyk, M., Race, M., Papirio, S., Esposito, G., Oleszczuk, P., 2022a. Low temperature-produced and VFA-coated biochar enhances phenanthrene adsorption and mitigates toxicity in marine sediments. Sep. Purif. Technol. 121414. https://doi.org/10.1016/j.seppur.2022.121414

Bianco, F., Race, M., Papirio, S., Esposito, G., 2023. A critical review of the remediation of PAH-polluted marine sediments: current knowledge and future perspectives. Resour. Environ. Sustain. 11, 100101. https://doi.org/10.1016/j.resenv.2022.100101

Bianco, F., Şenol, H., Papirio, S., Zenk, H., Kara, A., Atasoy, S., 2022b. Combined ultrasonic–hydrothermal pretreatment to improve the biomethane potential of hazelnut shell. Biomass and Bioenergy 165, 106554. https://doi.org/10.1016/j.biombioe.2022.106554

Breitwieser, M., Thomas-Guyon, H., Huet, V., Sagerup, K., Geraudie, P., 2018. Spatial and temporal impacts of the Skjervøy harbour diesel spill on native population of blue mussels: A sub-Arctic case study. Ecotoxicol. Environ. Saf. 153, 168–174. https://doi.org/10.1016/j.ecoenv.2018.01.033

Cai, L., Zhang, Y., Zhou, Y., Zhang, X., Ji, L., Song, W., Zhang, H., Liu, J., 2019. Effective Adsorption of Diesel Oil by Crab-Shell-Derived Biochar Nanomaterials. Materials (Basel). 12, 236. https://doi.org/10.3390/ma12020236

Diraki, A., Mackey, H.R., McKay, G., Abdala, A., 2019. Removal of emulsified and dissolved diesel oil from high salinity wastewater by adsorption onto graphene oxide. J. Environ. Chem. Eng. 7, 103106. https://doi.org/10.1016/j.jece.2019.103106

Erjavec, A., Plohl, O., Zemljič, L.F., Valh, J.V., 2022. Significant Fragmentation of Disposable Surgical Masks—Enormous Source for Problematic Micro/Nanoplastics Pollution in the Environment. Sustainability 14, 12625.

https://doi.org/10.3390/su141912625
Ferdous, S., Ioannidis, M.A., Henneke, D.E., 2012. Effects of temperature, pH, and ionic strength on the adsorption of nanoparticles at liquid–liquid interfaces. J. Nanoparticle Res. 14, 850. https://doi.org/10.1007/s11051-012-0850-4
Ge, J., Zhao, H.-Y., Zhu, H.-W., Huang, J., Shi, L.-A., Yu, S.-H., 2016. Advanced Sorbents for Oil-Spill Cleanup: Recent Advances and Future Perspectives. Adv. Mater. 28, 10459–10490. https://doi.org/10.1002/adma.201601812
Golnari, K., Alijani, H., Nobakht, V., Mokhtari, B., 2022. High-performance total sulfur removal from diesel fuel using amine functionalized biochar: Equilibrium, kinetic study and experimental design. Chem. Eng. Res. Des. 185, 253–266. https://doi.org/10.1016/j.cherd.2022.07.006
Grant, S.M., Waller, C.L., Morley, S.A., Barnes, D.K.A., Brasier, M.J., Double, M.C., Griffiths, H.J., Hughes, K.A., Jackson, J.A., Waluda, C.M., Constable, A.J., 2021. Local Drivers of Change in Southern Ocean Ecosystems: Human Activities and Policy Implications. Front. Ecol. Evol. 9, 365. https://doi.org/10.3389/fevo.2021.624518
Gurav, R., Bhatia, S.K., Choi, T.-R., Choi, Y.-K., Kim, H.J., Song, H.-S., Park, S.L., Lee, H.S., Lee, S.M., Choi, K.-Y., Yang, Y.-H., 2021. Adsorptive removal of crude petroleum oil from water using floating pinewood biochar decorated with coconut oil-derived fatty acids. Sci. Total Environ. 781, 146636. https://doi.org/10.1016/j.scitotenv.2021.146636
Guselnikova, O., Semyonov, O., Kirgina, M., Ivanov, A., Zinoviev, A., Postnikov, P., 2022. Polymer waste surgical masks decorated by superhydrophobic metal-organic frameworks towards oil spills clean-up. J. Environ. Chem. Eng. 10, 107105. https://doi.org/10.1016/j.jece.2021.107105
Hilner, E., Andersson, M.P., Hassenkam, T., Matthiesen, J., Salino, P.A., Stipp, S.L.S., 2015. The effect of ionic strength on oil adhesion in sandstone – the search for the low salinity mechanism. Sci. Rep. 5, 9933. https://doi.org/10.1038/srep09933
Hörsing, M., Ledin, A., Grabic, R., Fick, J., Tysklind, M., Jansen, J. la C., Andersen, H.R., 2011. Determination of sorption of seventy-five pharmaceuticals in sewage sludge. Water Res. 45, 4470–4482. https://doi.org/10.1016/j.watres.2011.05.033
Hossain, M.S., Omar, F., Asis, A.J., Bachmann, R.T., Islam Sarker, M.Z., Ab Kadir, M.O., 2019. Effective treatment of palm oil mill effluent using FeSO4.7H2O waste from titanium oxide industry: Coagulation adsorption isotherm and kinetics studies. J. Clean. Prod. 219, 86–98. https://doi.org/10.1016/j.jclepro.2019.02.069
Huang, D., Xu, B., Wu, J., Brookes, P.C., Xu, J., 2019. Adsorption and desorption of

phenanthrene by magnetic graphene nanomaterials from water: Roles of pH, heavy metal ions and natural organic matter. Chem. Eng. J. 368, 390–399. https://doi.org/10.1016/j.cej.2019.02.152

Huang, Y., Gancheva, T., Favis, B.D., Abidli, A., Wang, J., Park, C.B., 2021. Hydrophobic Porous Polypropylene with Hierarchical Structures for Ultrafast and Highly Selective Oil/Water Separation. ACS Appl. Mater. Interfaces 13, 16859–16868. https://doi.org/10.1021/acsami.0c21852

Inam, E., Etim, U.J., Akpabio, E.G., Umoren, S.A., 2017. Process optimization for the application of carbon from plantain peels in dye abstraction. J. Taibah Univ. Sci. 11, 173–185. https://doi.org/10.1016/j.jtusci.2016.01.003

Jiang, Y.F., Sun, H., Yves, U.J., Li, H., Hu, X.F., 2016. Impact of biochar produced from post-harvest residue on the adsorption behavior of diesel oil on loess soil. Environ. Geochem. Health 38, 243–253. https://doi.org/10.1007/s10653-015-9712-1

Jin, C., Geng, Z., Zhang, X., Ma, M., Ji, J., Wang, G., Guan, C., Liu, H., 2020. Study on the Solubility between Diesel and Acetone–Butanol–Ethanol with or without Water. Energy & Fuels 34, 1166–1176. https://doi.org/10.1021/acs.energyfuels.9b02150

Jung, S., Lee, S., Dou, X., Kwon, E.E., 2021. Valorization of disposable COVID-19 mask through the thermo-chemical process. Chem. Eng. J. 405, 126658. https://doi.org/10.1016/j.cej.2020.126658

Kathambi, B.E., Obiero, L.M., 2022. A Review of the Effects of COVID-19 Pandemic on Solid Waste Management. Eur. J. Sustain. Dev. Res. 6, em0196. https://doi.org/10.21601/ejosdr/12221

Kim, J.E., Bhatia, S.K., Song, H.J., Yoo, E., Jeon, H.J., Yoon, J.-Y., Yang, Y., Gurav, R., Yang, Y.-H., Kim, H.J., Choi, Y.-K., 2020. Adsorptive removal of tetracycline from aqueous solution by maple leaf-derived biochar. Bioresour. Technol. 306, 123092. https://doi.org/10.1016/j.biortech.2020.123092

Krasucka, P., Rombel, A., Yang, X.J., Rakowska, M., Xing, B., Oleszczuk, P., 2022. Adsorption and desorption of antiviral drugs (ritonavir and lopinavir) on sewage sludges as a potential environmental risk. J. Hazard. Mater. 425, 127901. https://doi.org/10.1016/j.jhazmat.2021.127901

Lee, K.-T., Cheng, C.-L., Lee, D.-S., Chen, W.-H., Vo, D.-V.N., Ding, L., Lam, S.S., 2022. Spent coffee grounds biochar from torrefaction as a potential adsorbent for spilled diesel oil recovery and as an alternative fuel. Energy 239, 122467. https://doi.org/10.1016/j.energy.2021.122467

Liu, L., Pu, X., Zhou, Y., Zhou, J., Luo, D., Ren, Z., 2020. Smart Pickering water-in-oil emulsion by manipulating interactions between nanoparticles and surfactant as potential oil-based drilling fluid. Colloids Surfaces A Physicochem. Eng. Asp. 586, 124246. https://doi.org/10.1016/j.colsurfa.2019.124246

Liu, Y., Liu, Y.-J., 2008. Biosorption isotherms, kinetics and thermodynamics. Sep. Purif. Technol. 61, 229–242. https://doi.org/10.1016/j.seppur.2007.10.002

Louati, H., Said, O. Ben, Soltani, A., Got, P., Cravo-Laureau, C., Duran, R., Aissa, P., Pringault, O., Mahmoudi, E., 2014. Biostimulation as an attractive technique to reduce phenanthrene toxicity for meiofauna and bacteria in lagoon sediment. Environ. Sci. Pollut. Res. https://doi.org/10.1007/s11356-013-2330-5

Luo, L., Lou, L., Cui, X., Wu, B., Hou, J., Xun, B., Xu, X., Chen, Y., 2011. Sorption and desorption of pentachlorophenol to black carbon of three different origins. J. Hazard. Mater. 185, 639–646. https://doi.org/10.1016/j.jhazmat.2010.09.066

Martins, L.S., Zanini, N.C., Botelho, A.L.S., Mulinari, D.R., 2021. Envelopes with microplastics generated from recycled plastic bags for crude oil sorption. Polym. Eng. Sci. 61, 2055–2065. https://doi.org/10.1002/pen.25734

Mitra, D., Tai, M.H., Abdullah, E.B., Wang, C.-H., Neoh, K.G., 2021. Facile fabrication of porous waste-derived carbon-polyethylene terephthalate composite sorbent for separation of free and emulsified oil from water. Sep. Purif. Technol. 279, 119664. https://doi.org/10.1016/j.seppur.2021.119664

Mohamed Nor, N.H., Koelmans, A.A., 2019. Transfer of PCBs from Microplastics under Simulated Gut Fluid Conditions Is Biphasic and Reversible. Environ. Sci. Technol. 53, 1874–1883. https://doi.org/10.1021/acs.est.8b05143

Mueller, A. V., Eden, M.J., Oakes, J.M., Bellini, C., Fernandez, L.A., 2020. Quantitative Method for Comparative Assessment of Particle Removal Efficiency of Fabric Masks as Alternatives to Standard Surgical Masks for PPE. Matter 3, 950–962. https://doi.org/10.1016/j.matt.2020.07.006

Muscetta, M., Minichino, N., Marotta, R., Andreozzi, R., Di Somma, I., 2021. Zero-valent palladium dissolution using NaCl/CuCl2 solutions. J. Hazard. Mater. 404, 124184. https://doi.org/10.1016/j.jhazmat.2020.124184

Muscetta, M., Russo, D., 2021. Photocatalytic Applications in Wastewater and Air Treatment: A Patent Review (2010–2020). Catalysts 11, 834. https://doi.org/10.3390/catal11070834

Navarathna, C.M., Bombuwala Dewage, N., Keeton, C., Pennisson, J., Henderson, R., Lashley, B., Zhang, X., Hassan, E.B., Perez, F., Mohan, D., Pittman, C.U., Mlsna, T., 2020. Biochar Adsorbents with Enhanced Hydrophobicity for Oil Spill

Removal. ACS Appl. Mater. Interfaces 12, 9248–9260. https://doi.org/10.1021/acsami.9b20924

Oliveira, L.M.T.M., Saleem, J., Bazargan, A., Duarte, J.L. da S., McKay, G., Meili, L., 2021. Sorption as a rapidly response for oil spill accidents: A material and mechanistic approach. J. Hazard. Mater. 407, 124842. https://doi.org/10.1016/j.jhazmat.2020.124842

Park, S., Kim, Y., Lee, W., Nam, C., 2022. Superhydrophobic polypropylene sorbent derived from discarded face masks: A highly efficient adsorbent for oil spill sorbent. Chemosphere 303, 135186. https://doi.org/10.1016/j.chemosphere.2022.135186

Qian, Y., Posch, T., Schmidt, T.C., 2011. Sorption of polycyclic aromatic hydrocarbons (PAHs) on glass surfaces. Chemosphere. https://doi.org/10.1016/j.chemosphere.2010.11.002

Saharan, Y., Singh, J., Goyat, R., Umar, A., Algadi, H., Ibrahim, A.A., Kumar, R., Baskoutas, S., 2022. Nanoporous and hydrophobic new Chitosan-Silica blend aerogels for enhanced oil adsorption capacity. J. Clean. Prod. 351, 131247. https://doi.org/10.1016/j.jclepro.2022.131247

Selvaranjan, K., Navaratnam, S., Rajeev, P., Ravintherakumaran, N., 2021. Environmental challenges induced by extensive use of face masks during COVID-19: A review and potential solutions. Environ. Challenges 3, 100039. https://doi.org/10.1016/j.envc.2021.100039

Senthil Kumar, P., Ramalingam, S., Senthamarai, C., Niranjanaa, M., Vijayalakshmi, P., Sivanesan, S., 2010. Adsorption of dye from aqueous solution by cashew nut shell: Studies on equilibrium isotherm, kinetics and thermodynamics of interactions. Desalination 261, 52–60. https://doi.org/10.1016/j.desal.2010.05.032

Shen, M., Zeng, Z., Song, B., Yi, H., Hu, T., Zhang, Y., Zeng, G., Xiao, R., 2021. Neglected microplastics pollution in global COVID-19: Disposable surgical masks. Sci. Total Environ. 790, 148130. https://doi.org/10.1016/j.scitotenv.2021.148130

Shojaei, N., Aminsharei, F., Abbastabar Ahangar, H., 2021. Application of hydrophobic polymers as solidifiers for oil spill cleanup. Int. J. Environ. Sci. Technol. 18, 1419–1424. https://doi.org/10.1007/s13762-020-02882-y

Sidik, S.M., Jalil, A.A., Triwahyono, S., Adam, S.H., Satar, M.A.H., Hameed, B.H., 2012. Modified oil palm leaves adsorbent with enhanced hydrophobicity for crude oil removal. Chem. Eng. J. 203, 9–18.

https://doi.org/10.1016/j.cej.2012.06.132

Song, Xiaowei, Wu, X., Song, Xiaoping, Shi, C., Zhang, Z., 2021. Sorption and desorption of petroleum hydrocarbons on biodegradable and nondegradable microplastics. Chemosphere 273, 128553. https://doi.org/10.1016/j.chemosphere.2020.128553

Sun, X., Fu, H., Bao, M., Liu, W., Luo, C., Li, Yang, Li, Yiming, Lu, J., 2022. Development of a new hydrophobic magnetic biochar for removing oil spills on the water surface. Biochar 4, 60. https://doi.org/10.1007/s42773-022-00184-9

Tang, J.W., Bahnfleth, W.P., Bluyssen, P.M., Buonanno, G., Jimenez, J.L., Kurnitski, J., Li, Y., Miller, S., Sekhar, C., Morawska, L., Marr, L.C., Melikov, A.K., Nazaroff, W.W., Nielsen, P.V., Tellier, R., Wargocki, P., Dancer, S.J., 2021. Dismantling myths on the airborne transmission of severe acute respiratory syndrome coronavirus-2 (SARS-CoV-2). J. Hosp. Infect. 110, 89–96. https://doi.org/10.1016/j.jhin.2020.12.022

Tong, H., Hu, X., Zhong, X., Jiang, Q., 2021. Adsorption and Desorption of Triclosan on Biodegradable Polyhydroxybutyrate Microplastics. Environ. Toxicol. Chem. 40, 72–78. https://doi.org/10.1002/ETC.4902

Uriu, K., Ito, J., Kosugi, Y., Tanaka, Y.L., Mugita, Y., Guo, Z., Hinay, A.A., Putri, O., Kim, Y., Shimizu, R., Begum, M.M., Jonathan, M., Saito, A., Ikeda, T., Sato, K., 2023. Transmissibility, infectivity, and immune evasion of the SARS-CoV-2 BA.2.86 variant. Lancet Infect. Dis. 0. https://doi.org/10.1016/S1473-3099(23)00575-3

Vannarath, A., Thalla, A.K., 2021. Synthesis and characterisation of an ultra-light, hydrophobic and flame-retardant robust lignin-carbon foam for oil-water separation. J. Clean. Prod. 325, 129263. https://doi.org/10.1016/j.jclepro.2021.129263

Wang, J., Guo, X., 2020. Adsorption kinetic models: Physical meanings, applications, and solving methods. J. Hazard. Mater. 390, 122156. https://doi.org/10.1016/j.jhazmat.2020.122156

Weaver, D.T., McElvany, B.D., Gopalakrishnan, V., Card, K.J., Crozier, D., Dhawan, A., Dinh, M.N., Dolson, E., Farrokhian, N., Hitomi, M., Ho, E., Jagdish, T., King, E.S., Cadnum, J.L., Donskey, C.J., Krishnan, N., Kuzmin, G., Li, J., Maltas, J., Mo, J., Pelesko, J., Scarborough, J.A., Sedor, G., Tian, E., An, G.C., Diehl, S.A., Scott, J.G., 2021. UV decontamination of personal protective equipment with idle laboratory biosafety cabinets during the COVID-19 pandemic. PLoS One 16, e0241734. https://doi.org/10.1371/journal.pone.0241734

Wu, W., Hu, Y., Guo, Q., Yan, J., Chen, Y., Cheng, J., 2015. Sorption/desorption behavior of triclosan in sediment–water–rhamnolipid systems: Effects of pH, ionic strength, and DOM. J. Hazard. Mater. 297, 59–65. https://doi.org/10.1016/j.jhazmat.2015.04.078

Yang, H., Sun, J., Zhang, Y., Xue, Q., Xia, S., 2021. Preparation of hydrophobic carbon aerogel using cellulose extracted from luffa sponge for adsorption of diesel oil. Ceram. Int. 47, 33827–33834. https://doi.org/10.1016/j.ceramint.2021.08.294

Yang, W., Wang, Y., Sharma, P., Li, B., Liu, K., Liu, J., Flury, M., Shang, J., 2017. Effect of naphthalene on transport and retention of biochar colloids through saturated porous media. Colloids Surfaces A Physicochem. Eng. Asp. https://doi.org/10.1016/j.colsurfa.2017.07.010

Yu, F., Yang, C., Huang, G., Zhou, T., Zhao, Y., Ma, J., 2020. Interfacial interaction between diverse microplastics and tetracycline by adsorption in an aqueous solution. Sci. Total Environ. 721, 137729. https://doi.org/10.1016/j.scitotenv.2020.137729

Zhang, H., Lin, K., Wang, H., Gan, J., 2010. Effect of Pinus radiata derived biochars on soil sorption and desorption of phenanthrene. Environ. Pollut. 158, 2821–2825. https://doi.org/10.1016/j.envpol.2010.06.025

Zheng, X., Lin, H., Tao, Y., Zhang, H., 2018. Selective adsorption of phenanthrene dissolved in Tween 80 solution using activated carbon derived from walnut shells. Chemosphere 208, 951–959. https://doi.org/10.1016/j.chemosphere.2018.06.025

Zhou, X., Wang, F., Ji, Y., Chen, W., Wei, J., 2016. Fabrication of Hydrophilic and Hydrophobic Sites on Polypropylene Nonwoven for Oil Spill Cleanup: Two Dilemmas Affecting Oil Sorption. Environ. Sci. Technol. 50, 3860–3865. https://doi.org/10.1021/acs.est.5b06007

CHAPTER 3. MOVING-BED BIOFILM REACTOR (MBBR) ALLEVIATES THE NEGATIVE EFFECT OF METHYLISOTHIAZOLINONE ON THE NITRIFICATION-DENITRIFICATION PROCESS

3.1 Introduction

Over the past ten years, there has been a noteworthy surge in interest regarding the emergence of novel pollutants, their environmental fate, and potential toxicity. Numerous of these substances are not recent discoveries but compounds that have been used for decades, now raising concerns. Despite the absence of regulations and restrictions, many are deemed potentially impactful environmental pollutants (Nowak-Lange et al., 2022).

Among these pollutants, 2-methyl-4-isothiazolin-3-one (MIT), known for its potent antimicrobial properties, has found widespread use as a non-oxidizing biocide and disinfectant (Speksnijder et al., 2010). MIT applications range from cosmetics and personal care products to controlling biofilm in membrane filtration systems (Peng et al., 2020). Due to its extensive use, MIT can be detected in natural water bodies and wastewater, posing threats to ecological balance and human health. For instance, epidemiological studies have revealed that MIT can induce contact allergy in humans, even at concentrations as low as 50 mg/L through repeated exposure (the limit for cosmetic application is 100 mg/L) (Lundov et al., 2013; Nowak et al., 2020).

Due to its long natural decay (i.e., from several days to weeks), the presence of MIT in wastewater (i.e., 5 – 150 mg/L) generated from industrial processes (e.g., cooling towers) introduces complexity to the treatment cycle since MIT can detrimentally influence the biological process (Amat et al., 2015; Nowak-Lange et al., 2022; Zeng et

al., 2020). Indeed, the occurrence of 5 mg/L of MIT in a paper mill wastewater markedly decreased the efficiency of the nitrification process from 90 to 20% in a Sequencing Batch Reactor (SBR) after 27 days (Amat et al., 2015). Similarly, the increase of MIT concentration from 10 to 40 mg/L led to the decrease of the denitrification rate from 62.4 to 17.6 mg NO_3–N/(g VSS·h) in an SBR treating saline wastewater (Zeng et al., 2020). MIT can undergo reactions with nucleophilic molecules due to a sulfur heterocycle, establishing bonds with the thiol groups found in proteins, thereby hindering the activity of enzymes vital for growth and metabolism. Consequently, this inhibition leads to the demise of microbial cells within a few hours of exposure (Berthet et al., 2017). For this purpose, a few investigations explored MIT chemical oxidation, including methods such as ozonation and electrochemical processes (Li et al., 2016; Peng et al., 2020).

However, it is worth noting that constructing and operating facilities for these techniques can be costly, and therefore, MIT can remain untreated in the industrial wastewater effluent. Thus, whether an MIT-containing industrial effluent meets specific criteria, such as chemical oxygen demand (COD), can be discharged into the civil sewage system (Directive, 2000), which coupled with MIT household use, can represent an issue for urban wastewater treatment plants (WTTPs) (Carbajo et al., 2015). Notwithstanding, insufficient information regarding MIT in civil WWTPs exists globally. MIT concentrations can vary from a few ng/L to several µg/L in an influent wastewater (Carbajo et al., 2015; Nowak et al., 2020; Paijens et al., 2021). Paijens et al. (Paijens et al., 2021) reported a removal efficiency above 55% achieved for MIT during sampling campaigns performed in the influent and effluent of a conventional WTTP.

To date, no studies have highlighted the effect of MIT-containing civil wastewater on the nitrification, denitrification, and anaerobic digestion (AD) processes. Indeed, it is still unclear whether the biological process in an urban WTTP can effectively remove this emerging pollutant and low MIT concentrations (i.e., 0.1 – 1.0 mg/L) can lead to the inhibition of the activated sludge biomass. Also, the only two studies available on nitrification or denitrification processes in the presence of MIT in industrial wastewater are only focused on an SBR configuration (Amat et al., 2015; Zeng et al., 2020).

Among the primary configurations employed for nitrification and denitrification purposes, attached-growth systems such as Moving-Bed Biofilm Reactors (MBBRs) facilitate the retention of microorganisms in the biofilm form (Pan et al., 2022). The effectiveness of an MBBR can rely on the fact that it can reduce the vulnerability of microbes to adverse environmental conditions, such as the presence of pollutants due to the addition of carriers, which are specifically designed with a large protected surface

area, defined as the surface area of the carrier available for biofilm growth in a protected environment (Kostrytsia et al., 2022).

Therefore, this thesis aims to investigate, as novel aspect, the effect of a MIT-containing urban wastewater solution (i.e., 0.1 – 1.0 mg/L) in an MBBR operated in a semi-continuous mode. The specific objectives of this thesis are *i*) investigate the effects of MIT on the nitrification process in fed-batch mode in the absence or the presence of supports for biofilm growth (i.e., classical K1); *ii*) evaluate the impact of MIT on the nitrification-denitrification process in two MBBRs operated in a semi-continuous mode; *iii*) study the influence of MIT on biochemical methane potential (BMP) tests at a low dosage (i.e., 0.001 mg/g TS); *iv*) assess the degradation kinetics and mechanisms of MIT under aerobic, anoxic and anaerobic conditions.

3.2 Materials and methods

3.2.1 Activated sludge, digestate and synthetic influent

An activated sludge taken from the pre-denitrification system in an urban WTTP was used as inoculum for the fed-batch reactor (F-BR) and semi-continuous MBBR. For the BMP tests, digestate was obtained downstream of the AD reactor in a plant treating zootechnical wastewater. The physical-chemical characteristics of both activated sludge and digestate are reported in Tab. 3.1.

The synthetic wastewater was replicated in the laboratory by dissolving 290 mg of ammonium chloride (NH_4Cl, purity ≥ 99.5%, Honeywell's Fluka™, USA) or 553 mg of potassium nitrate (KNO_3, purity ≥ 99%, Sigma-Aldrich, Germany) as a source of nitrogen (for nitrification or denitrification, respectively), 470 mg of glucose ($C_6H_{12}O_6$, purity ≥ 99.5%, Sigma-Aldrich, Germany) and 300 mg of sodium bicarbonate ($NaHCO_3$, purity ≥ 99.7%, Sigma-Aldrich, Germany) as a source of organic and inorganic carbon, respectively, and a mix of macro- and micro-nutrients (Iannacone et al., 2019). The resulting synthetic influent was characterized by a neutral pH and a concentration of water soluble organic carbon (WSOC) and nitrogen of approximately 188 and 77 mg/L, respectively (Bhave et al., 2020; Zangeneh et al., 2021). When the emerging pollutant was investigated, a variable amount of a concentrated MIT-containing solution (purity ≥ 95%, Sigma-Aldrich, Germany) was included in the synthetic wastewater to achieve the desired concentration (i.e., 0.1 – 1.0 mg MIT/L).

Table 3.1 – Physical-chemical characteristics of activated sludge and digestate. TS = total solids; VS = volatile solids; NO_3^-–N = nitrate; NH_4^+–N = ammonia nitrogen.

Parameters	Activated sludge	Digestate
TS (%)	2.67	7.84
VS (%)	1.46	5.57
pH	6.60	7.00
NO_3^-–N (mg/L)	7.93	–
NH_4^+–N (mg/L)	–	988.73

3.2.2 Experimental setup and bioreactor operations

3.2.2.1 F-BR

For the F-BR, a 1500 mL double-walled glass vessel was equipped with a mechanical overhead stirrer (Yellow line, IKA, USA) set at 300 rpm and a temperature control system (Julabo GmbH, Germany) at 20 ± 2 °C to avoid temperature fluctuations. Oxygen was supplied through an aeration pump, ensuring the necessary dissolved oxygen for nitrification (i.e., ≥ 2.0 mg O_2/L) (Morgenroth and Sørensen, 2023). The pH was controlled using an automatic control system (Milwaukee Instruments, Hungary) capable of introducing a 0.5 M sodium hydroxide solution (NaOH, purity ≥ 98%, Sigma-Aldrich, Germany) into the reactor when the pH values dropped below 7.3. An acrylic lid with sampling openings was employed to seal the F-BR (Bianco et al., 2023b).

The nitrification process was investigated for 39 days by performing 12 consecutive cycles as follows: 1) inoculum addition (i.e., 200 mL) in the presence of the synthetic wastewater (see Section 2.1); 2) startup between days 0 and 19 to guarantee biomass acclimation (Phase I), 3) MIT contamination (i.e., 0.1 mg/L) between days 20 and 29 (Phase II), and 4) 0.1 mg/L of MIT + Kaldnes K1 (10 mm diameter; 7 mm length) (Sweden) addition by respecting a filling level of 30% ($V_{carriers}/V_{reactor}$) (Aygun et al., 2008; Kostrytsia et al., 2022) between days 30 and 39 (Phase III). The completion of each cycle was determined either when the removal of WSOC ceased or when an ammonia removal efficiency exceeding 99% was achieved (Bianco et al., 2022a). After each cycle, the mechanical agitation was stopped for 30 minutes to allow biomass sedimentation and replace 50% of the overall liquid phase.

In addition to the previous F-BR, control reactors were employed to evaluate the potential removal of MIT through abiotic loss and adsorption. These control reactors, i.e., Inoculum-Free (IFCR) and Autoclaved Inoculum (AICR), contained 1000 mL of

autoclaved water and underwent the same operating conditions throughout the experimental phases. Approximately 200 mg/L of mercury chloride ($HgCl_2$, purity ≥ 98%, Alfa Aesar, USA) was introduced as a biocide agent into the synthetic wastewater solution to prevent biological activity (Bramwell and Laha, 2000).

3.2.2.2 Semi-continuous MBBR

Two MBBRs (i.e., nitrification and denitrification) with a similar reactor configuration described above (i.e., pH, temperature, mixing, filling ratio), except for the aeration in the denitrification vessel in which anoxic conditions were guaranteed, were operated simultaneously in semi-continuous mode by replacing the liquid solution with 500 mL of influent every day (simulating a water retention time of 2 days) to provide an adequate amount of ammonia and nitrate to the populations of nitrifying and denitrifying bacteria (see Section 2.1), respectively, and facilitate their colonization on the carriers before the addition of MIT. Before starting the MBBR operations, each vessel was inoculated with 200 mL of activated sludge, 800 mL of synthetic wastewater and 300 mL of K1 carriers. The "enrichment" process (1st Period) was considered stable after a period during which there was no significant difference in ammonia and nitrate removal between successive subcultures in the MBBRs. In this 2nd Period (i.e., steady phase), 500 mL influent was directly taken from the nitrification vessel (MBBR-N) and used as the influent solution for the denitrification reactor (MBBR-D) by respecting the required WSOC for denitrifying bacteria (Rodríguez et al., 2011) with an adequate amount of glucose. Afterwards, the effect of MIT on the nitrification and denitrification process was investigated in both MBBR-N and MBBR-D (3rd Period) at a concentration of 0.1 and 1.0 mg MIT/L between 98 – 120 and 121 – 136 days, respectively.

3.2.3 Biochemical methane potential tests

The BMP tests were conducted with 250 mL batch reactors (i.e., serum bottles) under 3 experimental conditions performed in triplicate: *i*) D: blanks with only inoculum (i.e., digestate); *ii*) C: controls containing inoculum and substrate (i.e., activated sludge); *iii*) M: containing inoculum, substrate, and MIT (i.e., 0.001 mg/g TS). A ratio of inoculum to substrate (ISR) equal to 2 was considered in each serum bottle, which received distilled water to reach a final working volume of 150 mL by ensuring an initial total solid (TS) content below 10% and an amount of volatile solids (VS) added of 2.5 g (Bianco et al., 2022c; Şenol and Zenk, 2020). Subsequently, the bottles were sealed with 20 mm diameter rubber stoppers, closed with aluminum crimps, and subjected to flushing with

N_2 for approximately 5 minutes to remove air from the headspace (i.e., 100 mL) (Bianco et al., 2022c). The BMP assays were placed in a temperature-controlled environment at 37 ± 1 °C, allowing operation under mesophilic conditions. Manual mixing was performed twice a day to prevent the formation of a sediment layer (Şenol et al., 2023). The assays were concluded only when the daily methane production for three consecutive days was < 1% of the accumulated CH_4 volume (Holliger et al., 2016).

3.2.4 Sampling, analytical methods and calculation

Concentrations of TS, VS, and volatile suspended solids (VSS) were assessed following the procedures outlined in Standard Methods (APHA, 2012). For VSS analysis, K1 carriers were sampled directly from each MBBR and sonicated in ultrapure water to allow biofilm detaching (Iannacone et al., 2019).

Liquid samples obtained from a sampling point located on the top of each F-BR and MBBR were filtered using 0.45 μm syringe filters with polypropylene membranes (VWR, USA) before nitrogen and WSOC analyses. The spectrophotometric indophenol blue method was employed 4 – 5 times per week to determine ammonia nitrogen concentrations (APAT and IRSA-CNR, 2003). Anion concentrations (i.e., nitrite and nitrate) were analyzed 4 – 5 times per week via ion chromatography (883 Basic IC Plus, Metrohm, Switzerland), and a Shimadzu TOC-L Series (Kyoto, Japan) was used to determine WSOC (Bianco et al., 2022b).

Biogas from the anaerobic reactors was quantified 3 – 5 times per week using the liquid displacement method, as previously described by Oliva et al (Oliva et al., 2022a). The composition of biogas, specifically methane, carbon dioxide, and hydrogen, was examined utilizing a 3400 GC-TCD gas chromatograph (Varian-Agilent, USA) (Bianco et al., 2020). The overall concentration of volatile fatty acids (VFAs), measured in acetic acid equivalents (mg HAc/L), was determined using HPLC following the method outlined by Bianco et al (Bianco et al., 2020). The samples were centrifuged at 10,000 rpm for 10 minutes and filtered via 0.22 μm PTFE filters (VWR, USA) prior to analysis.

The kinetic model employed via the Origin software (version 8.0, OriginLab Corporation, USA) for fitting the methane yield obtained in this thesis was the modified Gompertz and Logistic models (Oliva et al., 2022b). The resultant methane production (G_t), measured as mL CH_4/g VS_{added}, was calculated through the utilization of the following equations (Oliva et al., 2023):

$$G_t = G_u \cdot exp\left(-exp\left[\frac{R_m \cdot e(\lambda - t)}{G_u} + 1\right]\right)$$

$$G_t = \frac{G_u}{1 + exp^{\left(\frac{4R_m \cdot (\lambda - t)}{G_u} + 2\right)}}$$

where, G_u is the ultimate methane yield (mL CH_4/g VS), R_m represents the maximum methane production rate (mL CH_4/(g VS·d)), λ denotes the lag phase (d), and e is Euler's number (approximately 2.71828).

MIT was analyzed in both the nitrification-denitrification and AD processes using an LC-20AD HPLC (Shimadzu, Japan) equipped with a Kinetex® 5 μm C18 (250 × 4.6 mm) column (Phenomenex, USA) and an SPD-20A UV detector (Shimadzu, Kyoto, Japan) set at 274 nm (Aerts et al., 2015). An acid formic (0.1 %)/acetonitrile (VWR, HPLC grade) solution (90:10) was used as the eluent phase at a flow rate of 0.8 mL/min. The sample injection volume was 25 μL. Before the analyses, the samples were filtered through 0.22 μm PTFE filters (VWR, USA).

3.2.5 ANOVA test

The acquired data underwent analysis through one-way ANOVA followed by a Tukey's HSD test to explore significant differences ($p < 0.05$). The statistical computations were performed using an online web statistical calculator at https://astatsa.com/.

3.3 Results and discussion

3.3.1 The effects of MIT on the nitrification process in fed-batch reactor

An NH_4^+–N removal of about 68–100%, 83% and 96–99% (Fig. 3.1c) was achieved during Phases I, II and III, respectively, in the F-BR operated over 39 days.

From day 1 to day 19 (Phase I), NH_4^+–N concentration decreased ($p < 0.05$) from approximately 77 mg/L to below the detection limit of 0.2 mg/L in a period comprised between 1 and 2 days (Fig. 3.1a). The nitrification process typically involves two consecutive oxidation steps. In the initial step, ammonia-oxidizing bacteria (AOB) oxidize ammonia nitrogen to nitrite, utilizing 1.5 mol of O_2 per mol of N (Bianco et al., 2023a). During this reaction, the enzymes ammonia monooxygenase and hydroxylamine oxidoreductase are involved, with hydroxylamine serving as an intermediate product. In the subsequent step, nitrite-oxidizing bacteria (NOB) can employ the enzyme nitrite oxidoreductase to convert NO_2^-–N to NO_3^-–N, consuming 0.5 mol of O_2 per mol of N (Rahimi et al., 2020). The Gibbs free energy change (ΔG) for nitrification is approximately -94.3 kJ/mol (Tab 3.2) at ambient conditions, thus indicating that this process is thermodynamically favourable. A removal of WSOC comprised between 92 and 100% was also reached in the F-BR after each cycle (Fig. 3.1c). AOB and NOB commonly rely solely on inorganic carbon sources, with an approximate consumption of nearly 7.1 mg $CaCO_3$ for each mg of NH_4^+–N converted to NO_3^-–N (Villaverde, 1997), and therefore, the decrease of WSOC throughout F-BR operation (Fig. 3.1b) can be attributed to the presence of heterotrophic aerobic bacteria (HAB) in the inoculum.

From day 20 to day 29 (Phase II), the nitrification efficiency significantly decreased ($p < 0.05$) from 100 to 82% (Fig. 3.1c), and the remaining NH_4^+–N concentration in the F-BR was approximately 13 and 14 mg/L after cycles 9 and 10 (Fig. 3.1a), respectively. Typically, AOB and NOB such as *Nitrosomonas* and *Nitrobacter* genera, respectively, are acknowledged for their sensitivity to pollutants (e.g., MIT), making them valuable early indicators for assessing the influence of chemicals on wastewater microbial function and overall health (Kookana et al., 2022). Indeed, biological processes can be affected by MIT, which adversely impacts the wastewater treatment process by significantly decreasing nitrification efficiency from 80 to 20% at high MIT concentrations (i.e., 5 mg/L) (Amat et al., 2015). Similarly, Carbajo et al. (Carbajo et al., 2015) showed an EC_{50} (effective concentration causing manifestation of the observed effect in 50% of the tested organism) below 4 mg/L for a mixture of MIT and methylchloroisothiazolinone in

activated sludge. MIT inhibits cellular activity primarily by deactivating cell protein thiols through the reductive sulfur present in MIT molecules (Wang et al., 2020), as suggested by the reduction in MIT concentrations due to the biosorption and biodegradation mechanism (Fig. 3.4a). However, at low MIT concentrations (i.e., 0.1 mg/L) the nitrification process was partially inhibited (i.e., from 100 to approximately 83%) (Fig. 3.1c), but the time required for ammonia oxidation significantly increased ($p < 0.05$) up to 6 days (Fig. 3.1a). It is noteworthy that while Fig. 3.1c indicates a drastic VSS reduction ($p < 0.05$) from 1.6 to approximately 0.8 – 1.0 g/L upon the addition of MIT by further corroborating the toxicity towards nitrifying bacteria, there is no significant decrease ($p > 0.05$) of efficiency in the mineralization of WSOC, which suggests that MIT cannot affect the metabolization of the organic substrates such as glucose (Amat et al., 2015). Also, the organic load was relatively low and the liquid retention time sufficiently long, likely facilitating an effective substrate degradation by HAB (Amat et al., 2015; Iannacone et al., 2019).

From day 30 to day 39 (Phase III), the residual NH_4^+–N concentration in F-BR significantly decreased from about 14 to 1 – 3 mg/L (Fig. 3.1a) after 3 and 5 days in cycles 11 and 12, respectively. This was accompanied by increased VSS concentrations from approximately 0.8 to 1.8 g/L, whereas the WSOC removal remained at 100%. The carrier addition could be the reason for the improvement of nitrification efficiency (Fig. 3.1c). K1 carriers are engineered to possess a substantial Protected Surface Area (PSA), defined as the surface area of the carrier available for biofilm growth within a secure environment (Kostrytsia et al., 2022). Also, smaller aggregates (e.g., suspended biomass) may potentially render nitrifiers more susceptible to inhibition compared to larger clusters (e.g., formation of biofilm onto K1) (Piculell et al., 2016). For instance, Schopf et al. (Schopf et al., 2018) reported that inhibition could be avoided at influent copper concentrations of 0.13 – 0.61 mg/L in an MBBR during long-term nitritation. However, the time here studied for allowing a sufficient biofilm growth onto K1 could not be enough to support this theory, and therefore, a more complex reactor configuration and longer experiment was subsequently conducted in a nitrification-denitrification system for 136 days.

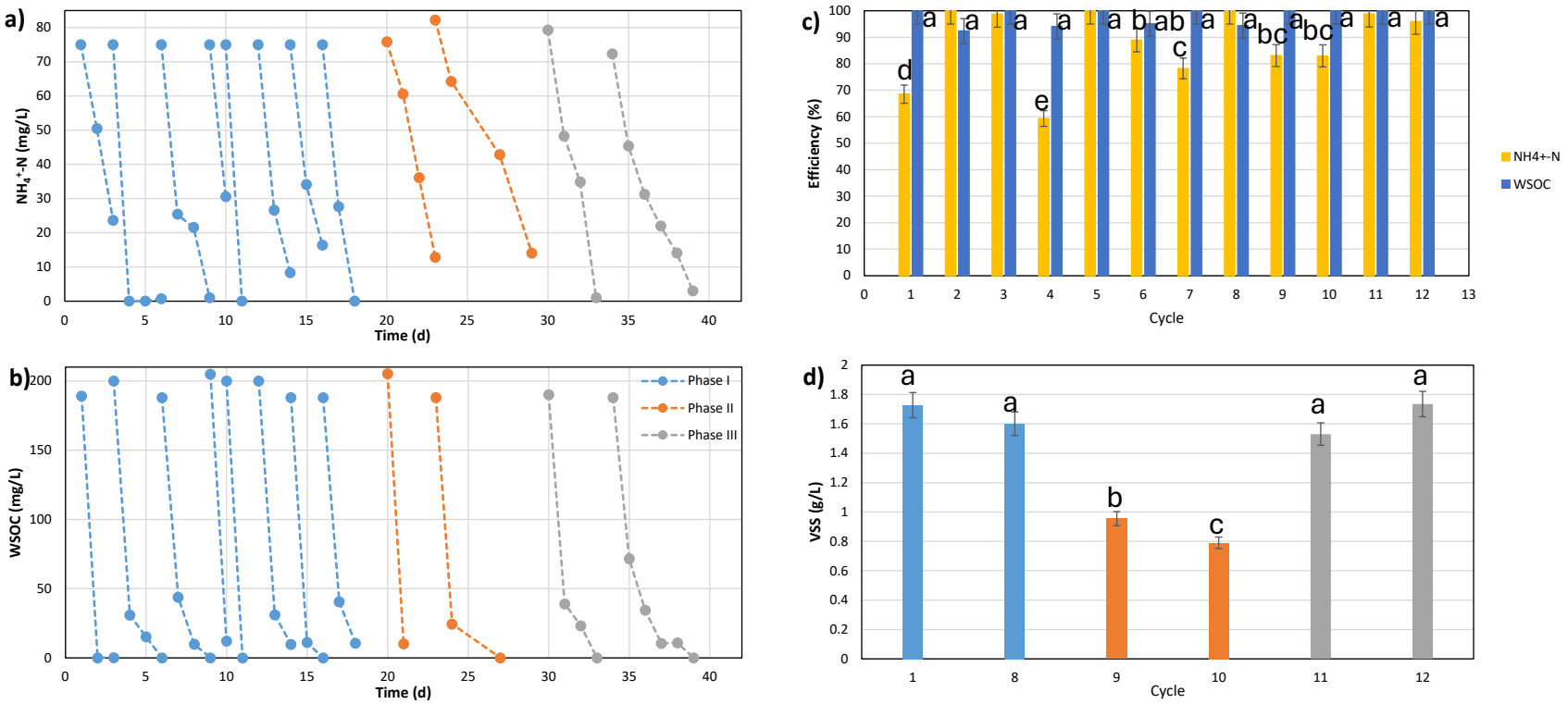


Figure 3.1 – Evolution of a) ammonia nitrogen (NH_4^+–N, mg/L), b) water soluble organic carbon (WSOC, mg/L), vs time (days) during Phases I, II, and III; and c) NH_4^+–N and WSOC removal efficiencies (%), d) volatile suspended solids (VSS, g/L) thorough 12 cycles of operation of the fed-batch reactor (F-BR).

3.3.2 The impact of MIT on the nitrification-denitrification process in moving-bed biofilm reactors

An NH_4^+–N and NO_3^-–N removal of approximately 13 – 87 and 42 – 100%, 75 – 100 and 58 – 100%, and 0 – 64 and 0 – 100% (Fig. 3.2a,b) was achieved during the 1st, 2nd, and 3rd Period in MBBR-N and MBBR-D, respectively, which were operated for over 136 days.

3.3.2.1 Nitrification

During the 1st Period (days 0 – 59), the ammonia nitrogen concentration in the MBBR-N statistically increased ($p < 0.05$) from approximately 10 to 42 mg/L (Fig. 3.2a). This could be attributed to the failure of the temperature control system due to a technical issue, which was used to maintain a constant temperature of 20 ± 2 °C throughout the studied periods. Indeed, temperature fluctuations can affect the nitrification efficiency, as shown by the variation of the Arrhenius coefficient (θ) of 1.086 – 1.109 reported for MBBRs in a temperature range between 10 and 28 °C (Young et al., 2017). A further reason could be the decline of ammonia removal occurring during the acclimation period. For instance, Delatolla et al. (Delatolla et al., 2010) reported lower measured ammonia removals by AOB biomass in an MBBR system due to the acclimatization phase. Afterwards (2nd Period, days 60 – 97), the temperature control was repristinated, and the nitrification efficiency significantly improved ($p < 0.05$), reaching an NH_4^+–N concentration of below 10 mg/L in the MBBR-N after 86 days. This would suggest that the operative chemoautotrophic bacteria (i.e., AOB and NOB) likely achieved a symbiotic relationship that contributed to the consistent maintenance of nitrification performance (Wittebolle et al., 2008). Therefore, in the 3rd Period a concentration of 0.1 and 1.0 mg MIT/L between 98 – 120 and 121 – 136 days was studied in the MBBR-N.

From day 98 to day 101, the ammonia nitrogen concentration reached approximately 77 mg/L (Fig. 3.2a) in the MBBR-N, thus indicating that the nitrification was wholly inhibited at only 0.1 mg MIT/L. This is generally shown after adding organic pollutants to a nitrification system (Amat et al., 2015). For instance, Yang et al. (Yang et al., 2023) reported that 5 mg/L of 2-chloro-6-trichloromethylpyridine was sufficient to inhibit nitrification by affecting AOB. Indeed, the presence of MIT, which induced toxicity towards nitrifying bacteria by probably deactivating cell protein thiols (see Section 3.1), was coupled with a water retention time of 2 days, which was not enough to achieve a complete NH_4^+–N oxidation (i.e., up to 5 days in the F-BR, Fig. 3.1a). This is further supported by the effective MIT dosage employed here (i.e., 0.041 mg MIT/g TS), which was similar to that used in the F-BR (i.e., 0.058 – 0.065 mg MIT/g TS). However, between

days 102 – 112, the nitrification efficiency gradually recovered ($p < 0.05$) reaching a NH_4^+–N removal of about 49%. Similarly, Kookana et al. (Kookana et al., 2022) showed a partial recovery of about 50% for nitrification efficiency in soils subjected to MIT, chloromethyl isothiazolinone, and triethanolamine. The continuous alkalinity addition could have improved nitrification (Yang et al., 2023). Interestingly, the increase of MIT concentration from 0.1 to 1.0 mg/L seemed not to affect NH_4^+–N oxidation, which was enhanced ($p < 0.05$) and achieved approximately 64% efficiency (Fig. 3.2a) between 121 and 136 days. Amat et al. (Amat et al., 2015) showed that a high MIT dosage and long cycle duration are determining factors for inhibiting of the ammonium transformation into nitrite in an SBR. This would suggest that MBBR operation supports nitrification in the presence of emerging organic pollutants (e.g., MIT), as previously shown for ibuprofen, sulfamethoxazole, iomeprol, trimethoprim, acetyl-sulfadiazine and sulfadiazine (Ooi et al., 2018).

3.3.2.2 Denitrification

From day 0 to day 59 (1st Period), the NO_3^-–N concentration rapidly reached 0 mg/L (Fig. 3.2b) in the MBBR-D, thus indicating that the denitrification process started with an efficiency of 100%. Denitrification is a process that entails the stepwise reduction of NO_3^-–N to NO_2^-–N, and ultimately N_2. Typically occurring in anoxic conditions, denitrifying bacteria (DNB) facilitate this process by utilizing organic carbon as an energy source, simultaneously generating alkalinity (Sabba et al., 2015). The heterotrophic denitrification process at ambient conditions is thermodynamically favourable, with the ΔG of about -1381.6 kJ/mol (Tab. 3.2). After 40 days, the NO_2^-–N concentration significantly increased ($p < 0.05$) from approximately 1 to 40 mg/L (Fig. 3.2c), suggesting that the MBBR-D was also inhibited, likely due to the temperature control system (Holtan-Hartwig et al., 2002), as discussed above (see Section 3.2.1). Indeed, in heterotrophic denitrification, the slower rate of NO_2^-–N reduction in the presence of NO_3^-–N can lead to nitrite accumulation, which, in turn, has the potential to hinder bacterial growth (Rezania et al., 2005). During the subsequent 2nd Period (days 60 – 97), the restoration of the temperature control system probably led to the significant decrease of NO_2^-N concentrations from 36 to 0.2 mg/L (Fig. 3.2c), and the denitrification efficiency was again above 99% after few days (Fig. 3.2b).

Between days 98 and 108 (at the beginning of the 3rd Period), the denitrification process was temporarily inhibited in the MBBR-D (Fig. 3.2b), likely due to the simultaneous introduction of MIT and the decrease of nitrate concentrations in the influent by nitrification malfunctioning (Fig. 3.2a). However, when the nitrification

recovered after 112 days (Fig. 3.2a), the NO_3^-–N concentration rapidly achieved approximately 1 mg/L (Fig. 3.2b) and was comparable ($p > 0.05$) to the condition without MIT (i.e., 1st and 2nd Periods) remaining below the threshold for wastewater discharge (Directive, 2000) at the end of the MBBR operation (i.e., 136 days). These results agree with those previously reported in the only study present in the literature (Zeng et al., 2020). Zeng et al. (Zeng et al., 2020) reported that 10 mg MIT/L did not negatively affect denitrification in an SBR, and NO_3^-–N removal was 100% since the first day, either with a continuous or intermittent addition. This is primarily due to insufficient exposure to MIT (i.e., below 1 mg/L), which resulted in challenges for close contact with thiols, rendering the generation of the inhibitory effect unlikely. Also, the increase of MIT concentrations from 0.1 to 1.0 mg/L in the MBBR-D influent seemingly had no impact on the electron consumption rates of denitrification reductases. Surprisingly, rather than inhibition, MIT increase appeared to improve the processes of NO_3^-–N and NO_2^-–N reduction (Fig. 3.2b,c), as reported by Zeng et al. (Zeng et al., 2020).

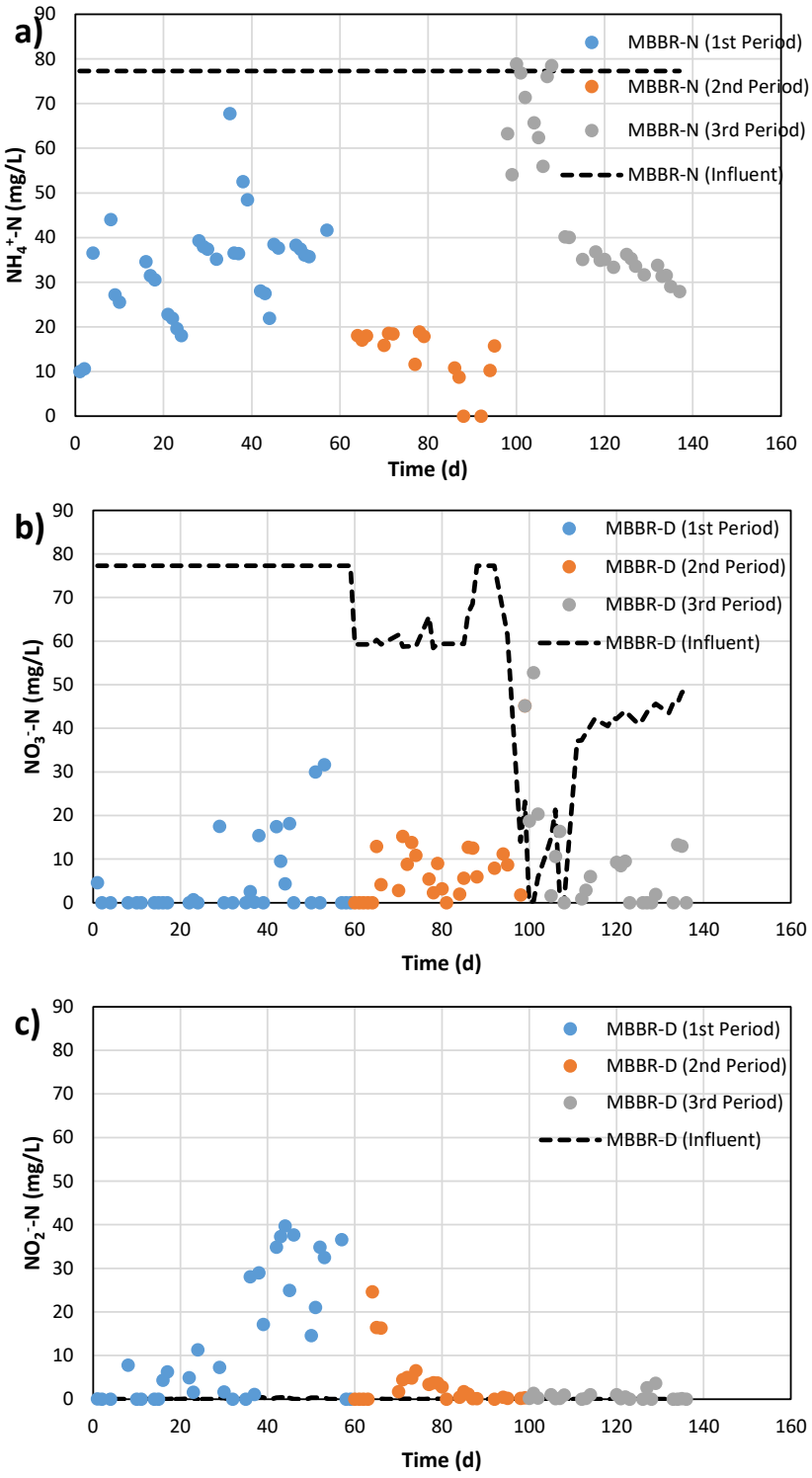


Figure 3.2 – Evolution of a) ammonia (NH_4^+–N, mg/L), b) nitrate (NO_3^-–N, mg/L), c) nitrite (NO_2^-–N, mg/L) vs time (days) in the 1st (enrichment), 2nd (steady phase), 3rd (methyl-4-isothiazolin-3-one) Period during 136 days of moving-bed biofilm reactor (MBBR) operation under nitrification (MBBR-N) and denitrification (MBBR-D) performed in semi-continuous mode.

3.3.3 The influence of MIT on biogas production during the AD process in the sludge line

3.3.3.1 Cumulative methane yield

After 109 days of anaerobic digestion of activated sludge, the cumulative methane production (measured in mL CH_4/g VS) was about 134 mL CH_4/g VS for the control group (Fig. 3.3a). This was not significantly different ($p > 0.05$) from the methane production in the presence of MIT (i.e., 129 mL CH_4/g VS, Fig. 3.3a). This would suggest that MIT slightly impacted the methanogens, which are instead known to be very sensitive to contaminants (Luo et al., 2020). The percentage of gases composing the biogas (i.e., about 53 and 47% for CH_4 and CO_2, respectively) (Fig. 3.2b) (Oslaj et al., 2010) further corroborates this theory as being not statistically different ($p > 0.05$) among the studied conditions. These results are in contrast to a recent study on anaerobic fermentation of waste-activated sludge conducted by Fang et al. (Fang et al., 2023), which obtained a significant reduction of methane yield with 40 mg/g TS of MIT compared to control (i.e., 74 mL CH_4/g VS). This is due mainly to the fact that in our study, the MIT dosage used for the experiment was low (i.e., 0.001 mg/g TS), which is nearer to that found for civil wastewater than that employed by Fang et al. (Fang et al., 2023). Also, the same authors obtained a similar methane yield in the presence of 10 mg MIT/g TS compared to the control test (Fang et al., 2023). In each case, more studies are needed to confirm this evidence.

The modified Gompertz model (Fig. 3.2a) better simulated the BMP data for the control and MIT conditions due to a higher adj. R^2 than the Logistic kinetic (Tab. 3.3). The kinetic parameters are shown in Tab. 3.2. The adj. R^2 of the modified Gompertz model for the control group was higher (i.e., 0.967, Tab. 3.3) than that obtained for the MIT condition (i.e., 0.963, Tab. 3.3), indicating that the model better represents the methane generation profile and the ultimate methane yield (G_u) (i.e., approximately 127 mL CH_4/g VS, Tab. 3.3), which was closer to the methane obtained experimentally (Fig. 3.3a) (Kafle and Chen, 2016). Also, the results showed that the maximum rate of methane production (R_m) for the control test was 0.044 mL CH_4/g VS·d (Tab. 3.3), which was similar to the value obtained with the MIT group (i.e., 0.046 mL CH_4/g VS·d). This suggests that there is a similar level of microbial activity (Oliva et al., 2021) after the MIT addition. Interestingly, the lag phase (λ) of the control was slightly lower (i.e., 13.367 days) than that of the MIT condition (i.e., 12.763 days) (Tab. 3.3), according to the modified Gompertz model. Therefore, MIT at low dosage (i.e., 0.001 mg/g TS) can even stimulate bacteria under anaerobic conditions during the first days due to a lower

acclimation time (Mainardis et al., 2019) and was likely used as a substrate for methane generation, as suggested by MIT degradation (Fig. 3.4b).

3.3.3.2 Volatile fatty acid generation

The AD of activated sludge leads to the production of VFAs as reaction intermediates, which are generally used as indicators of the stability of the process (Mancini et al., 2018). In this work, the overall VFA accumulation shown as the sum of acetic (HAc), isobutyric, butyric, isovaleric, valeric and heptanoic acids on an equivalent HAc basis (mg Hac/L), was monitored for 28 days in both control and MIT group (Fig. 3.3 c,d) (Rubio et al., 2022). The main components of VFAs were isobutyric, butyric, valeric, and heptanoic acids, which together accounted for more than 85% of the total VFA concentration (Fig. 3.3 c,d). There was an accumulation of VFAs within the first 2 – 5 days (Fig. 3.3 c,d), followed by a rapid depletion of VFAs from days 5 and 12 onwards in the control (i.e., from about 1,118 to 616 mg HAc/L) and MIT (i.e., from about 1,686 to 1,134 mg HAc/L) groups (Fig. 3.3 c,d), respectively. This confirms the onset of methanogenesis (Lin et al., 2017), as supported by the increase in biomethane yield and lag-phase values (Fig. 3.3 a, and Tab. 3.3). After 28 days, VFAs significantly decreased ($p > 0.05$) below 300 mg Hac/L (Fig. 3.3 c,d) until no accumulation was eventually detected from day 28 onward. The lack of VFAs buildup in the following days of AD suggests a gradual hydrolysis of the substrate, with methanogenic archaea operating at a pace comparable to hydrolytic and acidogenic bacteria (Oliva et al., 2022b).

However, the MIT condition had a 1.5-fold higher VFA concentration than the control (Fig. 3.3 c,d), which could indicate a decoupling between the acidogenic and methanogenic phases (Wahid et al., 2020). This phenomenon could be associated with the limited disruption of the activated sludge, resulting in the low release of bioavailable organics for microbial bioconversion in the control (Zhu et al., 2022). Thus, the occurrence of MIT can enhance VFA accumulation during AD. Fang et al. (Fang et al., 2023) reported a 2-fold higher VFA concentration in the presence of 10 mg MIT/g TS than the control group (i.e., 343 mg COD/L) during the anaerobic fermentation of activated sludge. Accordingly, the percentage of acetic acid was enhanced in the presence of an MIT dosage of 0.001 mg/g TS. Notwithstanding, the highest VFA production obtained with MIT never exceeded the threshold of about 2,000 mg HAc/L, which is known to inhibit methanogenic archaea (Xiao et al., 2013). This was probably due to the favorable I/S ratio of 2 used in this study for AD (Papirio, 2020), resulting in a similar methane yield to the control group.

Table 3.2 – The Gibbs free energy change (ΔG) for nitrification and denitrification processes is calculated as the difference between the standard Gibbs free energy of formation (ΔG°f) of products and reactants, obtained through a summary of each species involved.

Process	Reaction	ΔG^{of}(product) [kJ/mol]	$\Delta G°_f$(reactants) [kJ/mol]	ΔG° [kJ/mol]	$\Delta G°_{TOT}$ [kJ/mol]
Nitrification	$NH_3+(3/2)O_2 \rightarrow NO_2^- + 2H^+ + H_2O$	-340.8	-16.5	-324.3	-94.3
	$NO_2^- + (1/2)O_2 + H_2O \rightarrow NO_3^- + 2H^+$	-110.8	-340.8	230	
Denitrification	$2NO_3^- + 8H^+ + 6e^- \rightarrow 2NO_2^- + 4H_2O$	-1155.8	-221.6	-934.2	-1381.6
	$2NO_2^- + 4H^+ + 4e^- \rightarrow N_2O + 3H_2O$	-711.3	-207.4	-503.9	
	$2NO + 2H_2O \rightarrow N_2O + 4H^+ + 4e^-$	0	-293.6	293.6	
	$N_2O + 2H^+ + 2e^- \rightarrow N_2 + H_2O$	-237.1	0	-237.1	

Table 3.3 – Kinetic model of cumulative methane yield (mL CH_4/g VS) under the control and 2-methyl-4-isothiazolin-3-one (MIT) groups during 109 days of BMP test.

Kinetic parameters λ, R_m, G_u, Residual Sum of Squares (RSS) and the adjusted R^2 (correlation coefficient) refer to those used in the modified Gompertz and Logistic models.

Model	Kinetic parameters	*Control*	*MIT*
Gompertz $G_t = G_u \cdot exp\left(-exp\left[\frac{R_m \cdot e \cdot (\lambda - t)}{G_u} + 1\right]\right)$	λ (day)	13.637	12.763
	R_m (mL CH_4/g VS·d)	0.044	0.046
	G_u (mL CH_4/g VS)	127.181	121.398
	Adj. R^2	0.967	0.963
	RSS	1379.909	1443.639
Logistic $G_t = \frac{G_u}{1 + exp\left(\frac{4R_m \cdot (\lambda - t)}{G_u}\right)}$	λ (day)	22.191	21.055
	R_m (mL CH_4/g VS·d)	0.062	0,063

	G_u (mL CH_4/g VS)	124.210	118.890
	Adj. R^2	0.950	0.944
	RSS	2111.542	2167.301

3.3.4 Kinetics and mechanism of methylisothiazolinone removal under aerobic, anoxic and anaerobic conditions

Among the tested conditions (Fig. 3.4a,b), the microorganisms in the activated sludge demonstrated the ability to completely remove MIT within 60 and 1,440 minutes of incubation during the nitrification-denitrification process by increasing the initial MIT concentration from 0.1 to 1.0 mg/L in the MBBR influent. Amat et al. (Amat et al., 2015) achieved a 55 – 80% removal during nitrification in an SBR reactor after 12 hours. Zeng et al. (Zeng et al., 2020) showed a decrease of MIT concentration from 8 to only 5 mg/L during denitrification under saline conditions. This would further confirm the beneficial effect of MBBR configuration on the microbial community under MIT stress. Besides, the lower concentrations of MIT here studied to simulate a civil wastewater could have affected these results. Indeed, the increase of MIT concentrations from 0.1 to 1.0 mg/L led to the rise of MIT removal time from 30 and 60 to 360 and 1,440 minutes (Fig. 3.4a) under aerobic and anoxic conditions, respectively. Notwithstanding, the increase of MIT concentrations only increased the time to achieve 100% removal but would not justify the lower efficiency obtained in other studies (Amat et al., 2015; Zeng et al., 2020). This is further corroborated by the other culture conditions available in the literature. Wang et al. (Wang et al., 2020) showed that 3 mg MIT/L could be entirely degraded by *Scenedesmus* sp. LX1 (i.e., algal consortium) after 4 days. Nowak et al. (Nowak et al., 2020) employed *Phanerochaete chrysosporium* (fungal strain) in water and soil samples to achieve an MIT removal of 100% at 30 mg MIT/L after 1,440 minutes. In each case, to further reduce the stress on nitrifying bacteria in an MBBR configuration, a pre-denitrification process is recommended when the hydraulic retention time is approximately one day, i.e., time to degrade MIT under anoxic conditions completely (Fig. 3.4a).

Also, the time to reach a 100% MIT removal was significantly increased under anaerobic conditions up to 22 days (Fig. 3.4b) compared to aerobic and anoxic

environments (Fig. 3.4a). This behavior was also reported for emerging contaminants by Biel-Maeso (Biel-Maeso et al., 2019), which obtained the increase of half-life time from 1 to 103 days evaluating the degradation of pharmaceutical compounds (e.g., sulfamethoxazole, carbamazepine, hydrochlorothiazide). This would not represent an issue for wastewater discharge since the sludge age in a wastewater treatment plant is generally up to 20 days (Ge et al., 2013).

Biodegradation (Fig. 3.5) was the primary mechanism for removing MIT by likely involving heterotrophic bacteria (Zeng et al., 2020) since the effect of physical adsorption onto sludge and abiotic effect (e.g., adsorption onto carriers, abiotic degradation) did not significantly contribute to the MIT removal (Fig. 3.4a). The biodegradation followed a first-order exponential decay ($y = A_1 \cdot \exp(-x/t_1) + y_0$) and a linear kinetic ($y = a + b \cdot x$) for the aerobic/anoxic (adj. $R^2 = 0.882 – 0.991$) and anaerobic conditions (adj. $R^2 = 0.997$) (Tab. 3.4), respectively. These obtained results are in agreement with the scientific literature about the degradation of MIT or organic pollutants (Wang et al., 2020; Yap et al., 2020). The biotransformation of MIT likely followed three main steps (Wang et al., 2020): firstly, the sulfhydryl group underwent ring cleavage and methylation, which led to the loss of the nitrogenous group ($-NH-CH_3$); secondly, the aldehyde group was oxidized into a carboxyl group; lastly, the carboxyl group dissociated in alkaline conditions.

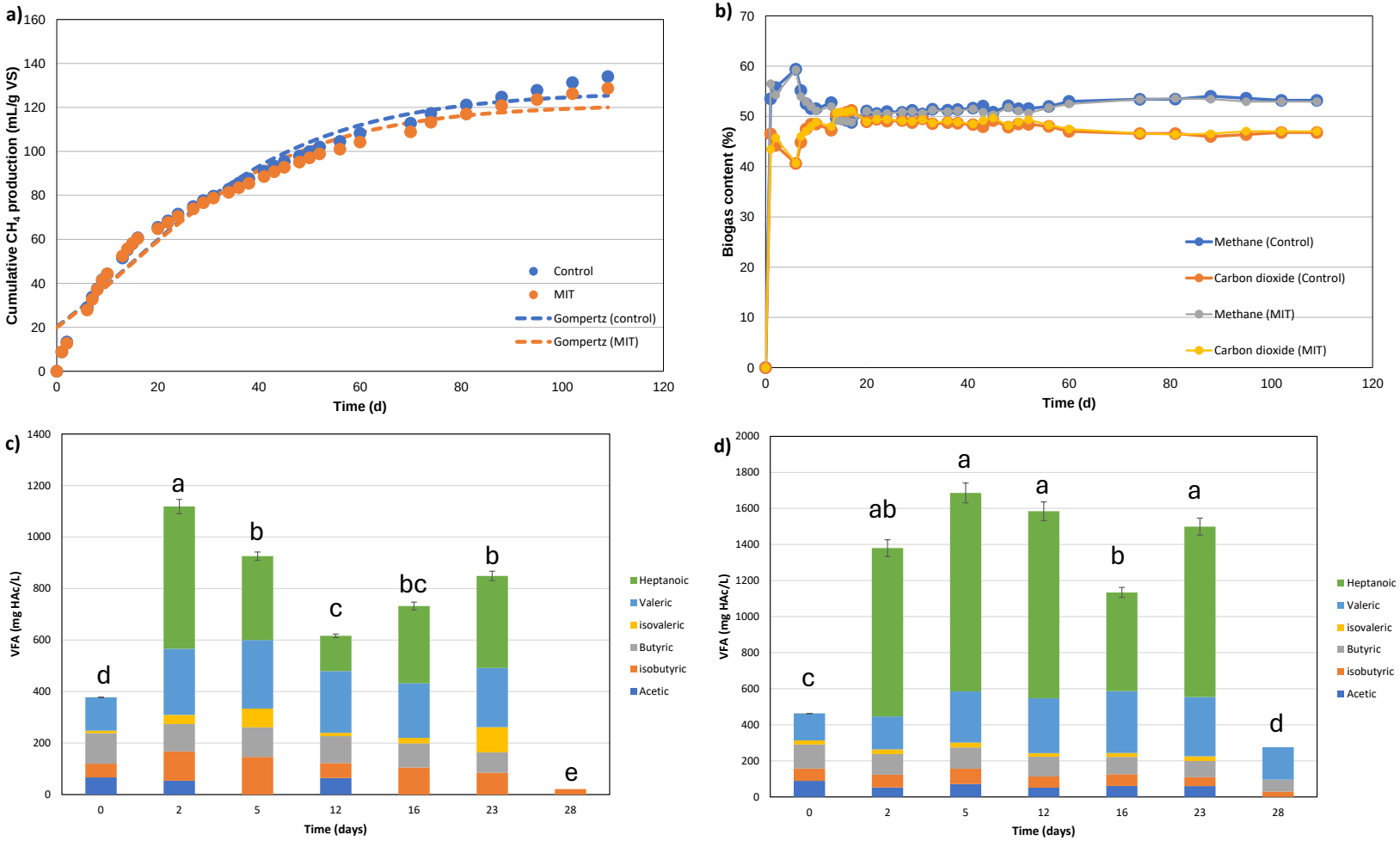


Figure 3.3 – a) Cumulative methane yield (mL CH_4/g VS); b) biogas composition (%) in terms of CH_4 and CO_2; total VFA evolution (mg HAc/L) in c) the control and d) methyl-4-isothiazolin-3-one (MIT) groups during 109 days of anaerobic digestion. The dissimilar letters (Tukey test) denote significant differences ($p < 0.05$).

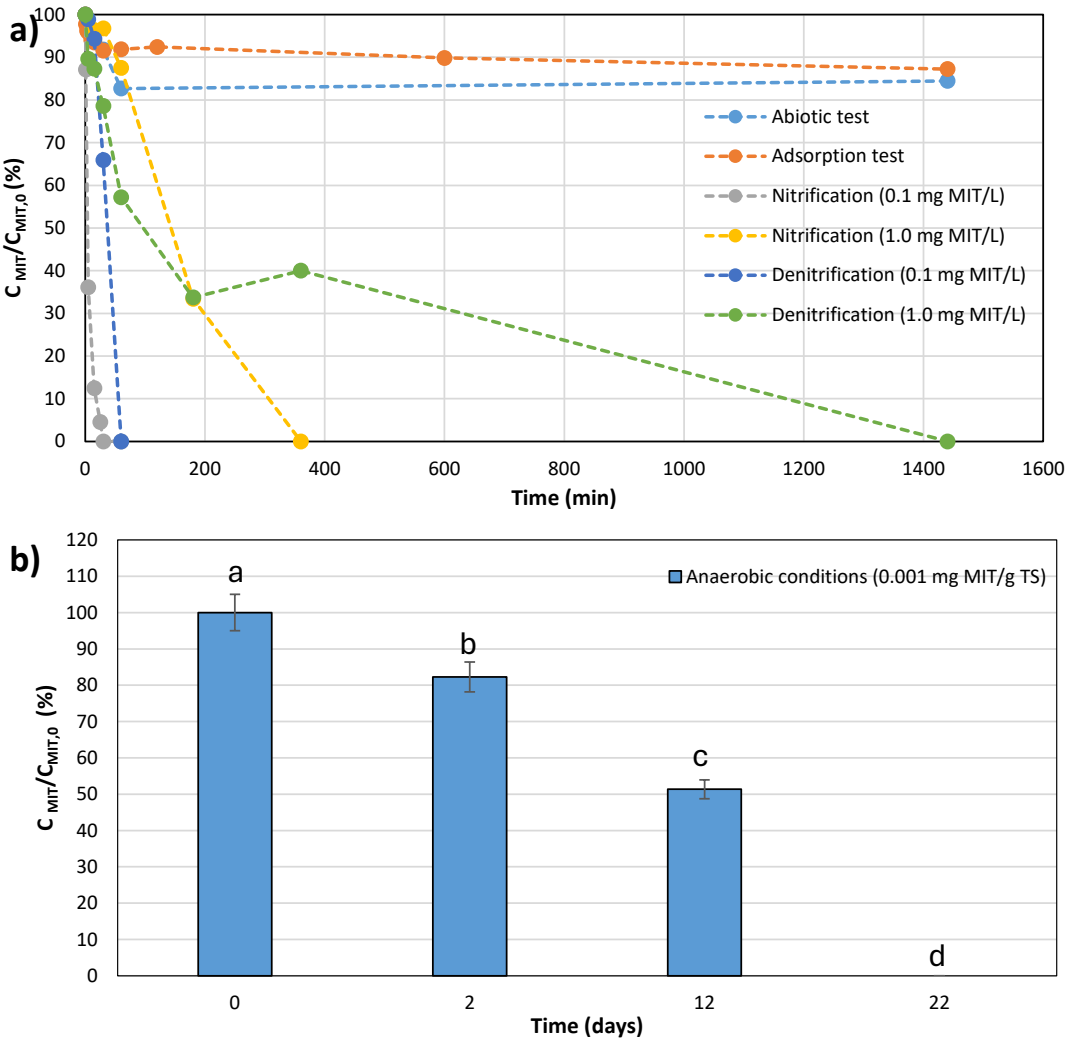


Figure 3.4 – Methyl-4-isothiazolin-3-one (MIT) degradation ($C_{MIT,i}/C_{MIT,0}$, %) during a) nitrification/denitrification processes and b) anaerobic digestion. The dissimilar letters (Tukey test) denote significant differences ($p < 0.05$).

Table 3.4 – Kinetic models of methyl-4-isothiazolin-3-one (MIT) degradation under aerobic, anoxic, and anaerobic groups in moving-bed biofilm reactors and biochemical methane potential test.

Model	Kinetic parameters	***Aerobic (0.1 mg MIT/L)***	***Aerobic (1.0 mg MIT/L)***	***Anoxic (0.1 mg MIT/L)***	***Anoxic (1.0 mg MIT/L)***
First-order exponential decay $y = A_1 \cdot \exp(-x/t_1) + y_0$	t_1	5.129	407.299	-41.323	187.976
	A_1	99.386	181.722	-31.496	83.316
	y_0	2.170	-76.852	134.215	8.654
	Adj. R^2	0.991	0.976	0.987	0.882
	RSS	62.971	153.237	47.159	699.314
		Anaerobic (0.001 mg MIT/ g TS)			
Linear kinetic $y = a + b \cdot x$	a	97.027			
	b	-0.003			
	Adj. R^2	0.977			
	RSS	87.618			

Kinetic parameters t_1, A_1, y_0, a, b, Residual Sum of Squares (RSS) and the adjusted R^2 (correlation coefficient) refer to those used in the first-order exponential decay and linear kinetic models.

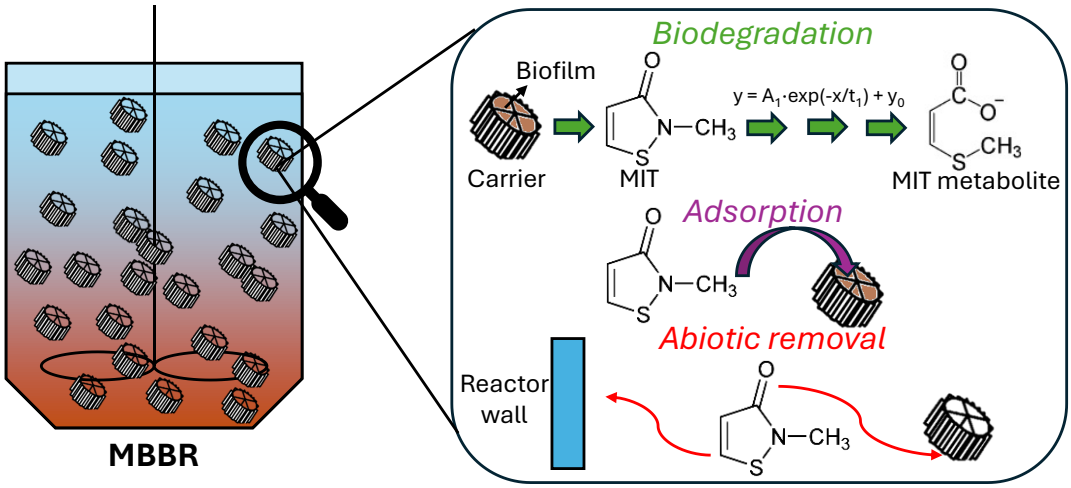


Figure 3.5 – Proposed mechanisms involved during methyl-4-isothiazolin-3-one (MIT) removal.

3.5 Conclusions

This thesis treated MIT-containing civil wastewater through nitrification-denitrification in an MBBR system for the first time. Nitrifying bacteria were initially inhibited entirely at only 0.1 mg MIT/L, and subsequently, the nitrification efficiency gradually recovered, reaching a NH_4^+–N removal of about 49%, which was enhanced at 1.0 mg MIT/L (i.e., 64%). The denitrification process was temporarily inhibited but achieved a 100% reduction of nitrite and nitrate after the increase of MIT concentration from 0.1 to 1.0 mg/L. The presence of sludge AD in an urban WWTP should not be of concern since the cumulative methane yield was not affected by MIT addition. MIT was completely removed under nitrification-denitrification and anaerobic conditions after 1 and 22 days, respectively, thus indicating the effectiveness of the MBBR. Future studies should evaluate the impact of possible MIT secondary metabolites in the sewage sludge via ecotoxicological tests.

3.6 References

Aerts, O., Meert, H., Janssens, S., Sprengers, M., Chapelle, K., Bensch, L., Apers, S., Lambert, J., 2015. A sudden flare-up of a quiescent oral lichen planus: methylisothiazolinone as the prime suspect? Contact Dermatitis 72, 186–189. https://doi.org/10.1111/cod.12343

Amat, A.M., Arques, A., López-Pérez, M.F., Nacher, M., Palacios, S., 2015. Effect of Methylisothiazolinone on Biological Treatment: Efficiency of SBRs and Bioindicative Studies. Environ. Eng. Sci. 32, 479–485. https://doi.org/10.1089/ees.2014.0283

APAT, IRSA-CNR, 2003. Agenzia per la Protezione dell'Ambiente e per i Servizi Tecnici (APAT), Istituto di Ricerca sulle Acque del Consiglio Nazionale delle Ricerche (IRSA-CNR). 2003. Manuali e linee Guid. 29.

APHA, 2012. Standard Methods for the Examination of Water and Wastewater, 22nd edition. Am. Public Heal. Assoc. Am. Water Work. Assoc. Water Environ. Fed. https://doi.org/10.1520/E0536-16.2

Aygun, A., Nas, B., Berktay, A., 2008. Influence of High Organic Loading Rates on COD Removal and Sludge Production in Moving Bed Biofilm Reactor. Environ. Eng. Sci. 25, 1311–1316. https://doi.org/10.1089/ees.2007.0071

Berthet, A., Spring, P., Vernez, D., Plateel, G., Hopf, N.B., 2017. Ex vivo human skin permeation of methylchloroisothiazolinone (MCI) and methylisothiazolinone (MI). Arch. Toxicol. 91, 3529–3542. https://doi.org/10.1007/s00204-017-1978-x

Bhave, P.P., Naik, S., Salunkhe, S.D., 2020. Performance Evaluation of Wastewater Treatment Plant. Water Conserv. Sci. Eng. 5, 23–29. https://doi.org/10.1007/s41101-020-00081-x

Bianco, F., Ali Saeed Al-Gheethi, A., Race, M., 2023a. Coupling of Anammox Activity and PAH Biodegradation: Current Insights and Future Directions. Processes 11, 458. https://doi.org/10.3390/pr11020458

Bianco, F., Monteverde, G., Race, M., Papirio, S., Esposito, G., 2020. Comparing performances, costs and energy balance of ex situ remediation processes for PAH-contaminated marine sediments. Environ. Sci. Pollut. Res. 27, 19363–19374. https://doi.org/10.1007/s11356-020-08379-y

Bianco, F., Race, M., Papirio, S., Esposito, G., 2023b. Phenanthrene removal from a spent sediment washing solution in a continuous-flow stirred-tank reactor. Environ. Res. 228, 115889. https://doi.org/10.1016/j.envres.2023.115889

Bianco, F., Race, M., Papirio, S., Esposito, G., 2022a. Phenanthrene biodegradation in a fed–batch reactor treating a spent sediment washing solution: Techno–economic implications for the recovery of ethanol as extracting agent. Chemosphere 286, 131361. https://doi.org/10.1016/j.chemosphere.2021.131361

Bianco, F., Race, M., Papirio, S., Oleszczuk, P., Esposito, G., 2022b. Coupling of desorption of phenanthrene from marine sediments and biodegradation of the sediment washing solution in a novel biochar immobilized–cell reactor. Environ. Pollut. 308, 119621. https://doi.org/10.1016/J.ENVPOL.2022.119621

Bianco, F., Şenol, H., Papirio, S., Zenk, H., Kara, A., Atasoy, S., 2022c. Combined ultrasonic–hydrothermal pretreatment to improve the biomethane potential of hazelnut shell. Biomass and Bioenergy 165, 106554. https://doi.org/10.1016/j.biombioe.2022.106554

Biel-Maeso, M., González-González, C., Lara-Martín, P.A., Corada-Fernández, C., 2019. Sorption and degradation of contaminants of emerging concern in soils under aerobic and anaerobic conditions. Sci. Total Environ. 666, 662–671.

https://doi.org/10.1016/j.scitotenv.2019.02.279

Bramwell, D.A.P., Laha, S., 2000. Effects of surfactant addition on the biomineralization and microbial toxicity of phenanthrene. Biodegradation 11, 263–277. https://doi.org/https://doi.org/10.1023/A:1011121603049

Carbajo, J.B., Perdigón-Melón, J.A., Petre, A.L., Rosal, R., Letón, P., García-Calvo, E., 2015. Personal care product preservatives: Risk assessment and mixture toxicities with an industrial wastewater. Water Res. 72, 174–185. https://doi.org/10.1016/j.watres.2014.12.040

Delatolla, R., Tufenkji, N., Comeau, Y., Gadbois, A., Lamarre, D., Berk, D., 2010. Investigation of Laboratory-Scale and Pilot-Scale Attached Growth Ammonia Removal Kinetics at Cold Temperature and Low Influent Carbon. Water Qual. Res. J. 45, 427–436. https://doi.org/10.2166/wqrj.2010.042

Directive, W.F., 2000. Directive 2000/60/EC of the European Parliament and of the Council of 23 October 2000 establishing a framework for Community action in the field of water policy. Off J Eur Comm L 327, 1–73.

Fang, S., Cao, W., Wu, Q., Cheng, S., Yang, Y., Liu, J., Wu, Y., Fang, F., Feng, Q., Cao, J., Luo, J., 2023. Multifaceted roles of methylisothiazolinone intervention in sludge disintegration and acidogenic and methanogenic pathways for efficient carboxylate production during anaerobic fermentation. Chem. Eng. J. 472, 145022. https://doi.org/10.1016/j.cej.2023.145022

Ge, H., Batstone, D.J., Keller, J., 2013. Operating aerobic wastewater treatment at very short sludge ages enables treatment and energy recovery through anaerobic

sludge digestion. Water Res. 47, 6546–6557. https://doi.org/10.1016/j.watres.2013.08.017

Holliger, C., Alves, M., Andrade, D., Angelidaki, I., Astals, S., Baier, U., Bougrier, C., Buffière, P., Carballa, M., de Wilde, V., Ebertseder, F., Fernández, B., Ficara, E., Fotidis, I., Frigon, J.-C., de Laclos, H.F., Ghasimi, D.S.M., Hack, G., Hartel, M., Heerenklage, J., Horvath, I.S., Jenicek, P., Koch, K., Krautwald, J., Lizasoain, J., Liu, J., Mosberger, L., Nistor, M., Oechsner, H., Oliveira, J.V., Paterson, M., Pauss, A., Pommier, S., Porqueddu, I., Raposo, F., Ribeiro, T., Rüsch Pfund, F., Strömberg, S., Torrijos, M., van Eekert, M., van Lier, J., Wedwitschka, H., Wierinck, I., 2016. Towards a standardization of biomethane potential tests. Water Sci. Technol. 74, 2515–2522. https://doi.org/10.2166/wst.2016.336

Holtan-Hartwig, L., Dörsch, P., Bakken, L.., 2002. Low temperature control of soil denitrifying communities: kinetics of N2O production and reduction. Soil Biol. Biochem. 34, 1797–1806. https://doi.org/10.1016/S0038-0717(02)00169-4

Iannacone, F., Di Capua, F., Granata, F., Gargano, R., Pirozzi, F., Esposito, G., 2019. Effect of carbon-to-nitrogen ratio on simultaneous nitrification denitrification and phosphorus removal in a microaerobic moving bed biofilm reactor. J. Environ. Manage. 250, 109518. https://doi.org/10.1016/j.jenvman.2019.109518

Kafle, G.K., Chen, L., 2016. Comparison on batch anaerobic digestion of five different livestock manures and prediction of biochemical methane potential (BMP) using different statistical models. Waste Manag. 48, 492–502. https://doi.org/10.1016/j.wasman.2015.10.021

Kookana, R.S., Williams, M., Gregg, A., Semmler, A., Du, J., Apte, S.C., 2022. Sorption, degradation and microbial toxicity of chemicals associated with hydraulic fracturing fluid and produced water in soils. Environ. Pollut. 309, 119754. https://doi.org/10.1016/j.envpol.2022.119754

Kostrytsia, A., Papirio, S., Khodzhaev, M., Morrison, L., Collins, G., Lens, P.N.L., Ijaz, U.Z., Esposito, G., 2022. Biofilm carrier type affects biogenic sulfur-driven denitrification performance and microbial community dynamics in moving-bed biofilm reactors. Chemosphere 287, 131975. https://doi.org/10.1016/j.chemosphere.2021.131975

Li, A., Wu, Q.-Y., Tian, G.-P., Hu, H.-Y., 2016. Effective degradation of methylisothiazolone biocide using ozone: Kinetics, mechanisms, and decreases in toxicity. J. Environ. Manage. 183, 1064–1071. https://doi.org/10.1016/j.jenvman.2016.08.057

Lin, Y., Liang, J., Zeng, C., Wang, D., Lin, H., 2017. Anaerobic digestion of pulp and paper mill sludge pretreated by microbial consortium OEM1 with simultaneous degradation of lignocellulose and chlorophenols. Renew. Energy 108, 108–115. https://doi.org/10.1016/j.renene.2017.02.049

Lundov, M.D., Opstrup, M.S., Johansen, J.D., 2013. Methylisothiazolinone contact allergy – a growing epidemic. Contact Dermatitis 69, 271–275. https://doi.org/10.1111/cod.12149

Luo, J., Zhang, Q., Zhao, J., Wu, Y., Wu, L., Li, H., Tang, M., Sun, Y., Guo, W., Feng, Q., Cao, J., Wang, D., 2020. Potential influences of exogenous pollutants

occurred in waste activated sludge on anaerobic digestion: A review. J. Hazard. Mater. 383, 121176. https://doi.org/10.1016/j.jhazmat.2019.121176

Mainardis, M., Flaibani, S., Trigatti, M., Goi, D., 2019. Techno-economic feasibility of anaerobic digestion of cheese whey in small Italian dairies and effect of ultrasound pre-treatment on methane yield. J. Environ. Manage. 246, 557–563. https://doi.org/10.1016/j.jenvman.2019.06.014

Mancini, G., Papirio, S., Lens, P.N.L., Esposito, G., 2018. Anaerobic Digestion of Lignocellulosic Materials Using Ethanol-Organosolv Pretreatment. Environ. Eng. Sci. 35, 953–960. https://doi.org/10.1089/ees.2018.0042

Morgenroth, E., Sørensen, K.H., 2023. Biofilm modelling and biofilm reactors, in: Biological Wastewater Treatment. IWA Publishing, pp. 539–559. https://doi.org/10.2166/9781789062304_0539

Nowak-Lange, M., Niedziałkowska, K., Lisowska, K., 2022. Cosmetic Preservatives: Hazardous Micropollutants in Need of Greater Attention? Int. J. Mol. Sci. 23, 14495. https://doi.org/10.3390/ijms232214495

Nowak, M., Zawadzka, K., Lisowska, K., 2020. Occurrence of methylisothiazolinone in water and soil samples in Poland and its biodegradation by Phanerochaete chrysosporium. Chemosphere 254, 126723. https://doi.org/10.1016/j.chemosphere.2020.126723

Oliva, A., Papirio, S., Esposito, G., Lens, P.N.L., 2023. Impact of Chemical and Physical Pretreatment on Methane Potential of Peanut Shells. Energies 16, 4698. https://doi.org/10.3390/en16124698

Oliva, A., Papirio, S., Esposito, G., Lens, P.N.L., 2022a. Ultrasounds application for nut and coffee wastes valorisation via biomolecules solubilisation and methane production. Waste Manag. 150, 373–382. https://doi.org/10.1016/j.wasman.2022.07.010

Oliva, A., Tan, L.C., Papirio, S., Esposito, G., Lens, P.N.L., 2022b. Use of N-Methylmorpholine N-oxide (NMMO) pretreatment to enhance the bioconversion of lignocellulosic residues to methane. Biomass Convers. Biorefinery 1, 1–18. https://doi.org/10.1007/s13399-022-03173-x

Oliva, A., Tan, L.C., Papirio, S., Esposito, G., Lens, P.N.L., 2021. Effect of methanol-organosolv pretreatment on anaerobic digestion of lignocellulosic materials. Renew. Energy 169, 1000–1012. https://doi.org/https://doi.org/10.1016/j.renene.2020.12.095

Ooi, G.T.H., Tang, K., Chhetri, R.K., Kaarsholm, K.M.S., Sundmark, K., Kragelund, C., Litty, K., Christensen, A., Lindholst, S., Sund, C., Christensson, M., Bester, K., Andersen, H.R., 2018. Biological removal of pharmaceuticals from hospital wastewater in a pilot-scale staged moving bed biofilm reactor (MBBR) utilising nitrifying and denitrifying processes. Bioresour. Technol. 267, 677–687. https://doi.org/10.1016/j.biortech.2018.07.077

Oslaj, M., Mursec, B., Vindis, P., 2010. Biogas production from maize hybrids. Biomass and Bioenergy 34, 1538–1545. https://doi.org/10.1016/j.biombioe.2010.04.016

Paijens, C., Bressy, A., Frère, B., Tedoldi, D., Mailler, R., Rocher, V., Neveu, P.,

Moilleron, R., 2021. Urban pathways of biocides towards surface waters during dry and wet weathers: Assessment at the Paris conurbation scale. J. Hazard. Mater. 402, 123765. https://doi.org/10.1016/j.jhazmat.2020.123765

Pan, D., Shao, S., Zhong, J., Wang, M., Wu, X., 2022. Performance and mechanism of simultaneous nitrification–denitrification and denitrifying phosphorus removal in long-term moving bed biofilm reactor (MBBR). Bioresour. Technol. 348, 126726. https://doi.org/10.1016/j.biortech.2022.126726

Papirio, S., 2020. Coupling acid pretreatment and dosing of Ni and Se enhances the biomethane potential of hazelnut skin. J. Clean. Prod. 262, 121407. https://doi.org/10.1016/j.jclepro.2020.121407

Peng, L., Liu, H., Wang, W.-L., Xu, Z.-B., Ni, X.-Y., Wu, Y.-H., Wu, Q.-Y., Hu, H.-Y., 2020. Degradation of methylisothiazolinone biocide using a carbon fiber felt-based flow-through electrode system (FES) via anodic oxidation. Chem. Eng. J. 384, 123239. https://doi.org/10.1016/j.cej.2019.123239

Piculell, M., Suarez, C., Li, C., Christensson, M., Persson, F., Wagner, M., Hermansson, M., Jönsson, K., Welander, T., 2016. The inhibitory effects of reject water on nitrifying populations grown at different biofilm thickness. Water Res. 104, 292–302. https://doi.org/10.1016/j.watres.2016.08.027

Rahimi, S., Modin, O., Mijakovic, I., 2020. Technologies for biological removal and recovery of nitrogen from wastewater. Biotechnol. Adv. 43, 107570. https://doi.org/10.1016/j.biotechadv.2020.107570

Rezania, B., Cicek, N., Oleszkiewicz, J.A., 2005. Kinetics of hydrogen-dependent

denitrification under varying pH and temperature conditions. Biotechnol. Bioeng. 92, 900–906. https://doi.org/10.1002/bit.20664

Rodríguez, D.C., Ramírez, O., Mesa, G.P., 2011. Behavior of nitrifying and denitrifying bacteria in a sequencing batch reactor for the removal of ammoniacal nitrogen and organic matter. Desalination 273, 447–452. https://doi.org/10.1016/j.desal.2011.01.068

Rubio, J.A., Fdez-Güelfo, L.A., Romero-García, L.I., Wilkie, A.C., García-Morales, J.L., 2022. Start-up of the mesophilic anaerobic co-digestion of two-phase olive-mill waste and cattle manure using volatile fatty acids as process control parameter. Fuel 325, 124901. https://doi.org/10.1016/j.fuel.2022.124901

Sabba, F., Picioreanu, C., Pérez, J., Nerenberg, R., 2015. Hydroxylamine Diffusion Can Enhance N 2 O Emissions in Nitrifying Biofilms: A Modeling Study. Environ. Sci. Technol. 49, 1486–1494. https://doi.org/10.1021/es5046919

Schopf, A., Delatolla, R., Mathew, R., Tsitouras, A., Kirkwood, K.M., 2018. Investigation of copper inhibition of nitrifying moving bed biofilm (MBBR) reactors during long term operations. Bioprocess Biosyst. Eng. 41, 1485–1495. https://doi.org/10.1007/s00449-018-1976-2

Şenol, H., Çakır, İ.T., Bianco, F., Görgün, E., 2023. Improved methane production from ultrasonically-pretreated secondary sedimentation tank sludge and new model proposal: Time series (ARIMA). Bioresour. Technol. 129866. https://doi.org/10.1016/j.biortech.2023.129866

Şenol, H., Zenk, H., 2020. Determination of the biogas potential in cities with hazelnut

production and examination of potential energy savings in Turkey. Fuel 270, 117577. https://doi.org/10.1016/j.fuel.2020.117577

Speksnijder, P., van Ravestijn, J., de Voogt, P., 2010. Trace analysis of isothiazolinones in water samples by large-volume direct injection liquid chromatography tandem mass spectrometry. J. Chromatogr. A 1217, 5184–5189. https://doi.org/10.1016/j.chroma.2010.06.010

Villaverde, S., 1997. Influence of pH over nitrifying biofilm activity in submerged biofilters. Water Res. 31, 1180–1186. https://doi.org/10.1016/S0043-1354(96)00376-4

Wahid, R., Romero-Guiza, M., Moset, V., Møller, H.B., Fernández, B., 2020. Improved anaerobic biodegradability of wheat straw, solid cattle manure and solid slaughterhouse by alkali, ultrasonic and alkali-ultrasonic pre-treatment. Environ. Technol. 41, 997–1006. https://doi.org/10.1080/09593330.2018.1516802

Wang, X.-X., Wang, W.-L., Dao, G.-H., Xu, Z.-B., Zhang, T.-Y., Wu, Y.-H., Hu, H.-Y., 2020. Mechanism and kinetics of methylisothiazolinone removal by cultivation of Scenedesmus sp. LX1. J. Hazard. Mater. 386, 121959. https://doi.org/10.1016/j.jhazmat.2019.121959

Wittebolle, L., Vervaeren, H., Verstraete, W., Boon, N., 2008. Quantifying Community Dynamics of Nitrifiers in Functionally Stable Reactors. Appl. Environ. Microbiol. 74, 286–293. https://doi.org/10.1128/AEM.01006-07

Xiao, K.K., Guo, C.H., Zhou, Y., Maspolim, Y., Wang, J.Y., Ng, W.J., 2013. Acetic

acid inhibition on methanogens in a two-phase anaerobic process. Biochem. Eng. J. 75, 1–7. https://doi.org/10.1016/j.bej.2013.03.011

Yang, L., Yuan, C., Chen, X., Xue, W., Cao, G., Meng, S., Bai, L., 2023. The effect of nitrification inhibitors on the aerobic biodegradation of tetracycline antibiotics in swine wastewater. Chemosphere 311, 136849. https://doi.org/10.1016/j.chemosphere.2022.136849

Yap, C.C., Chan, Y.J., Loh, S.K., Supramaniam, C.V., Soh, A.C., Chong, M.F., Chew, C.L., Lim, L.K., 2020. Comparison of different industrial scale palm oil mill effluent anaerobic systems in degradation of organic contaminants and kinetic performance. J. Clean. Prod. 262, 121361. https://doi.org/10.1016/j.jclepro.2020.121361

Young, B., Delatolla, R., Kennedy, K., Laflamme, E., Stintzi, A., 2017. Low temperature MBBR nitrification: Microbiome analysis. Water Res. 111, 224–233. https://doi.org/10.1016/j.watres.2016.12.050

Zangeneh, A., Sabzalipour, S., Takdatsan, A., Yengejeh, R.J., Khafaie, M.A., 2021. Ammonia removal form municipal wastewater by air stripping process: An experimental study. South African J. Chem. Eng. 36, 134–141. https://doi.org/10.1016/j.sajce.2021.03.001

Zeng, D., Liang, K., Guo, F., Wu, Y., Wu, G., 2020. Denitrification performance and microbial community under salinity and MIT stresses for reverse osmosis concentrate treatment. Sep. Purif. Technol. 242, 116799. https://doi.org/10.1016/j.seppur.2020.116799

Zhu, L., Wu, B., Liu, Y., Zhang, J., Deng, R., Gu, L., 2022. Strategy to enhance semi-continuous anaerobic digestion of food waste by combined use of calcium peroxide and magnetite. Water Res. 221, 118801. https://doi.org/10.1016/j.watres.2022.118801

CONCLUSIONS AND FUTURE PERSPECTIVES

Various techniques have been developed to address soil contamination when environmental remediation is involved. These methodologies range from ex-situ to in-situ processes and have been instrumental in helping to diminish environmental matrix contamination levels.

This thesis focuses on the soil-washing techniques specific to the reagents' use and efficiency in detoxifying the soil. Reagents, particularly biodegradable, are critical to permitting a more cost-effective and environmentally friendly practice in the soil remediation industry to avoid harmful wastewater. Many of such reagents have promising characteristics, including foul-molecular-weight organic acids (LMWOA), chelating agents, and biosurfactants. This study has critically evaluated these extractant agents and what makes them remove some Potentially Toxic Elements (PTEs). Furthermore, previous studies highlight the prerequisite to conducting preliminary inquiries at the laboratory scale to apply factors and adjust process conditions to different soil properties, making the treatment process achievable and cost-effective. Although chelating agents have been prevailing over all these years, future studies show promising evidence for LMWOA and biosurfactants due to the possibly significantly affordable production in the prospect via bio-processes. In this way, the proposed method could prevent ecosystems from being severely affected by accidental soil-washing effluent spills.

The marine environment remains another distinctive domain, and especially the most important social entities, such as harbors, remain constantly threatened due to diesel spills and toxic pollution. The current thesis presents an interesting solution due to its usage of a low-cost and environment-friendly approach. More broadly, this methodology also addresses an ever more pressing issue of polymeric waste produced by hospitals, which is particularly relevant concerning the explosion of mask usage during the pandemic. Thus, this thesis also evaluated the utilization of surgical masks as an adsorbent for diesel removal from saline solutions. The results indicate that such an approach could be used to limit the environmental impact and reduce the pressure

on the waste management system. Moreover, the ability to operate within various parameters, such as the ones concerning pH changes in ionic force, should not be understated, and using the masks multiple times appears to be a viable application. Affordable adsorbents are still to be understood for other emerging pollutants.

Indeed, in wastewater treatment, methylisothiazolinone (MIT) occurs as an emerging contaminant that threatens biological processes. This thesis first investigated the impact of MIT on nitrification-denitrification using an Moving-bed biofilm reactor (MBBR), which could be an alternative approach to the use of adsorbents. The experimental campaign resulted in crucial insights on the inhibitory effect of MIT over nitrification, recovery, and enhanced efficiency of removal at higher concentrations. More importantly, the denitrification processes led to a real decrease in the total measured concentration of nitrite and nitrate and only showed temporary inhibitory effects. The microbial communities demonstrated resilience to MIT presence levels. In the interim, concurrent research showed MIT's impact with no importance or relevance on the methanogenic community.

Future experiments should explore, enhance, and test current mitigation techniques thoroughly. Thus, several areas remain open to further significant development. This process approach should only be tested using full-scale approaches to determine the applicability and scalability in a real-world environment. In particular, long-term ecotoxicity testing is essential to determining the real environmental impacts of ecological measures. Pilot-scale testing might also be a critical piece of evidence when determining the most optimal reagents and regimes for soil washing. Indeed, preliminary lab-experiments only create a scientific background for developing remediation actions that are cost-effective and environmentally friendly. In detail, future works should also examine the effectiveness of surgical masks on other organic pollutants. Also, the toxicity of treated water toward organisms should be investigated to ensure the integrity of ecological measures purposed to treat pollution. Studies are also necessary to improve treatment methods against contamination to avoid nitrification treatment inhibition. The solution lies in interdisciplinary research and creative techniques, allowing for productive collaboration and the development of sustainable approaches to protect the environment and human health.